DEVELOPMENT OF
LINEAR STRIP ION THRUSTORS

Prepared by

J.R. ANDERSON, R. KUBEREK, J.W. PFEIFER,

J.D. SMITH, S.A. THOMPSON, and M.D. BENTON

Prepared for

NATIONAL AERONAUTICS and SPACE ADMINISTRATION

CONTRACT NO. NAS 3-7927

SEMIANNUAL REPORT

DEVELOPMENT OF LINEAR STRIP ION THRUSTORS

by

J. R. Anderson, R. Kuberek, J. W. Pfeifer,
J. D. Smith, S. A. Thompson, and M. D. Benton

prepared for

NATIONAL AERONAUTICS AND SPACE ADMINISTRATION

January 1966

CONTRACT NAS 3-7927

Technical Management
NASA Lewis Research Center
Cleveland, Ohio
Daniel M. Shellhammer
Project Manager

HUGHES RESEARCH LABORATORIES
A Division of Hughes Aircraft Company
Malibu, California

TABLE OF CONTENTS

LIST OF ILLUSTRATIONS

ABSTRACT

This report describes the first half of a program for the development of a linear ion thrustor and a cesium feed system for possible satellite control systems application. The major effort is being devoted to cyclic tests of two thrustors with cesium and development of a liquid-transfer cesium feed system for zero-gravity applications in space. Related tasks are directed toward determining the thrustor vibration sensitivity and advanced development of the thrustor, and demonstrating a two-thrustor station with electrostatic ion beam deflection.

I.   INTRODUCTION AND SUMMARY

The purpose of this program is to continue development of a 0.3 millipound force cesium-contact, linear strip ion thrustor in conjunction with a liquid cesium feed system which will lead to development of a satellite control system. Specific major contractual tasks are (1) thrustor vibration analysis and test; (2) long-duration cyclic thrustor tests with cesium; (3) liquid cesium feed system development; (4) fabrication of two single-thrustor stations using the new zero-gravity feed system; and (5) advanced development of the thrustor, including demonstration of a two-engine station having beam deflection capability for thrust vector control.

During the first six months of the contract, considerable effort was necessarily devoted to the fabrication and construction of the experimental hardware. Because of the long duration of many of the tests, most of the experimental data will be generated and available only during the second half of the contract period.

An analysis of thrustor vibration sensitivity has been completed. Initial tests were conducted with the thrustor on a vibration shake table. The thrustor electrodes were instrumented with low mass accelerometers so that quantitative data could be obtained for correlation with the theoretical results. In general, the correlation between theory and experiment was good; the few deviations were traced to a change in the shape of the focus electrode, which is the main structural member in the present thrustor design. The analysis will be modified to account for this discrepancy between the mathematical model and the real ion engine.

Prior to testing two thrustors for 50,000 cycles each with a cesium ion beam, a number of preparatory tasks were necessary. In particular, one of the 2 foot diameter by 6 foot long vacuum chambers was modified to permit operation of two ion thrustors in the one facility. This was accomplished principally by including a vacuum lock at one end of the chamber, so that the two ion thrustors can be separated into their own vacuum environment and removed for any necessary repairs. An automatic console has been constructed and checked out for automatically cycling the two thrustors during the life test. In addition, an improved solenoid-valve cesium feed system was designed for use with the thrustors that are to be cycled. At the conclusion of this first six month report period all of these items, including the two thrustors, were completed and ready for integration.

Design of the liquid cesium feed system has been established and subjected to detailed thermodynamic analysis. This analysis showed that the vaporizer section of the feed tube could be heated to operating temperature in approximately 15 seconds, which is within the warmup time of the ionizer itself. In addition, the vaporizer could be cooled within 10 seconds to a temperature corresponding to 1 percent of the peak vapor flow. These results indicate that rapid startup and shutdown can be achieved. In order to maintain cesium in a clean state during storage and prior to use, a passive burst disc using a frangible diaphragm has been designed and is on order. If one atmosphere of an inert gas, such as argon, is placed on the internal side of the burst disc, it is possible to maintain the cesium feed system hermetically sealed during all handling and storage operations. The cesium becomes available only when a vacuum is pulled on the downstream side, bursting the diaphragm.

A number of experiments have been conducted for thermal improvement of the thrustor. The results are promising for further reductions of ionizer heater power requirements. A new structural design for the thrustor has been established in order to improve its high voltage integrity. In particular, the high voltage insulators in the

2

modified design are referenced with respect to ground in order to reduce the voltage standoff requirement on each insulator. In addition, the insulators are positioned more favorably for minimizing surface leakage effects resulting from cesium deposition.

Electrolytic tank simulation studies were conducted to define the ion optical characteristics of both the present thrustor electrode structure and several possible electrode modifications. It was found that in the present design, the neutralizer filament is swamped in a negative electric field. The addition of a grounded decel electrode was shown to provide a superior electrode structure.

The study of a double-beam station with electrostatic beam deflection capability in each thrustor has been included in this contractual effort. Analysis and experiment has shown that the ion beam may be deflected to angles greater than 10 degrees from the normal beam axis. With this amount of deflection a large fraction of the thrust can be directed perpendicular to the normal thrust vector. Therefore, a single linear-strip thrustor could be used for both station keeping and attitude control about one axis. If two such thrustors are mounted with the ionizers in one plane, but with the electrode structures perpendicular to each other, two-axis control from a single station is possible. Using this concept, one two-thrustor station with electrostatic beam deflection performs the functions of five separate static thrustors.

II.   THRUSTOR VIBRATION ANALYSIS AND TEST

Vibration tests to determine the mechanical integrity of a sub-system following design changes are often tedious, time consuming, and expensive. These disadvantages would be eliminated if a proven computer program could quantitatively evaluate a mathematical model of the device or subsystem subject to excitation accelerations specified as a function of frequency. Such a digital computer program has been developed at Hughes. The purpose of this portion of the contract is to prove the applicability of this computer program to analysis of the dynamical behavior of ion thrustor systems. Therefore, a detailed analytic study of the vibration sensitivity of the linear strip ion thrustor has been completed. The computer results are to be verified by determining the principal vibration modes and resonances which occur during actual vibration tests of a thrustor. Once verified, the computer program can be used to confirm any design changes which may subsequently occur in a development program without requiring repeated vibration tests. This should significantly reduce the time and expense involved in vibration qualification.

The program was run using the Linear Elastic Structural Analysis Routine (LESAR) in conjunction with the IBM 7094 digital computer. This routine is essentially a stiffness matrix normal mode technique. The program is capable of solving the dynamic responses of a structure subjected to any arbitrary time dependent input force. The forces may act either separately or simultaneously at the selected reference stations. LESAR will handle three-dimensional structures with up to 102 degrees of freedom. Displacement and/or rotational constraints may be put into any station. This imposition of arbitrary constraints is quite essential since it permits "blanking" out normal modes which are not excited by the particular forcing function. The contributions of up to twelve normal modes may be used for the response calculations if necessary.

Results of the program include the following:

a.   Natural frequencies and the corresponding mode shapes.

b.   Displacements, velocities, and accelerations at each station and for all degrees of freedom at points selected in time. Axial and shearing forces and bending and torsional moments are also found at the times of interest.

c.   Maximum values of the forces and moments of (b) and the time at which they occur.

A mathematical dynamic model of the ion thrustor used in the study was simulated by a series of lumped masses connected by elastic members, as shown in Fig. 1. The neutralizer filament assembly was treated separately, since it was assumed that this assembly would have little dynamic effect on the rest of the system because of its relatively small mass. The model was assumed to have a damping coefficient of 1% of critical for all modes and to be fixed at two points on the focus electrode. (The mounting as taken in the model was not the same as on the test thrustor because of an engineering change that had taken place. The actual mounting was as shown in phantom lines in Fig. 1.)

The computer study has shown that the first two natural frequencies of the thrustor, excluding the neutralizer assembly, should occur at 1774 cycles per second (cps) and 2473 cps. In these modes the neutralizer bar experiences relatively large motion with respect to the rest of the system. In actual vibration tests a first resonant frequency of 200 cps became apparent. This was attributed to the difference in mounting between the model and the test specimen. The model is being changed to simulate the new mounting configuration and the computer program will be rerun to determine whether the analysis predicts the 200 cps resonant frequency.

The test procedure used consisted of mounting the unit to an aluminum fixture on an MB Electronics Model C-10 vibration exciter (see Fig. 2). Two CEC Model 4-275 miniature, 1.5 gram (g) accelerometers were located at various locations on the thrustor as shown in Fig. 3, to measure response. One Endevco Model 2213 accelerometer

NEUTRALIZER
BAR

ACCELERATOR
ELECTRODE

FOCUS
ELECTRODE

IONIZER
BASE
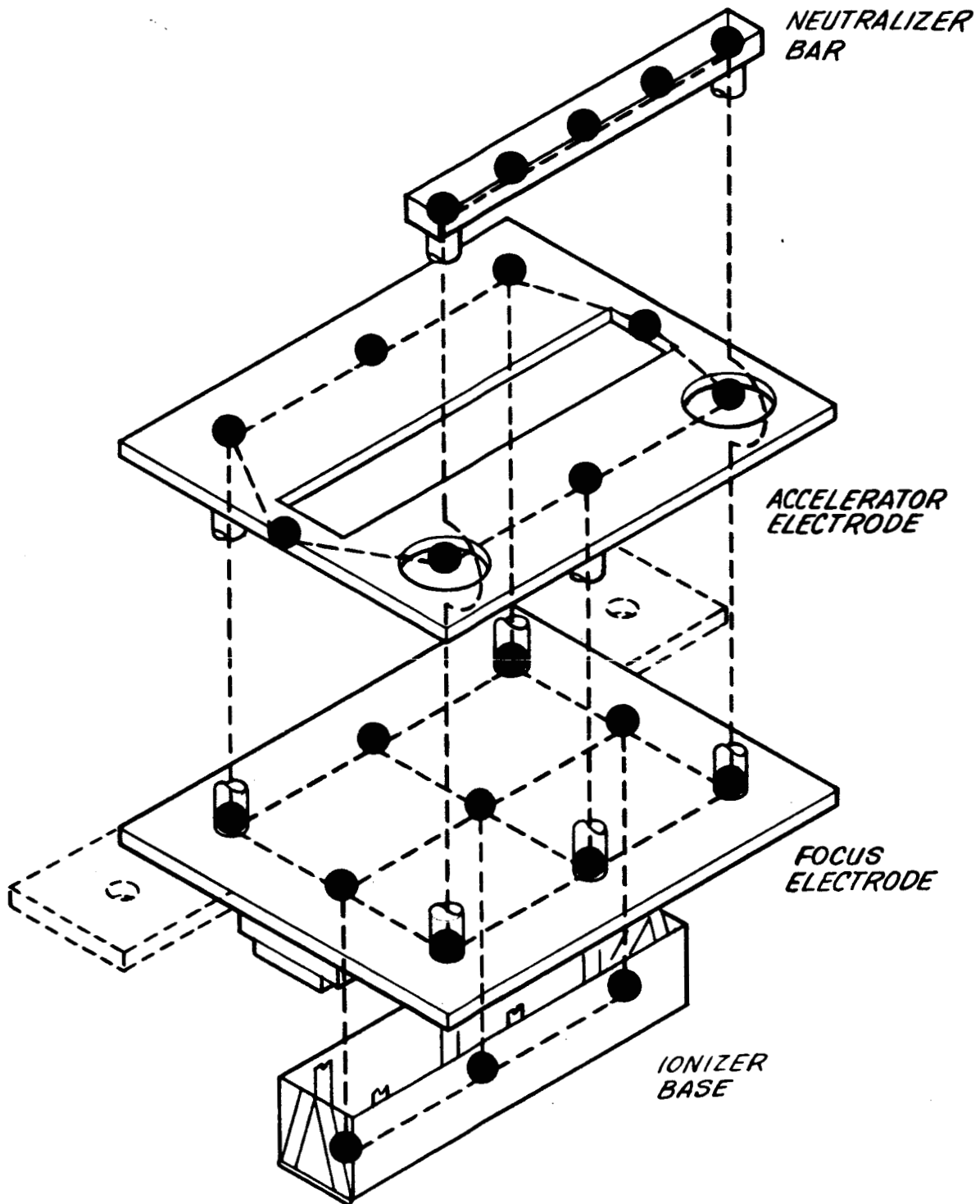
Fig. 1.   Model used for the mathematical analysis
of ion thrustor vibration sensitivity.
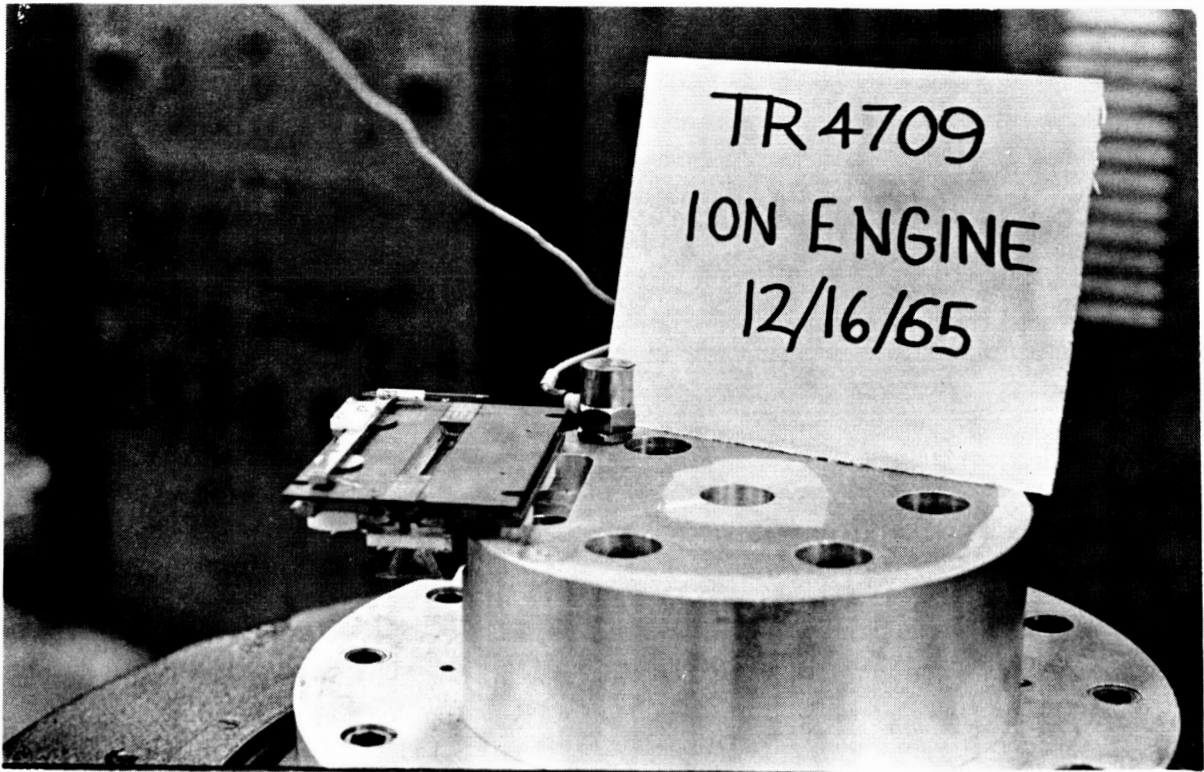
Fig. 2. Photograph of ion thrustor mounted on vibration table.
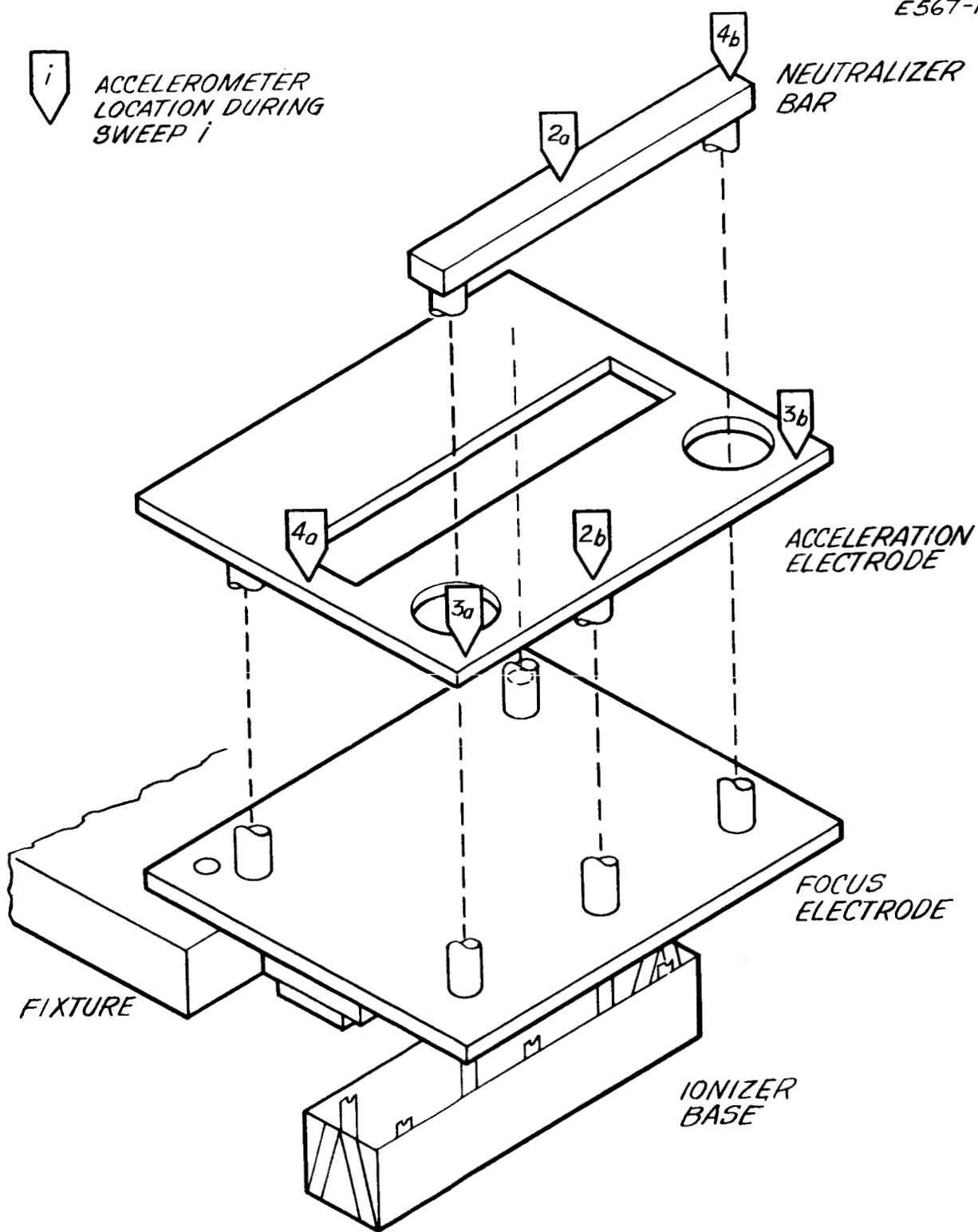
Fig. 3. Location of accelerometers during vibration tests.

was located on the fixture to measure input accelerations. The three accelerometer signals, plus the shaker drive oscillator signal and a voice identification channel, were recorded on Frequency Modulation (FM) tape at a tape speed of 15 inches/second (in./sec). A block diagram is shown in Fig. 4.

The test consisted of four 10 minute (min) sweeps. For each sweep the rate was as follows: 50 to 800 cps logarithmically in 4 min followed by 800 to 4000 cps logarithmically in 6 min. During the first sweep no accelerometers were mounted on the thrustor. Visual and audio observations; of the thrustor during the vibration sweep were made, and possible resonant conditions were noted. Dwells were then made at the noted frequencies, and the input level was increased to tune in the particular frequency mode.

During the last three sweeps the two response accelerometers were located as indicated in Fig. 3, and an x-y plot was made of the accelerometer output versus frequency. The x-y plot was then used to locate resonant points and dwells were made at these points to determine exact response magnitude. The input amplitude was 1 g in all sweeps but was increased to 3 g during dwells to locate exact frequencies.

The transmissibility data shown in Figs. 5 through 10 show that the entire thrustor has a fundamental resonant frequency at 200 cps when a two-point mount is used. It is believed that the lack of agreement between the computer study (see Appendix A) and the low frequency test results is caused by the difference in mounting. This is now being investigated and will be studied in the next period, together with tests of a thrustor with a four-point mounting arrangement.
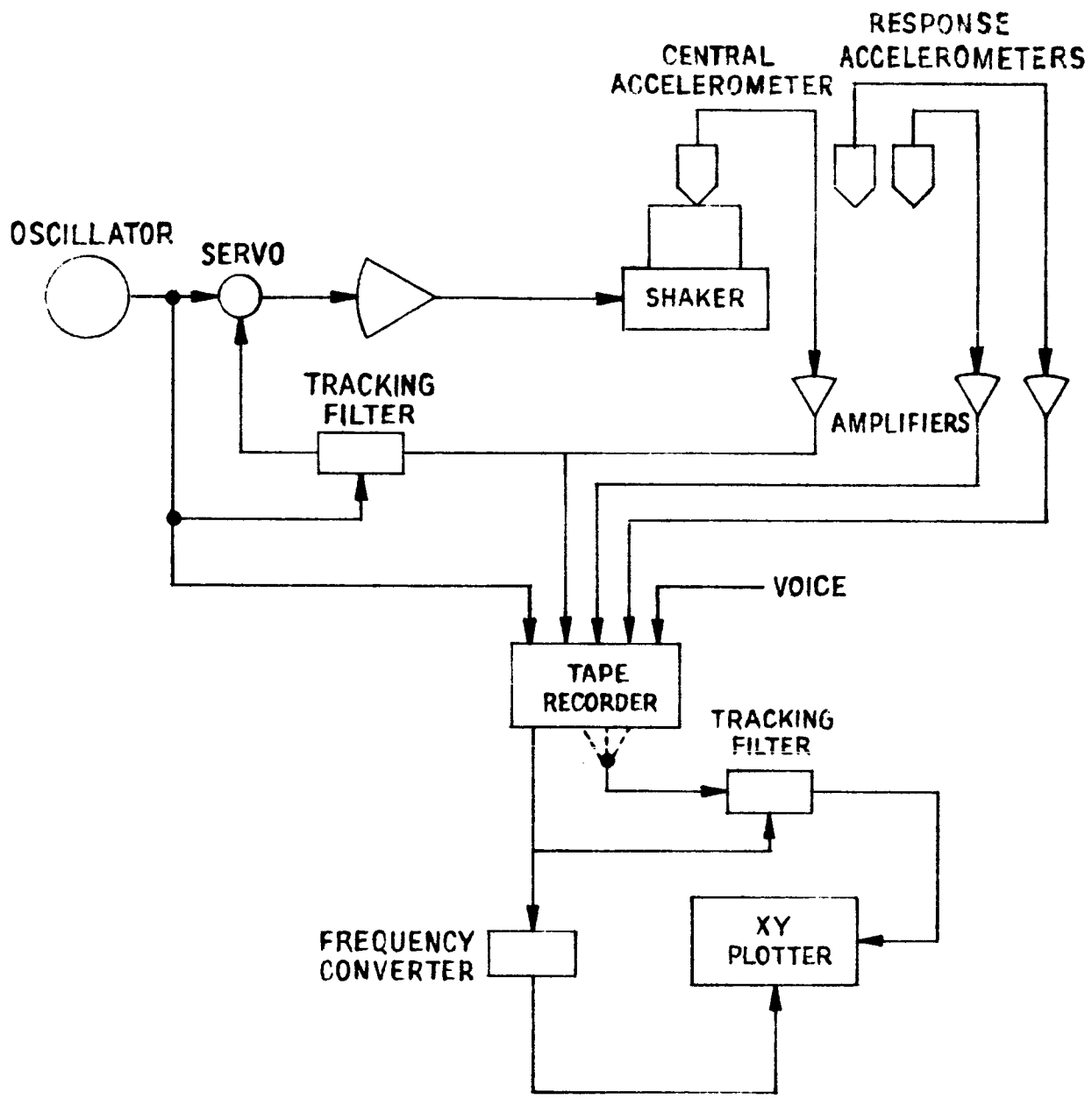
Fig. 4. Block diagram of vibration test arrangement.
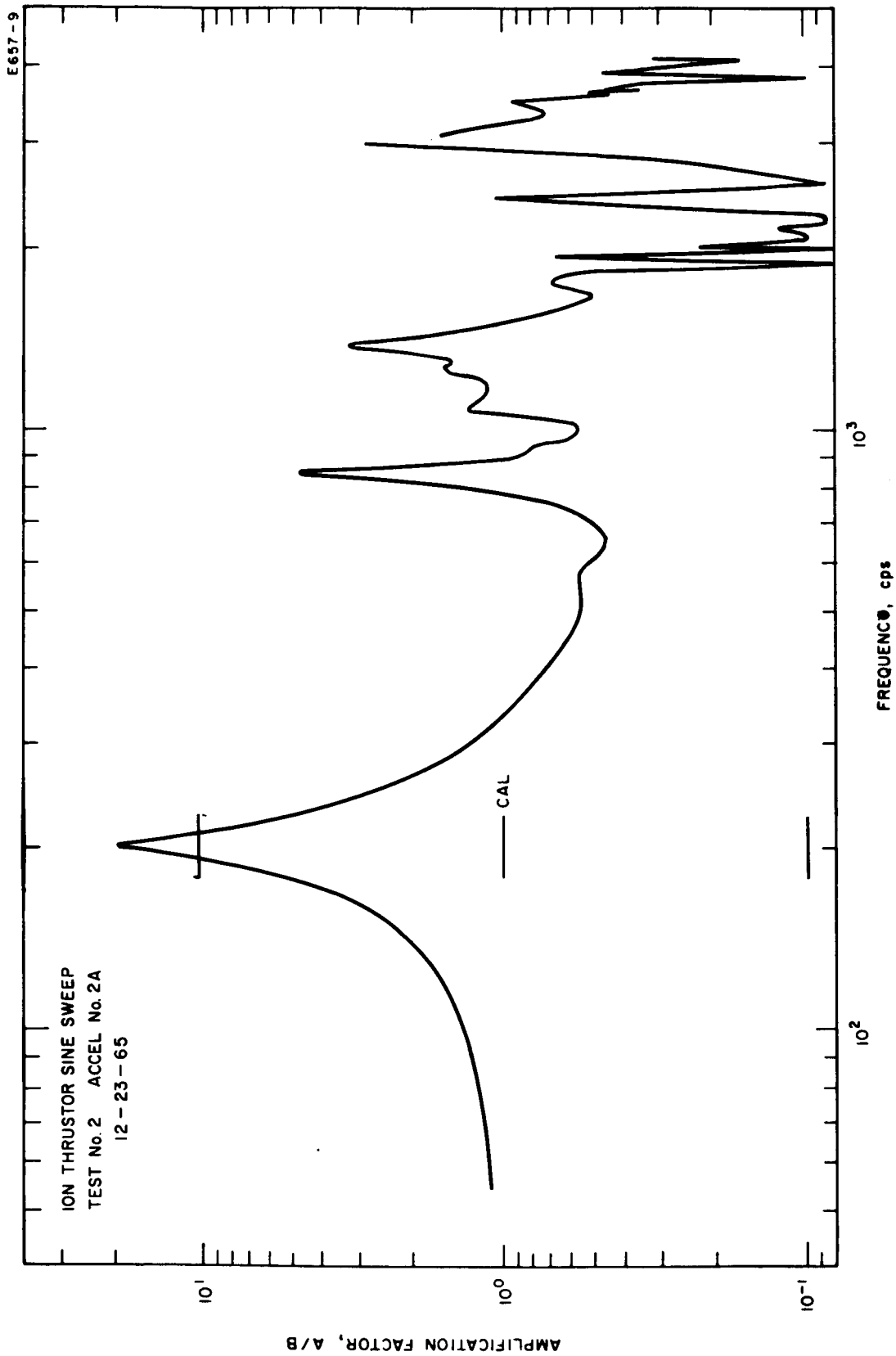
Fig. 5. Transmissibility data from vibration tests.

12
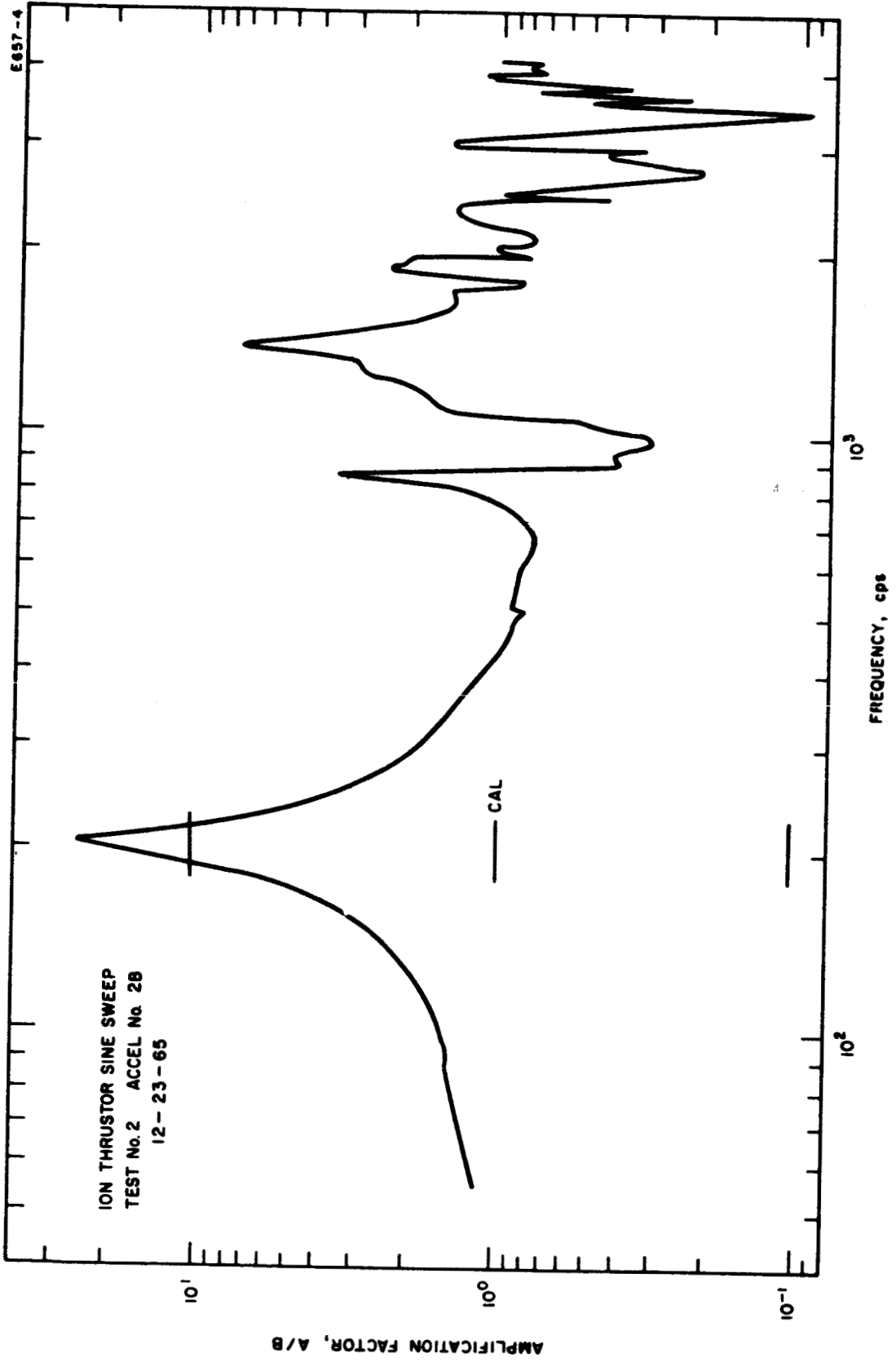
Fig. 6. Transmissibility data from vibration tests.

13
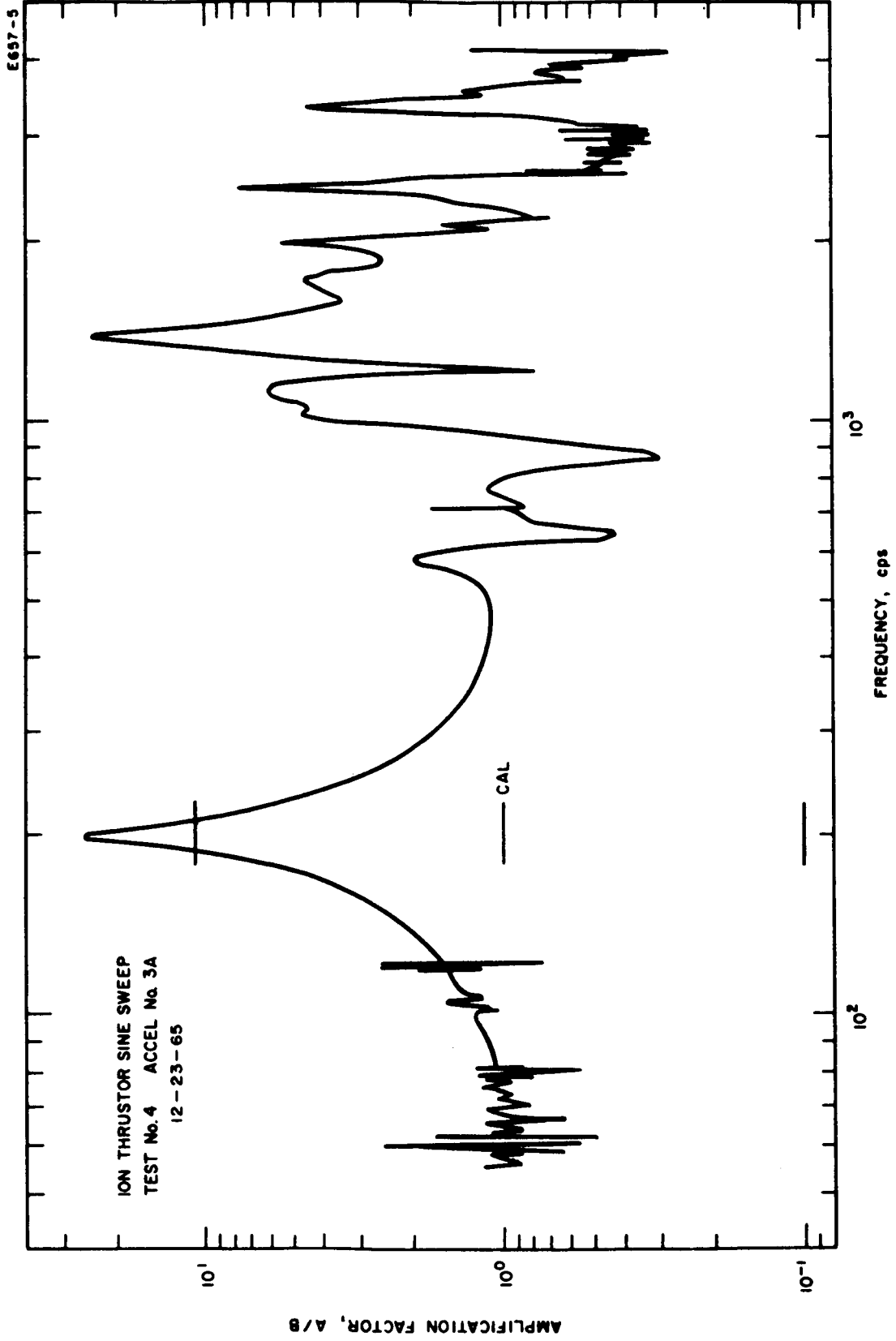
Fig. 7. Transmissibility data from vibration tests.

14
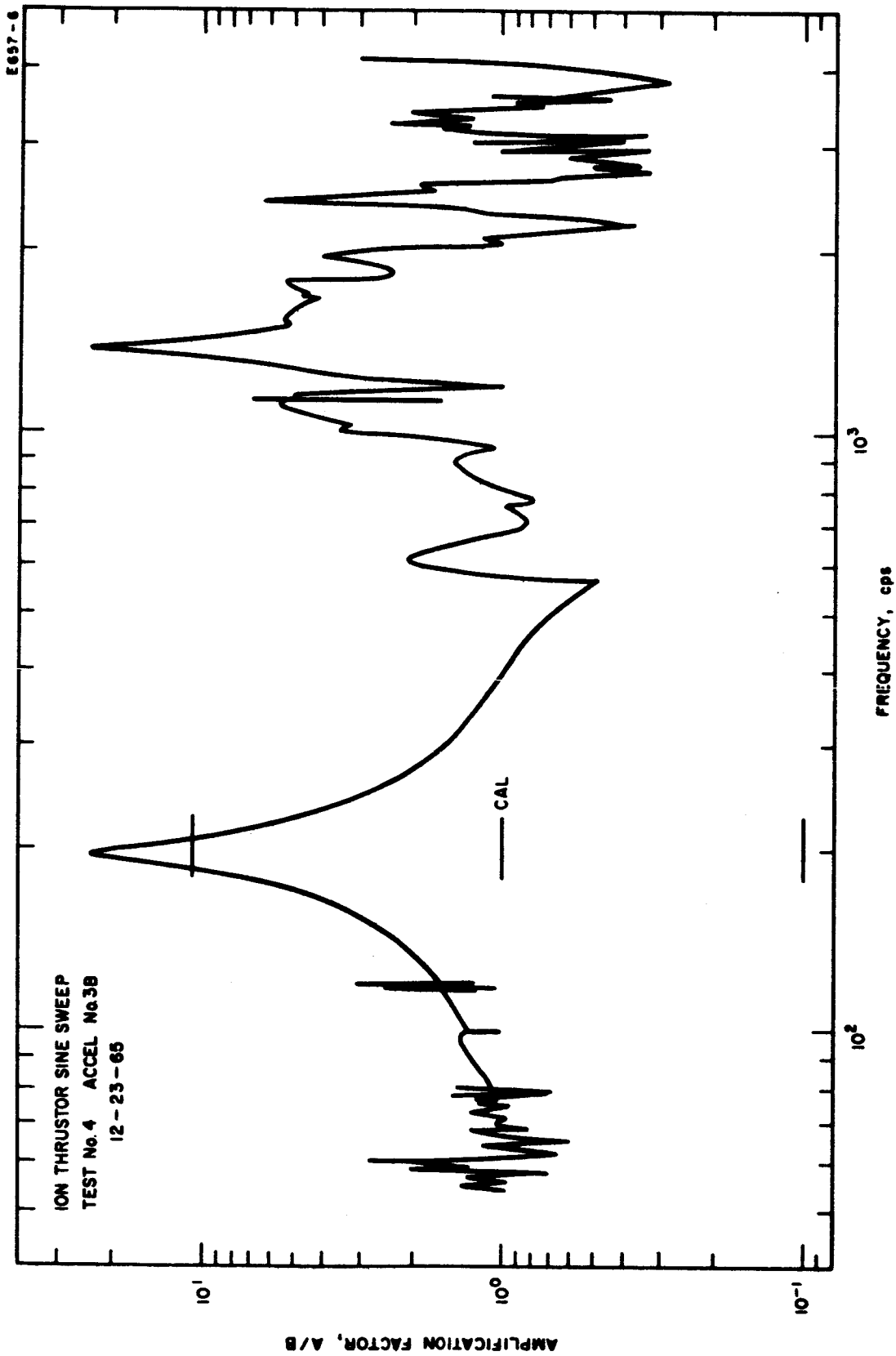
Fig. 8. Transmissibility data from vibration tests.

15
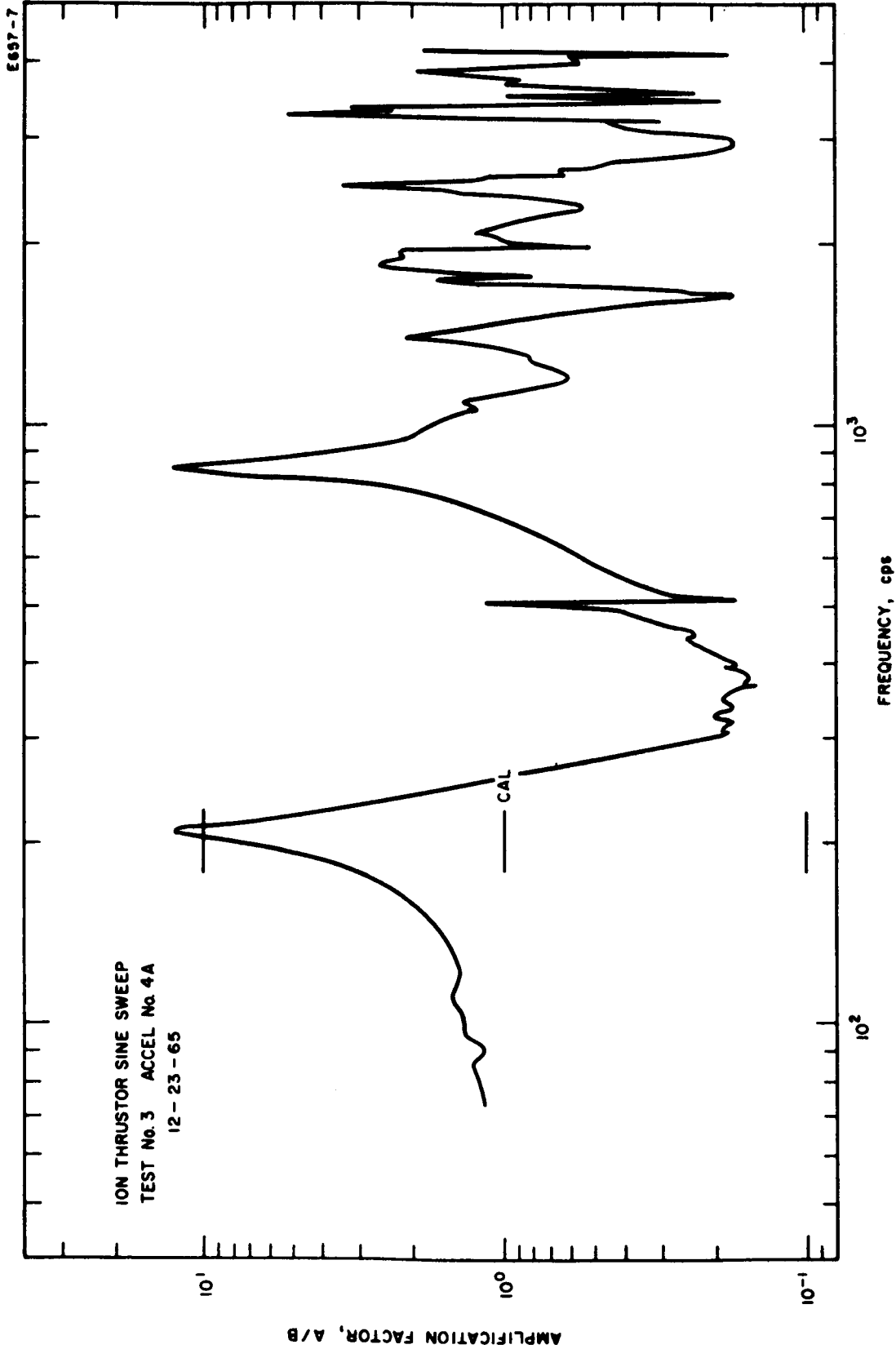
Fig. 9. Transmissibility data from vibration tests.

16
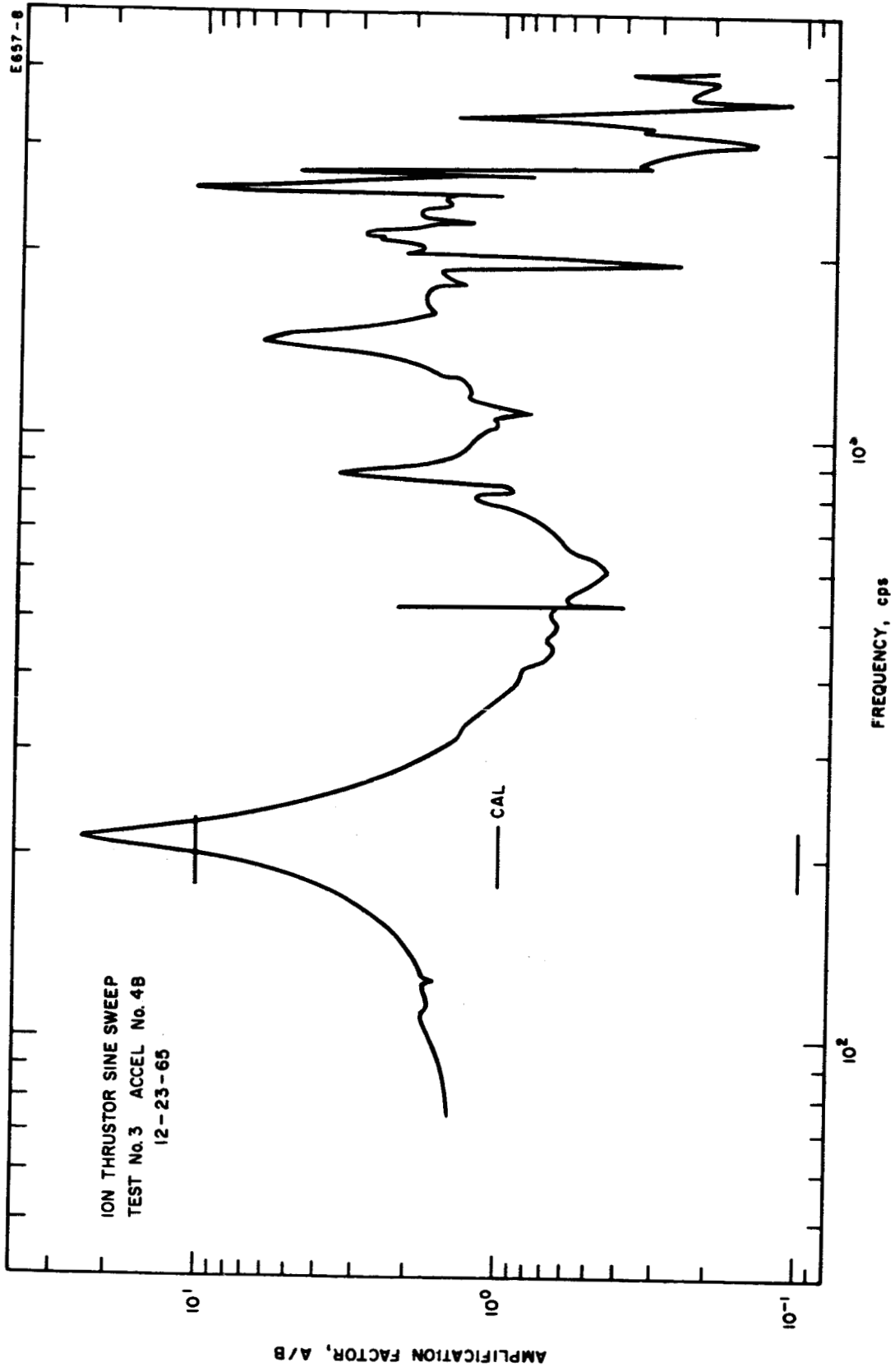
Fig. 10. Transmissibility data from vibration tests.

17

III.   LONG-DURATION CYCLIC TESTS

The purpose of this task is to demonstrate that the linear ion thrustor electrical design is suitable for repeated thrust operation. This is to be verified by cyclic operation of two thrustors, each for 50,000 beam-on cycles. Each test cycle is to simulate the attitude-control mode of operation as follows: a nominal 20 sec warmup period, a 10 sec thrust period at a level of 0.3 millipound force (mlbf), and a 3 min off period. Warmup is required to be consistent with a warmup energy of 0.60 watt-hour (W-hr) to an ionizer temperature of 1100 degrees Centigrade (^{O}C).

A.   THRUSTORS

Two thrustors of the LD design, designated LD-4 and LD-5, have been fabricated for long-duration cyclic testing. The Model LD, 4.6 centimeter (cm) thrustor is a scaled down version of the Model LB (8 cm) thrustor, for which a complete set of drawings was submitted under Contract NAS 3-4117, and utilizes a short F-2 type heater. Both LD-4 and LD-5 use Philips, Mod E, 82 percent (%) density (2.86 micron (μ) average particle size) porous tungsten ionizers. Accel electrodes are of the laminated copper and stainless steel construction used in previous life tests. Neutralizer filaments are carburized thoriated tungsten. A photograph of thrustor LD-4 and its accompanying neutral detector is shown in Fig. 11.

B.   LABORATORY FEED SYSTEM

The original planning for this thrustor test anticipated the use of several 250 g capacity laboratory-type cesium feed systems available from a previous program. Early in the program the cesium feed system requirement was reviewed, and it was concluded that a new feed system was needed. The available laboratory feed system had two disadvantages when considered for use on the cyclic life test: (1) it was sensitive to attitude, thus restricting engine installation in the vacuum facility; (2) the cycle life of the solenoid valve was too short.

19
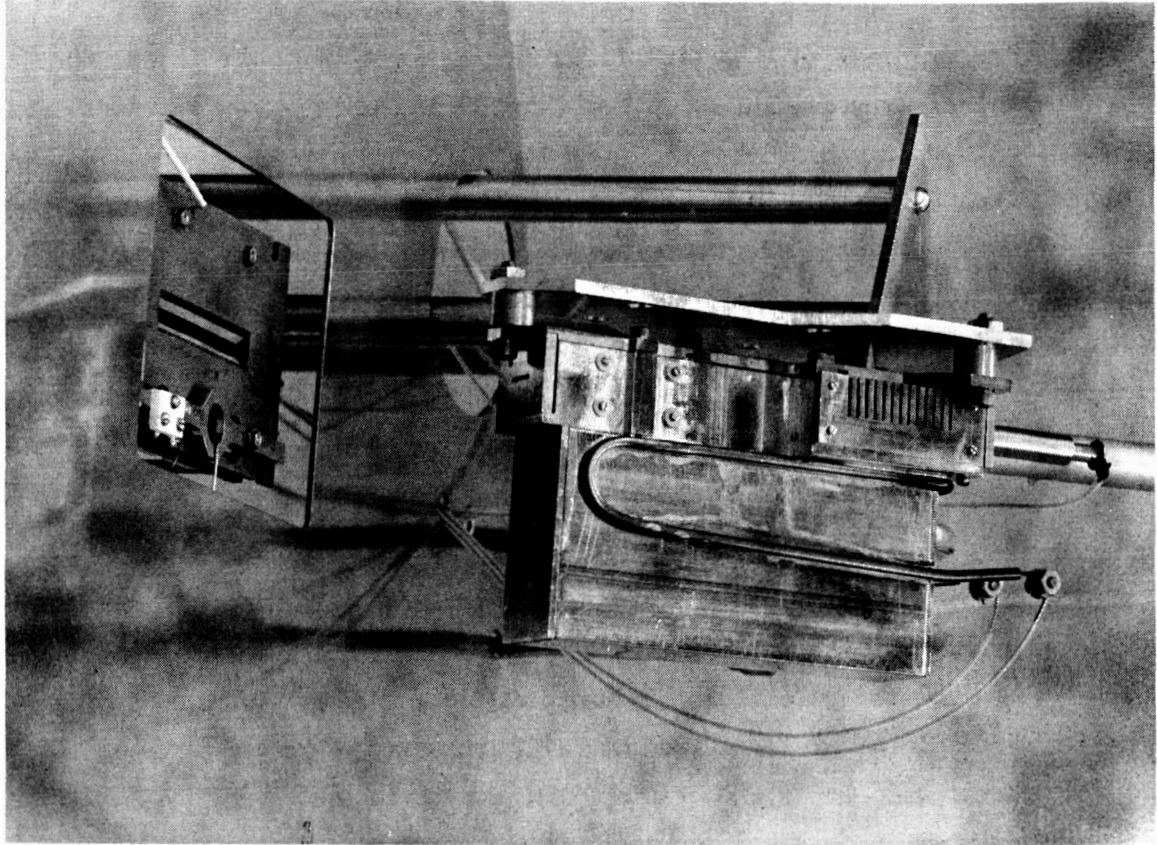
Fig. 11. Photograph of ion thrustor LD-4
and accompanying neutral detector.

A new vapor-transfer cesium feed system was designed and fabricated with the following features:

Cesium capacity: 80 g

Thermal time constant: 10 min maximum (max) (for 1% beam change)

Operating temperature $300^{\circ}C$

Insensitive to attitude

Minimum length feed tube to thrustor

All heaters brazed in place

No super heater

Hermetic seal and piercing mechanism

Solenoid on/off vapor flow control

This feed system, shown in Figs. 12 through 14, is essentially a new arrangement of previously developed components and techniques. In order to reduce thermal mass and improve thermal efficiency, the solenoid-operated feed valve is in the center of an annular capillary reservoir. A hermetic seal to protect the cesium during storage and station assembly, a piercing mechanism, and a heater complete the feed system.

The solenoid valve is similar to that developed for the 250 g laboratory feed system; some modifications were made to improve valve reliability and cycle life. The cesium flow path was altered to avoid exposure of the valve plunger cavity to air when the system was let down to ambient conditions. This redesign has the added advantage of minimizing the volume of the cesium flow path between the valve and the thrustor. In addition, coil potting techniques were modified to improve valve reliability. The remaining changes in the valve were designed to improve its cyclic life.

A minimal solenoid valve improvement program, supported by design and engineering effort, was started to verify valve redesigns. This phase of the work was not intended to produce a new valve design, but rather to define and eliminate valve failure modes, thus increasing valve reliability and life. A more comprehensive program of solenoid valve development and reliability testing is required than can be done under this contract.

PIERCING   FELT METAL   VALVE COIL   HEATER
MECHANISM
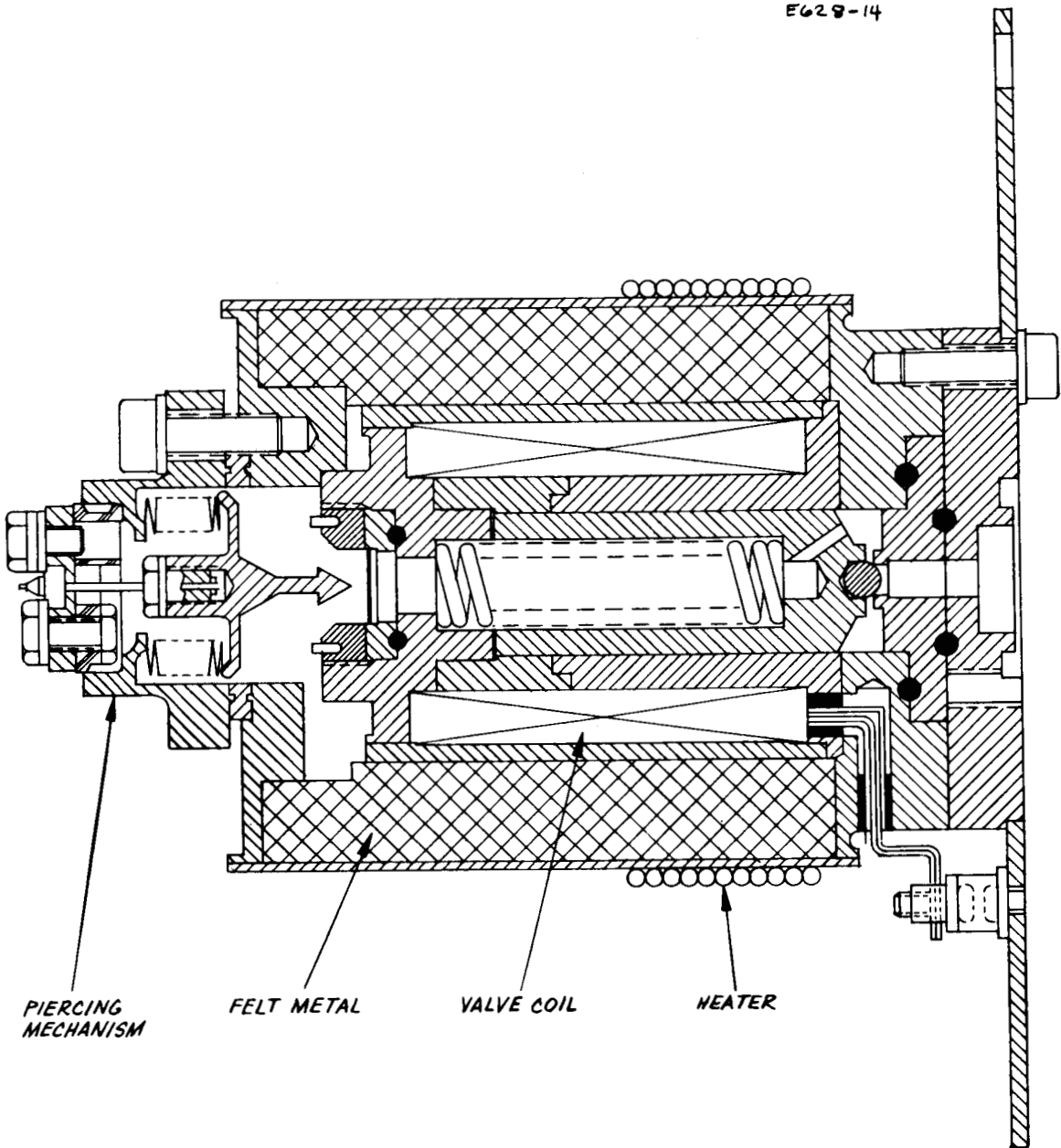
Fig. 12. Schematic of improved solenoid-valve feed
system for use in thrustor cyclic tests.
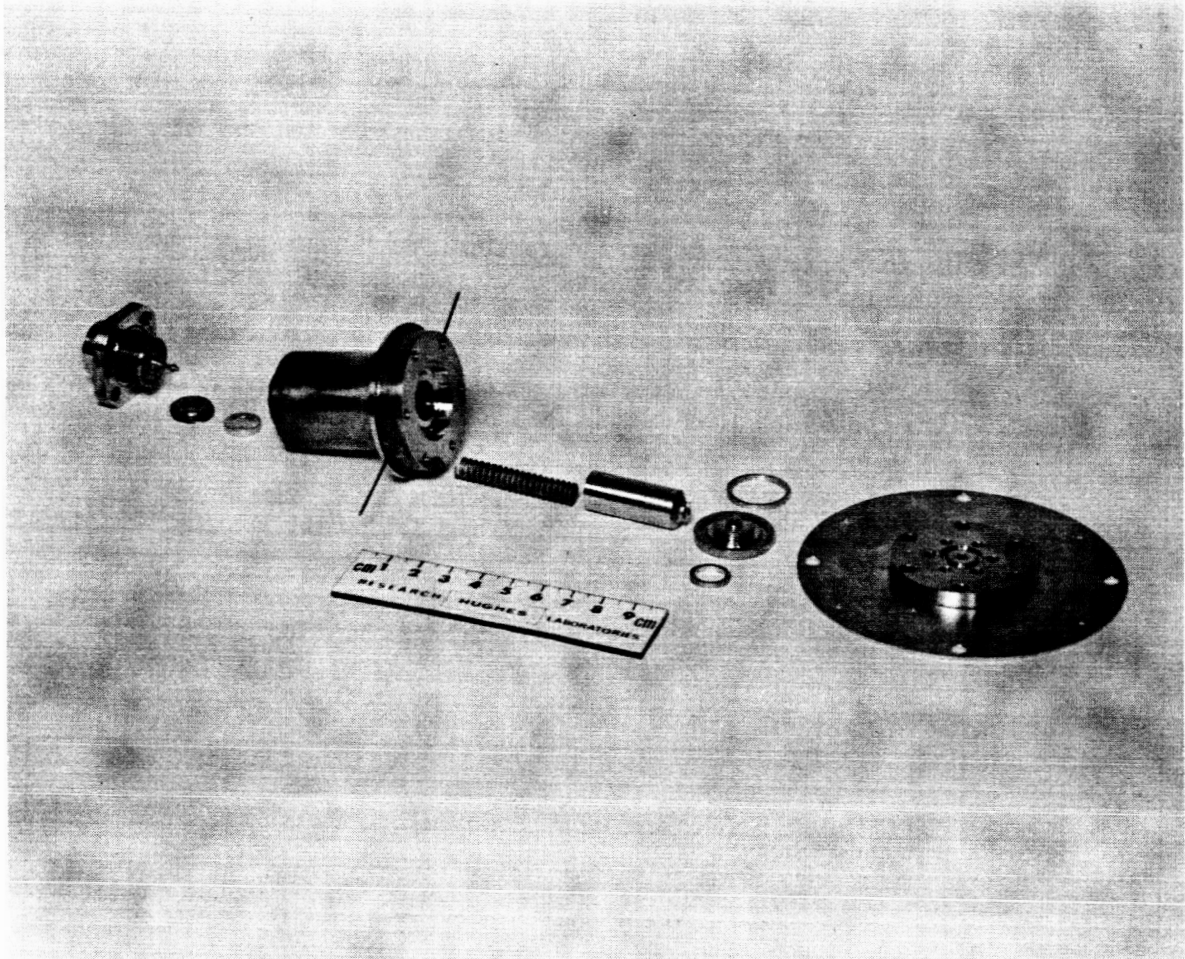
Fig. 13.   Photograph of redesigned solenoid valve.
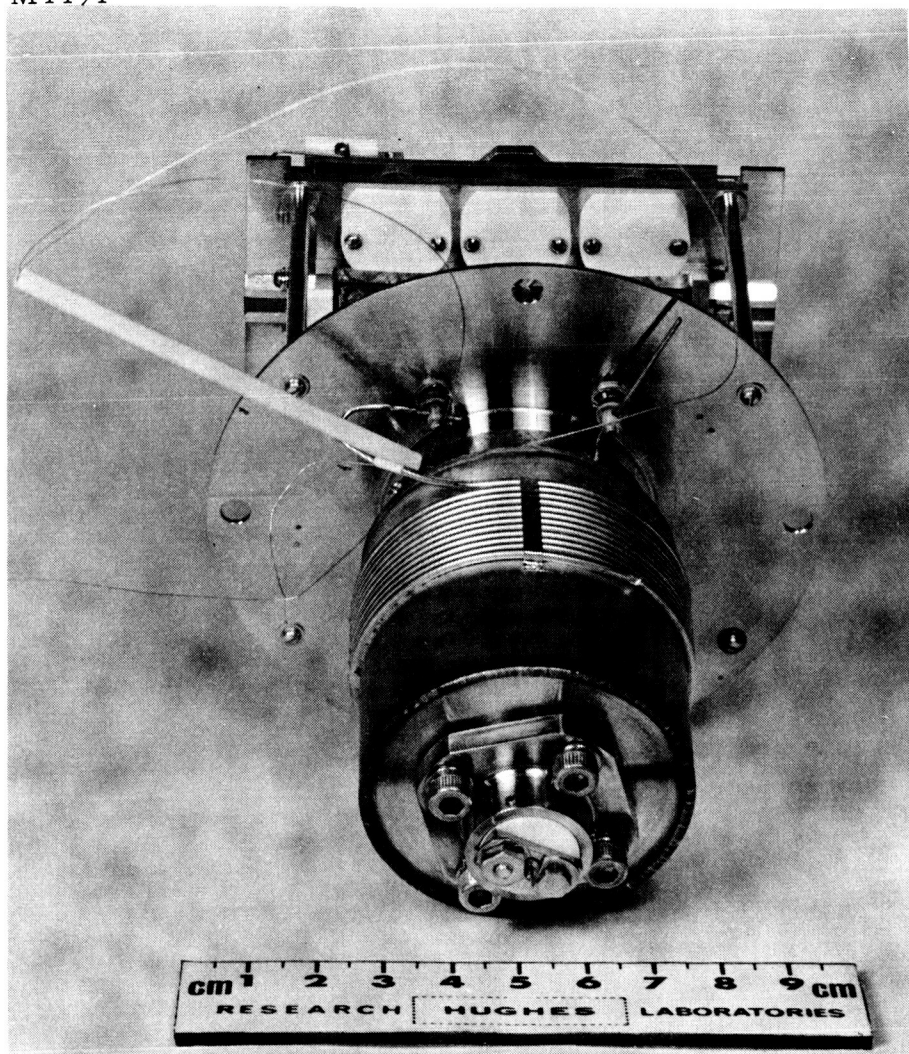
Fig. 14. Photograph of 80 g solenoid-
valve cesium feed system.

All tests were conducted under the temperature and vacuum conditions which the valve will experience in use, but without cesium in the lines. Figure 15 shows one of the development valves under test. Review of previous valve failures experienced with the basic valve showed that four failure modes were likely to be dominant: (1) insulation breakdown in the ceramic coil potting material; (2) galling between the valve plunger and valve bore; (3) deformation of the valve seat; and (4) deformation of the plunger where it is attached to the valvular element. Preliminary life testing verified the last three failure modes without introducing any evidence of others. Subsequent life testing established the effectiveness of the several proposed valve modifications outlined below.

Potting technique:	Change to eliminate crossed turns where electrical leads are brought out of valve
	Obtain magnet wire with substantially better quality ceramic insulation
Galling:	Apply precision hard chrome plating to plunger
Valve seat deformation:	Change material to increase hardness from Rockwell scale C (RC) 43 to RC 57
	Reduce valve spring force from 7 pounds (lb) to 3 lb
Plunger deformation:	Modify plunger to incorporate hardened retainer for the valvular element and to improve method of retention.

Tests of these modifications were limited to available valve bodies. Over 10,000 cycles were accumulated without failure of the new valve seat or plunger. Modified parts were incorporated in feed systems as they became available so that the first feed system delivered for thrustor test has an intermediate configuration, while the second feed system includes all the design improvements. A new valve including all of the changes is being fabricated for life test next month.
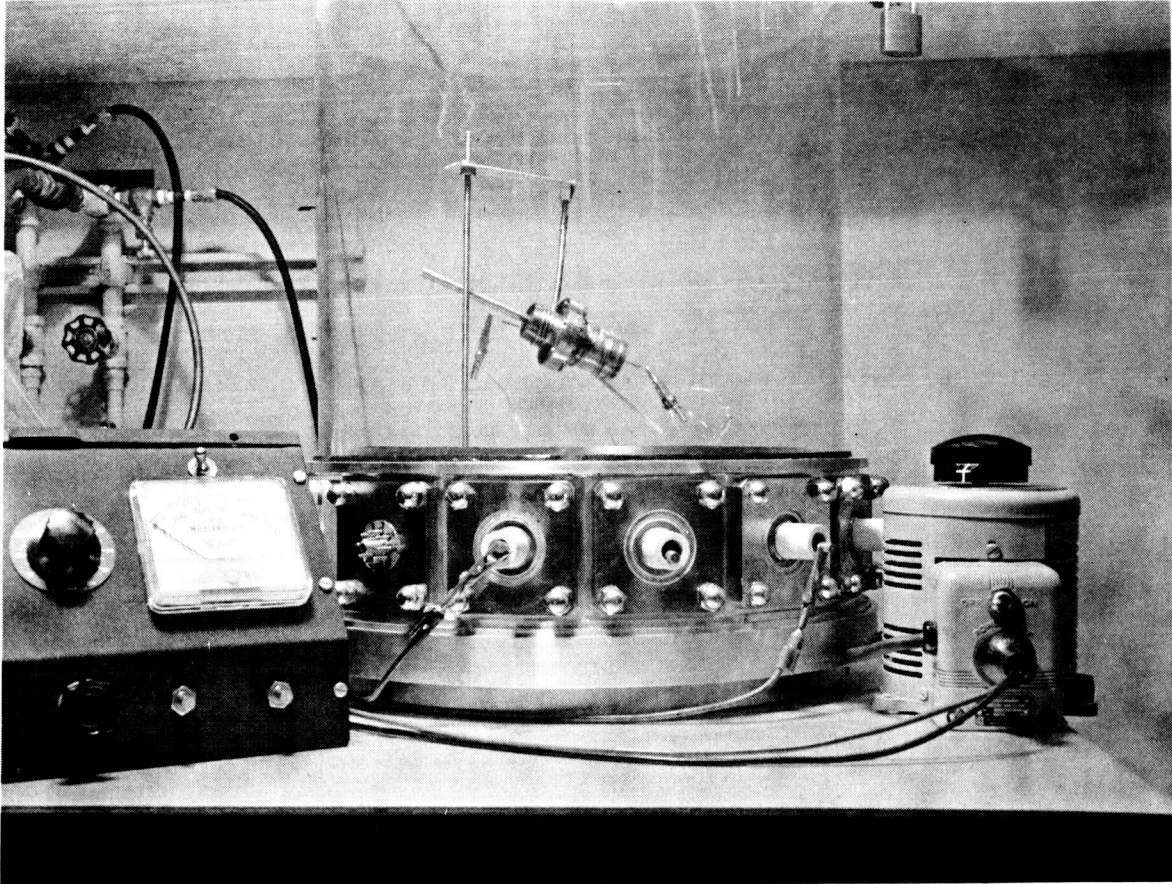
Fig. 15. Experimental arrangement for thermal-vacuum
evaluation of cyclic life of redesigned solenoid
valve.

The hermetic seal and piercing mechanism used on this new feed system was developed under Contract NAS 3-4117 and has been incorporated without significant change. Filler material used in the annular capillary reservoir is the same 10% dense nickel Feltmetal used for previous programs. The reservoir was sized to provide a convenient mechanical arrangement which results in a unit with a capacity of 80 g of cesium.

Reservoir filling procedure consists of evacuating the reservoir, then using atmospheric pressure (argon) to force the desired quantity of liquid cesium into the capillary filler, and finally backfilling the reservoir with argon to a pressure of 1 atm. The reservoir is then sealed with the piercing mechanism. Two of these feed systems have been completed, and two more are being fabricated.

C.   TEST CHAMBER MODIFICATION

For the cyclic operation of two thrustors, modifications were made on the 2C vacuum chamber. In particular a CEC Residual Gas Analyzer (RGA) and vacuum lock were added. A double ended collector assembly was constructed, and the pumping system was trapped. The new chamber is shown in Fig. 16.

The modifications to the chamber consisted of adding two 4 in. diameter view ports for observing the thrustors and making optical pyrometer measurements, and one 6 in. port for mounting a neutral detector. New view ports through the cryowall were aligned with the new ports in the tank wall, and externally operated shutters were provided.

The RGA lock assembly was mounted on an existing 6 in. port. The RGA lock is provided with an evacuation valve and a small ion pump so that it may be isolated from the chamber when the RGA is not in use or the chamber is vented.

The thrustor vacuum lock is designed so that either thrustor may be removed from the test chamber without the other being exposed to atmospheric pressure. The lock consists of a 12 in. diameter by 12 in. long chamber which is separated from the 2 foot diameter chamber by
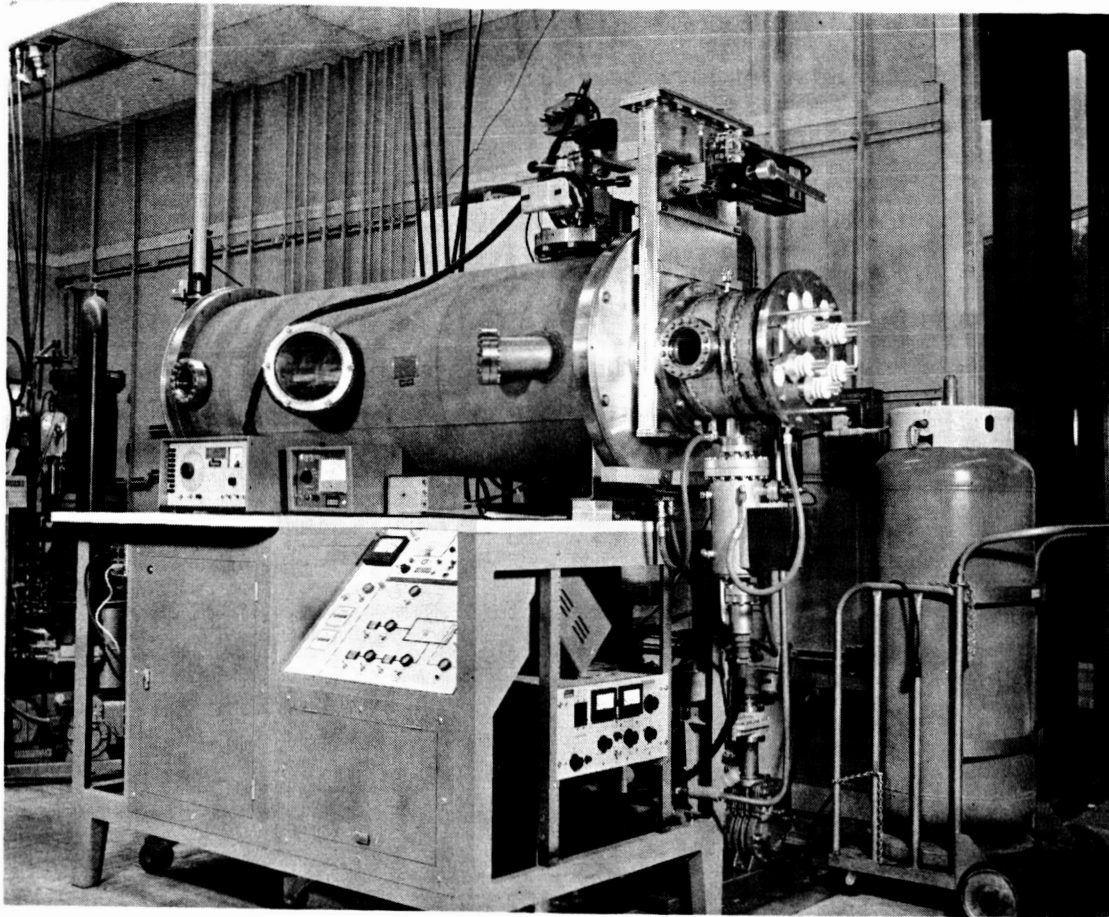
Fig. 16. Photograph of modified vacuum chamber.

a 10 in. diameter gate valve. The lock chamber is equipped with a
4 in. diameter view port, an evacuation valve, and a combination ion-
sublimation pump. The ion-sublimation pump reduces the lock pres-
sure nearly to that of the main chamber so that no large pressure rise
occurs when the 10 in. gate valve is opened.

The collector assembly consists of a chevron baffle which is
common to both engines and a series of truncated cone baffles mounted
on a frame which is isolated from the cryowall by teflon support pads.
The collector assembly is constructed of oxygen free copper and the
chevrons and cones are of 1/32 in. sheet.

The chamber is pumped by a 10 in. oil diffusion pump using
Don Corning (DC) 705 oil. Trapping of the diffusion pump consists of
an ambient or splash baffle and a combination liquid nitrogen (LN_2)
and zeolite trap. The pumping system is isolated from the chamber by
a 10 in. right angle valve. The LN_2-zeolite trap features bakeout
heaters, thermocouples, and a gas purge valve. The chamber roughing
pump is trapped with an uncooled zeolite trap. An auxiliary roughing
line is provided to rough the thrustor vacuum lock.

In operation the thrustor vacuum lock indicated a pressure of
approximately 1×10^{-6} Torr after an overnight pumpdown (empty,
no thrustor). With the chamber indicating 5×10^{-8} Torr, the lock
valve was opened at this pressure. A pressure rise in the chamber to
2×10^{-7} Torr was observed. During a longer pumpdown period
(24 hours) a lock pressure of less than 1×10^{-7} Torr was indicated
which should have less effect on the main chamber pressure when the
lock valve is opened.

D.   AUTOMATIC CYCLIC LIFE TEST CONSOLE

This console was designed to operate two ion rocket thrustors, of the linear-strip type. The console is fully automated for alternately operating each thrustor during cyclic life tests.

The following power conditioning modules are contained within the console (see Fig. 17):

1.	One Ionizer Heater power supply:	0 to 30 Vac at 5A
2.	One Feed Valve power supply:	0 to 60 Vdc at 1 A
3.	One Neutralizer Heater power supply:	0 to 15 Vac at 0.5 A
4.	One Main Drive power supply:	0 to +5 kV at 60 mA
5.	One Accel power supply:	0 to -5 kV at 30 mA
6.	Two Boiler Heater power supplies:	0 to 30 Vac at 1 A
7.	Two Feed Tube Heater power supplies:	0 to 20 Vac at 3A

These power supplies receive their input from two Space Electric Rocket Test (SERT)-I 2 kc square-wave inverters. The input to these inverters is furnished from +30 volt direct current (Vdc) and +50 Vdc regulated power supplies built into the console.

Included in the console are all the circuits and controls necessary to provide the following functions:

1.   Primary power ON-OFF switching

2.   Automatic or manual mode selection

3.   Automatic thrustor station cycling and voltage application in the automatic mode

4.   Manual thrustor station selection and manual voltage application in the manual mode

5.   Manual ON-OFF control of each power supply and independent output level adjustment of each voltage for both thrustor stations

6.   Servo control of the boiler heater input power to maintain the beam current at the preselected level.
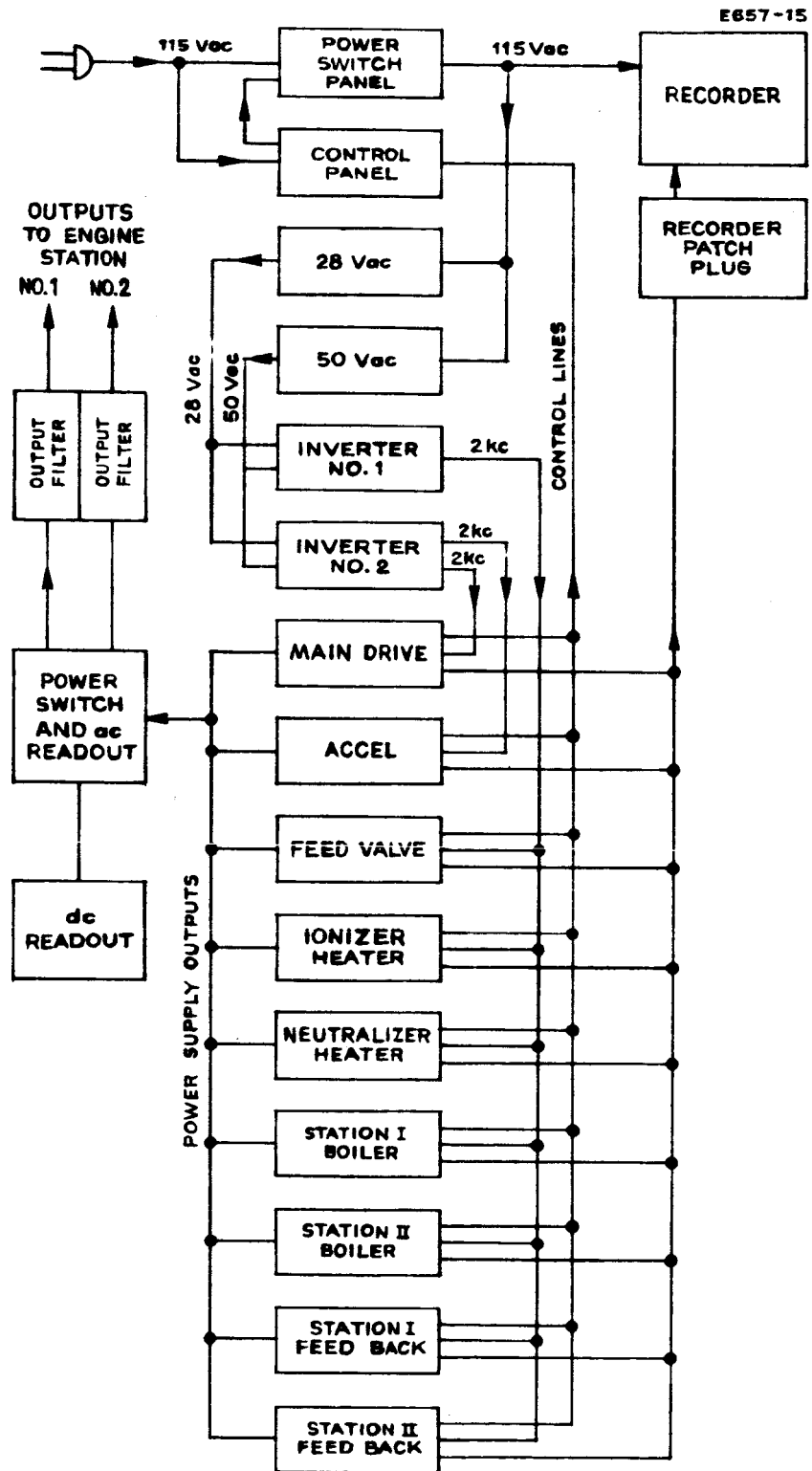
Fig. 17. Block diagram of automatic cyclic test console.

The control unit contains the cycle timers for automatic control of the console. A standard two-thrustor automatic cycle is described below. For the purpose of this discussion, it is assumed that the cycle begins with all time shared power supplies connected to Station I.

Time (in seconds)

0		The Ionizer Heater power supply is turned on. The Station I Ionizer Heater Warm Up potentiometer controls the power to the Ionizer.
18	a.	The Ionizer Heater power supply is switched from warm up to regulate. The Station I Regulate potentiometer controls the power to the ionizer heater.
	b.	The Main Drive supply is turned on. The voltage level is controlled by the Station I Main Drive potentiometer.
	c.	The Accel supply is turned on. The voltage level is controlled by the Station I Accel potentiometer.
	d.	The Neutralizer Heater supply is turned on. The voltage level is controlled by the Station I Neutralizer Heater potentiometer.
20		The Feed Valve power supply is turned on. The voltage level is controlled by the Station I Feed Valve potentiometer.
22		Station I beam current level is sensed by the Station I boiler control circuitry. The Station I boiler power control voltage is changed if the beam is not at the preselected level.
30		All shared supplies are turned off (the Boiler Heater and Feed Tube Heater supplies for both engines remain on during thrustor cyclic operation). Station I controls are disconnected from their respective power supplies and

		Station II controls are connected. The outputs of the shared power supplies are switched from Station I to Station II. The console is now ready for the Station II cycle.
105		The Ionizer Heater power supply is turned on. The Station II Warm Up potentiometer controls the power to the ionizer.
123	a.	The Ionizer Heater power supply is switched from warm up to regulate. The Station III Regulate potentiometer controls the power to the ionizer heater.
	b.	The Main Drive supply is turned on. The voltage level is controlled by the Station II Main Drive potentiometer.
	c.	The Accel supply is turned on. The voltage level is controlled by the Station II Accel potentiometer.
	d.	The Neutralizer Heater power supply is turned on. The voltage level is controlled by the Station II Neutralizer Heater potentiometer.
125		The Feed Valve power supply is turned on. The voltage level is controlled by the Station II Feed Valve potentiometer.
127		Station II beam current level is sensed by the Station II boiler control circuitry. The Station II boiler power control voltage is changed if the beam is not at the preselected level.
135		All shared supplies are turned off. The console control circuits and output connections are switched back to the Station I condition.

The console contains all instrumentation necessary to read out all voltages supplied by the power conditioning to the thrustor. Six thermocouple meters and a recorder which can continuously monitor up to eight channels of information are also included. There are two cycle counters, two feed valve cycle counters, and two elapsed time meters which indicate beam-on time for each thrustor. A photograph of the completed console is shown in Fig. 18.

33

M4573
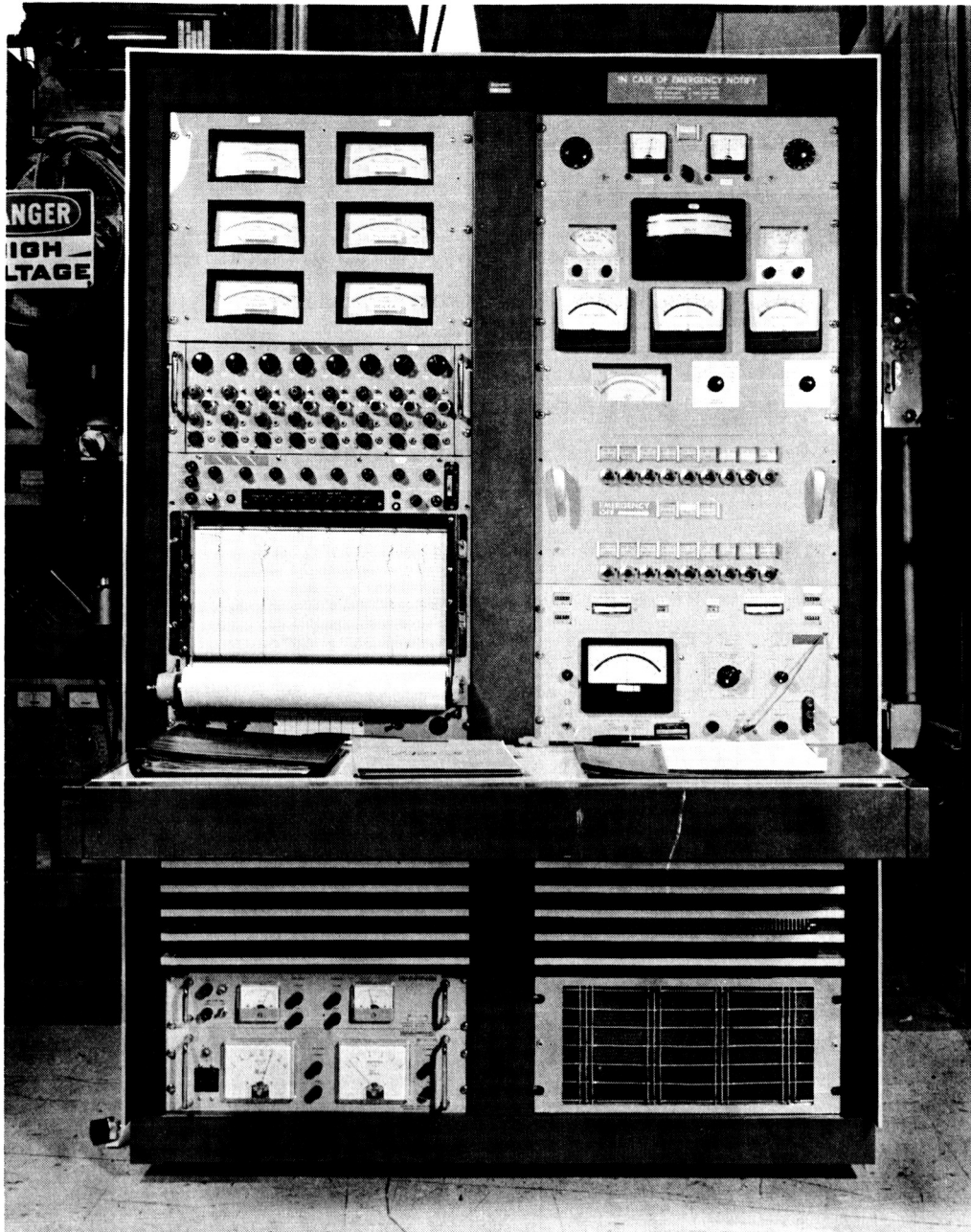
Fig. 18. Photograph of automatic cyclic test console.

The cyclic life test console operates unattended virtually 100% of the time. All heater supplies are fused at 100% overload to protect them in the event of a short. Overload trips on the high voltage supplies are set at approximately 15 to 20% overload, so that an arc or a short will trip off the inverter. One second later, voltage will be reapplied and if the condition persists, a series of trips will result. The series is short because during any given cycle only 12 sec elapse from regulate, when the high voltage is applied initially, to when the station is switched off, independent of arcing. Because the duty cycle of the supplies is so low and the power dissipation during arcing so small, no damage will be done to the console should such a malfunction occur.

Since 2 sec must elapse from high voltage application until the feed valve opens, no cesium can flow during prolonged arcing. This tends to clean up any cesium induced malfunction. Since the sample circuit is not activated until 4 sec after the feed valve opens, and if it is not activated the power to the reservoir is gradually reduced, reservoir temperature will gradually decline, further inhibiting cesium flow. This has the effect of shutting down the thrustor and also reduces the effects of excess cesium, as might be produced if the feed valve stuck open.

If the feed valve remains shut, the console simply continues cycling and the reservoir temperature will rise to the allowable maximum because no beam current would be registered during the sample portion of the cycle. The upper limit is usually set a few degrees above the normal operating point. Should the valve reactivate during a later cycle, the beam current would be high and the sample circuit would reduce reservoir power, or arcing will occur which also effects a reservoir power reduction as described above. The console is also interlocked to the vacuum gauge and will completely shut down if there is an indication that pressure is above the gauge setting.

IV.   LIQUID CESIUM FEED SYSTEM

A.   INTRODUCTION

This contract task is directed toward development of a valve-less liquid-transfer cesium feed system optimized for both laboratory and zero-gravity space applications.   This effort differs from that discussed in Section II.B, where the feed system was designed for the specific task of laboratory thrustor testing.

The feed system discussed in this section is being developed to provide a controllable cesium vapor flow to an ion thrustor operating in either a steady state or pulsed mode.   This feed system is designed to meet the following basic system requirements:

1. operable in a zero-gravity space environment
2. operable in any attitude in a laboratory environment
3. minimum standby power
4. storage capacity: 2 lb cesium
5. minimum weight.

Before actual design work was begun, a literature study was undertaken to establish the present state of the art in cesium feed systems and to avoid duplication of previous effort.   Appendix B lists the literature reviewed.   Following the literature review, the preliminary feed system analysis continued with particular emphasis on defining the requisite component functions and anticipated problem areas.   The basic component functions are as follows:

1. liquid storage reservoir
2. liquid transfer mechanism
3. hermetic seal (for handling and storage protection)
4. vaporizer
5. vapor flow control
6. rapid on/off vapor flow control

Primary consideration was given to cesium feed systems which provide passive cesium control. Typical of this class of feed system is the unit developed by Hughes Research Laboratories (HRL) under Contract NAS 3-2510 and that developed by Electro-Optical Systems (EOS) under Contract NAS 3-2516. Also considered were feed systems utilizing spring force or other means to maintain liquid pressure, with a thermally controlled impedance for vapor-flow-rate control.

In the simplest feed system design considered, only three of the above functions are separately identifiable, while the others are provided by the inherent characteristics of the components used. This system consists of a liquid-cesium storage reservoir, a hermetic seal, and a porous-metal vaporizer. Liquid cesium would be transferred from the storage tank to the vaporizer and both proportional and on/off control of cesium vapor flow would be achieved by thermal control of the vaporizer. The key element in the design is the vaporizer, since its characteristics determine both liquid storage and transfer component requirements and vapor-flow control component requirements.

Analytical investigation of the feed system continued with a thorough study of the three reservoir types: bellows tank, porous metal lined tank, and solid porous metal tank. All three concepts utilized a similar porous-metal vaporizer where the cesium is changed from the liquid to the vapor state.

The bellows tank using the bellows spring force as an expulsion mechanism, creates excessive pressure in its filled position. Liquid cesium would be forced through the vaporizer when heat was removed; therefore, it is essential to include a solenoid valve in such a system.

The porous metal lined system was studied with liquid cesium in the center of the reservoir and a porous metal lining with graded capillary pore sizes serving as a surface-tension pump to force the liquid cesium into the even smaller pore size vaporizer region. This system also presents a pressure head behind the vaporizer which can force liquid cesium through the vaporizer when heat is removed.

The third, and most promising, system is a hybrid. The reservoir is filled with a graded large-pore porous metal, with a small-pore porous metal wick through the center of the storage medium. This provides capillary suspension and a surface-tension pump action in the reservoir, in addition to flow through the wick into the vaporizer for an acceleration range greater than -1 gravity (g) to +1 g. By properly heat sinking the vaporizer in conjunction with thermal shielding the reservoir and vaporizer, the flow and rapid on-off control requirements can be met by controlling the heat input to the vaporizer.

Previous HRL feed systems have been variable-position interface systems, in which the liquid vapor interface migrates toward the fuel supply and away from the heater element as the fuel is consumed. This type of system results in a high standby power requirement, since the entire feed system must be maintained at vaporizer temperature unless startup times on the order of several hours can be tolerated. Movement of the interface is caused by a force imbalance acting upon the effective cross section of the liquid cesium at the interface. In this type of design, the vapor pressure forces dominate the capillary forces and result in a net force directed toward the fuel supply.

The new HRL feed system design should result in the capillary forces dominating the vapor pressure forces, causing the fuel to migrate toward the end of the vaporizer wick and maintain a constant heat load on the heater element. Therefore, the liquid vapor interface should be stationary throughout the fuel cycle. The feed system design requires that the capillary forces always be larger than the vapor pressure forces for all conditions of operation. A detailed discussion of the vaporizer wick design and its limitations is presented in Section IV-B-2.

B.   DESIGN CONSIDERATIONS

The most promising feed system concept defined during the review of both new designs and prior art was reduced to the specific configuration shown in Fig. 19 and subjected to detailed analysis.

In order to meet the basic system requirements, the following constraints were imposed upon the system design:

1. Operation in a zero-g space environment.
2. Operation in a ±1 g laboratory environment.
3. Fast response of vapor flow, i.e., maximum vapor flow within 20 sec of command and complete shutdown of vapor flow within 20 sec of command.
4. Cesium vapor flow for 0.3 mlb of thrust.
5. Valveless vapor transfer system.
6. Minimum electrical heater power requirement for "full" and "depleted" cesium supply.
7. Stable liquid-vapor interface at prescribed operating location.
8. Utilization of a single heating element to generate cesium vapor pressure and utilization of waste heat to maintain cesium in the storage supply in a liquid state.

1.   Description of Feed System Elements

The primary elements in the "zero-g" feed system are the stainless steel fuel container, the graded low-density nickel Feltmetal[*] storage matrix within the container, the high-density nickel Feltmetal wick, an electron bombardment vaporizer heating element, the one-shot burst-disc diaphragm, the radiative heat shielding, and the heat rejection surface.

---

[*]Trademark of the Huyck Corp. Feltmetal is an aggregate of fine nickel wires which is pressed and sintered to produce a random matrix of controlled pore size.
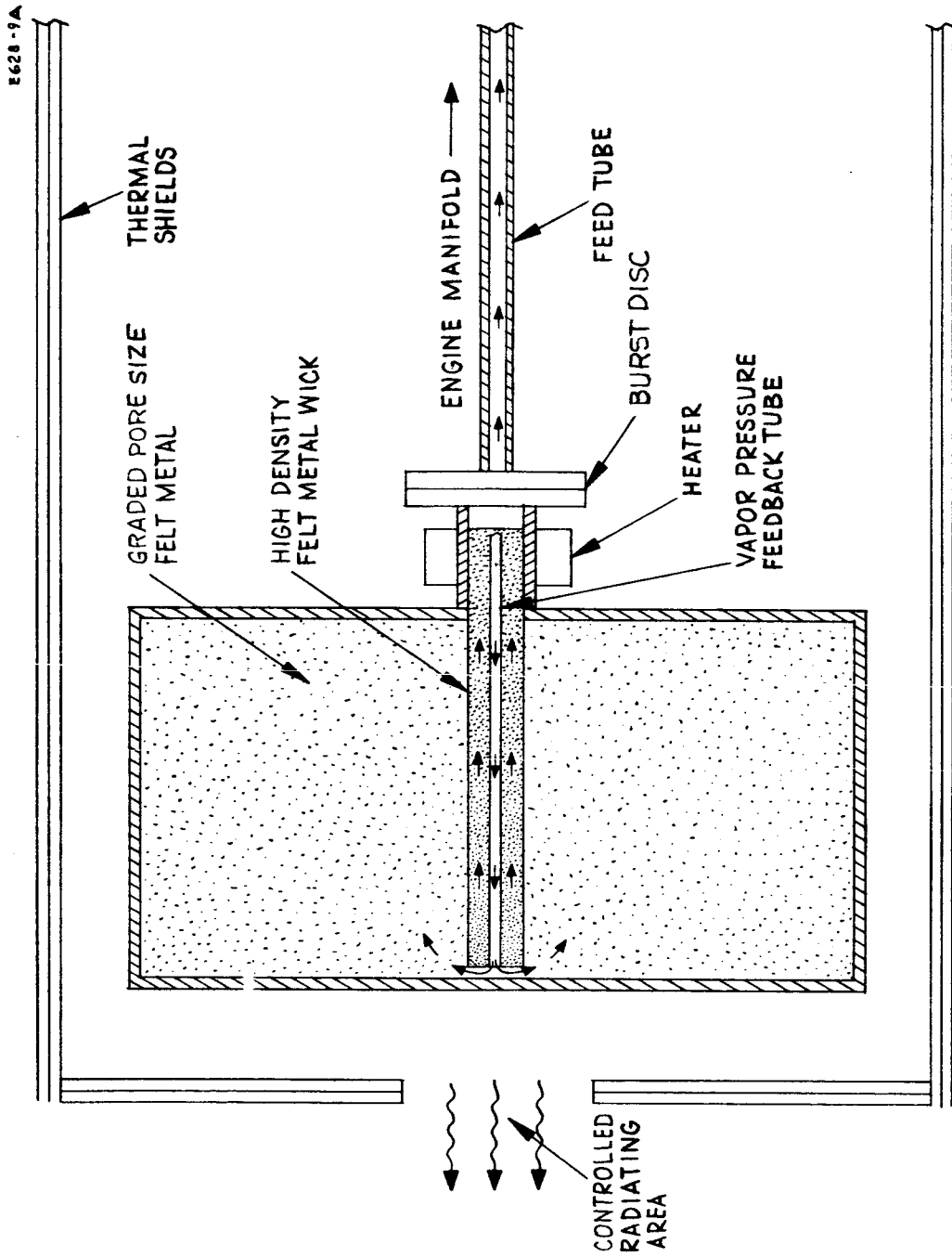
Fig. 19. Schematic of feedback pressure compensated, zero-gravity liquid cesium feed system.

THERMAL SHIELDS

ENGINE MANIFOLD →

FEED TUBE

BURST DISC

HEATER

VAPOR PRESSURE FEEDBACK TUBE

GRADED PORE SIZE FELT METAL

HIGH DENSITY FELT METAL WICK

CONTROLLED RADIATING AREA

E628-9A

The fuel container and the large-pore-size nickel Feltmetal filler provide a high capacity storage volume for the cesium fuel while providing sufficient surface tension to retain the liquid cesium within the container, regardless of attitude. The small-pore Feltmetal wick provides the capillary pumping action which draws from the fuel supply contained within the large-pore Feltmetal storage. Through capillary pumping action, the small-pore Feltmetal wick should maintain a completely wetted condition throughout the fuel cycle.

The thermal profile of the system was designed using analog computer programming of the system physical equations to provide an optimum thermal gradient. This design method yielded an optimum system thermodynamic response. The electron bombardment heater will provide instantaneous power availibility and removal to the vaporizer section for on-off control of cesium vapor flow. Heat contributions to the vaporizer section include vaporizer heater power and the heat conducted down the feed tube from the ionizer manifold. The excess heat from the vaporizer and thrustor manifold are conducted into the storage chamber to maintain the cesium in a liquid state.

The pressure feedback passage can provide relief from the vapor pressure forces acting on the liquid metal cross section within the vaporizer and assists in removal of contaminants from the surfaces of the porous-metal matrix. The one-shot burst disc opens the feed tube passage (normally sealed) just prior to system startup. Radiative heat shielding provides design operation management of the feed system total electrical power requirement. The heat rejection area is designed to provide an optimum temperature gradient along the feed system during operation.

2.   Description of Operation

A block diagram of the cesium feed system is shown in Fig. 20. The system provides liquid-metal storage, liquid-vapor separation, and fine flow control of vapor. The liquid metal is normally contained in the large pore Feltmetal section and is drawn upon by capillary pumping action as a function of the engine demand through the fine pore Feltmetal wick.

42

E657-17
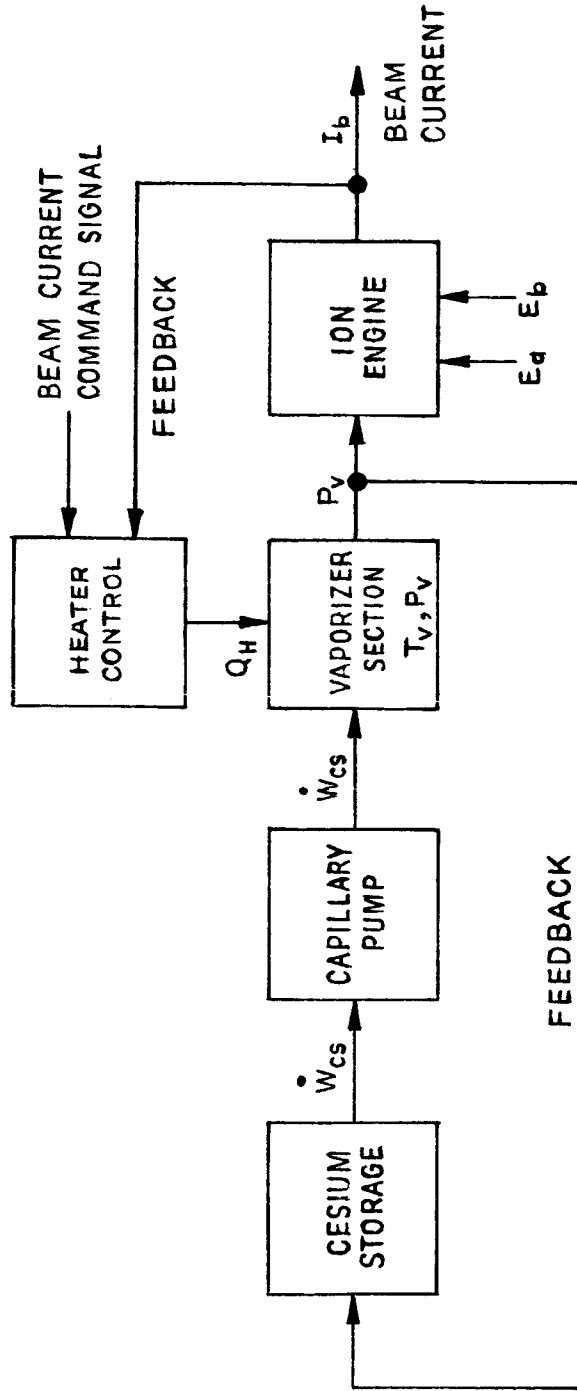
Fig. 20. Block diagram of liquid cesium feed system.

43

Cesium vapor flow control is attained by temperature control of the vaporizer section as a function of engine beam current demand. The provision of a low mass vaporizer section allows fast heatup and cooldown and therefore relatively fast startup, control, and shutdown operations. The vaporizer section also acts as a shutoff valve. When the electron bombardment heater is deactivated, the vaporizer section of the wick rapidly cools to condense the cesium vapor and shut off the vapor flow. Complete shutdown of the vapor flow is accomplished when the control temperature drops below the liquid metal vaporization temperature (approximately 450° Kelvin) and the cesium is condensed into the liquid state. Capillary action in the Feltmetal wick prevents the liquid metal from leaving the vaporizer wick.

This feed system concept allows a single storage reservoir for a number of vaporizers by the simple addition of more wicks. Separate adjustment of the vaporizer temperatures permits individual mass flow control of metal vapor to a number of thrustors, as well as individual engine shutdown. Feltmetal storage also provides protection against micrometeorite penetration and ultimate total loss of the fuel supply, as could result in a metal bellows arrangement.

3.   Vaporizer Design and Analysis

In a capillary pumping system, such as that designed for the zero-g feed system, the capillary forces of the liquid cesium must dominate the vapor pressure forces. Otherwise, the liquid vapor interface will tend to migrate toward the fuel supply and/or away from the heater section of the wick. This interface instability will cause an increasing heater power requirement as the interface moves away from the heater section, and will ultimately result in premature vapor shutdown. Therefore, for a minimum-power vaporizer with fast response, the liquid vapor interface must be precisely located and must not deviate from this location throughout the fuel cycle or lifetime.

A design analysis was made to determine the capillary force characteristics of cesium as the wetting agent in various types of porous nickel. The Feltmetal selected for use in the feed system will be provided by the Huyck Corporation. Figure 21 shows a graph of average pore size versus Feltmetal density. Also shown is the relative distribution of 80% of the pore size population, and the maximum and minimum pore size for various densities of Type A30 Nickel Feltmetal supplied by Huyck. Six data points are provided by the supplier. These are for 15%, 20%, 30%, 40%, and 60% dense Type A30 Feltmetal. All other graphical information was determined by either interpolation or extrapolation of the given vendor data.

Consider now the use of the graphical information supplied in Fig. 21. For 60% dense Feltmetal, the pore size ranges from 0 to 25 μ, with 80% of the pore size population within the range of 4 to 13 μ. The average pore size for the 60% dense Feltmetal is 7 μ. Preliminary analysis indicates that the finest Feltmetal material should be used for the wick in order to provide maximum capillary force and that coarse material should be used for the storage element in order to provide a maximum storage volume and still meet the environmental requirement.

Consider now the design of a vaporizer wick which will produce a capillary force greater than the vapor pressure force. Capillary pressure is derived by Carman[*] as equal to the surface tension of the liquid multiplied by the cosine of the contact angle of the liquid divided by the hydraulic radius normal to flow, i.e.,

$$P_c = \frac{\gamma \cos \theta}{m} \tag{1}$$

---

[*] P. C. Carman, Flow of Gases through Porous Media (Academic Press, New York, 1956).
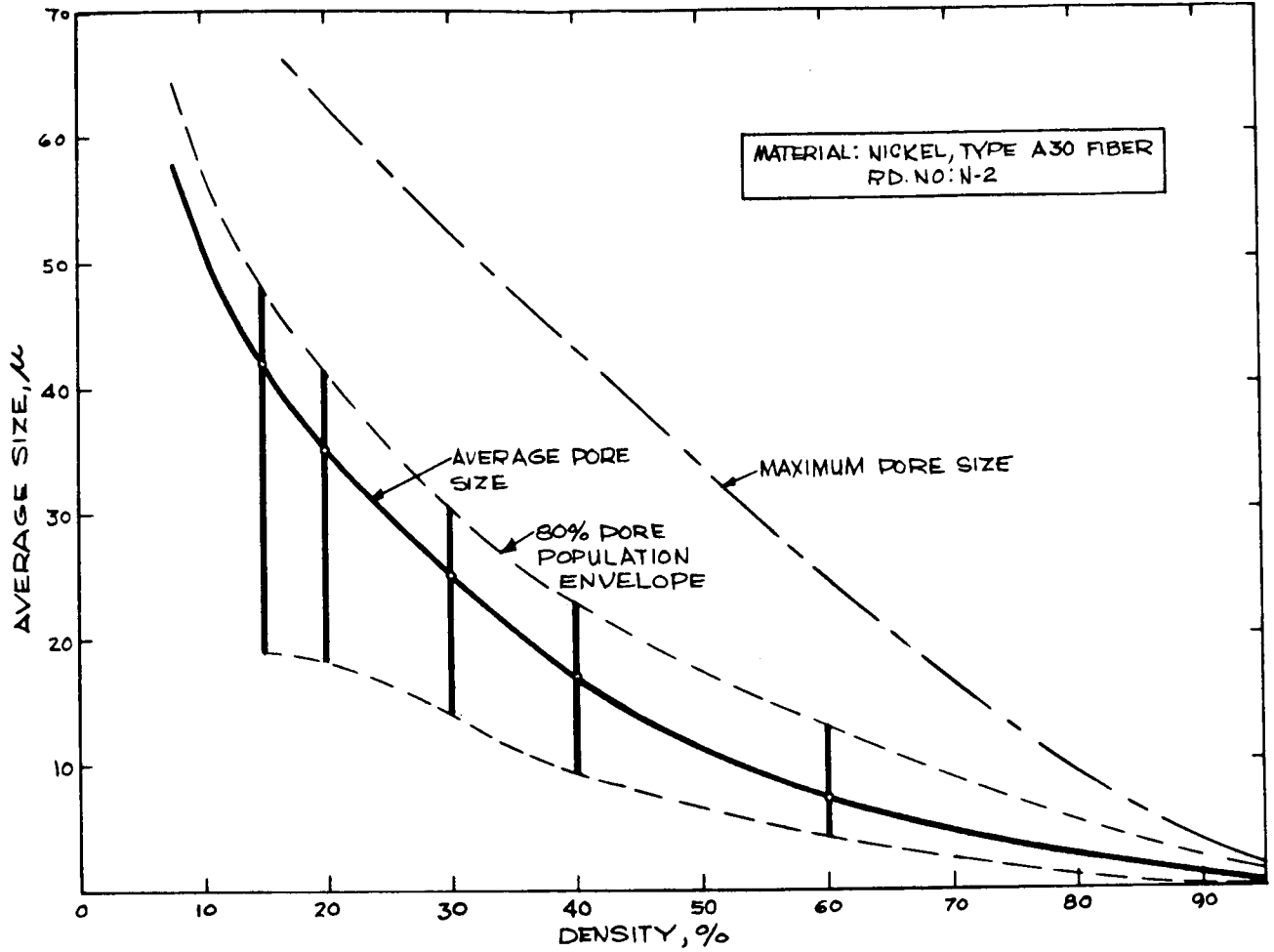
Fig. 21. Pore size as a function of density for nickel Feltmetal.

where

γ $\equiv$ surface tension of the wetting agent

θ $\equiv$ contact angle of the wetting agent

m $\equiv$ hydraulic radius normal to flow.

Hydraulic radius is defined as

$$m \equiv \frac{\text{cross sectional area normal to flow}}{\text{wetted perimeter}} \tag{2}$$

or

$$m \equiv \frac{\text{volume filled with liquid}}{\text{wetted surface}} . \tag{3}$$

Because the nickel Feltmetal is basically a random matrix of sintered wires, an accurate calculation for hydraulic radius becomes exceedingly complex. Therefore, an approach to the problem is to calculate a simple solution based on a worst-condition analysis. In analyzing the definition of hydraulic radius and its relationship to the capillary pressure, it is noted that in order to maximize capillary pressure, the hydraulic radius should be minimized. If one concludes that the sintered wires comprising the Feltmetal can be considered as cylindrical geometry then for a given average pore size it is concluded that small spheres provide a minimum wetted surface area per unit of filled volume compared with cylinders. Since a sphere has minimum surface area per unit volume, a cylinder must exhibit more surface area regardless of twisted configuration. Thus a worst-case design can be established by considering that the Feltmetal is composed of tiny spheres.

Carman further defines hydraulic radius by considering the porous media as uniform spheres. Substituting,

$$m = \epsilon / S$$

$$S = S_o (1 - \epsilon)$$

$$S_o = 6/d \quad \text{(for uniform spheres only)}$$

47

Equation (1) can be rewritten as:

$$P_c = \frac{6\gamma(1 - \epsilon)\cos\theta}{\epsilon d} \tag{4}$$

where

$\epsilon \equiv$ porosity

$S \equiv$ particle surface for unit volume of bed

$d \equiv$ diameter of sphere, cm.

The following conditions have been assumed for problem solution.

$d = 2.5 \times 10^{-3}$ cm (diameter of Type A30 Feltmetal wire)

$\epsilon = 0.2$ and 0.8 (coarse and fine Feltmetal)

$\theta = 30$ deg.

The surface tension of cesium at the interface is a function of temperature at the interface. Figure 22 shows cesium surface tension versus temperature. The following equations present expressions for the capillary pressure in Torr under the assumption that the Feltmetal is comprised of either uniform sized spheres or a uniform sized bundle of straight capillary tubes. The uniform sized sphere assumption is preferred because it yields the worst-case design. However, the straight capillary tube assumption is also presented for completeness:

$$P_c = \frac{6\gamma(1 - \epsilon)\cos\theta}{\epsilon d_1 (1.333)} , \text{ Torr (uniform sized spheres)} \tag{5}$$

$$P_c = \frac{4\gamma\cos\theta}{d_2 (1.333)} , \text{ Torr (uniform sized capillary tubes)} \tag{6}$$

where

$$\gamma = \gamma_o - \left(\frac{d\gamma}{dT}\right) T_v , \text{ dyn/cm} \tag{7}$$

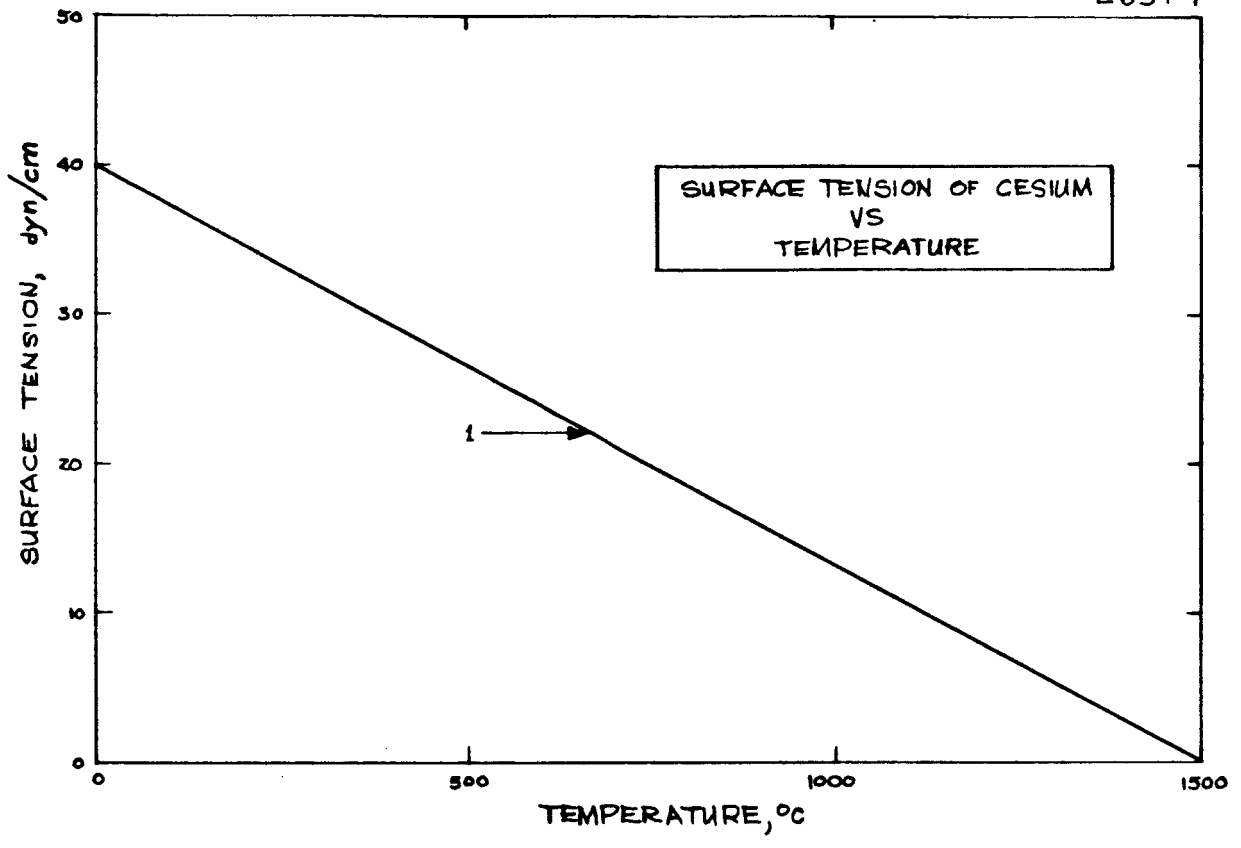$d_1 \equiv$ sphere diameter

$d_2 \equiv$ capillary tube diameter.

48

Fig. 22. Surface tension of cesium versus temperature.

Figure 23 presents graphs of equations (5) and (6) for constant values of porosity ϵ or average tube diameter d_2 versus vaporizer temperature. Also plotted on this graph is the cesium vapor pressure curve.

For any given cross section, the vapor pressure must not exceed the capillary pressure for stability. The unstable region shown in Fig. 23 is defined as the region where, for a given temperature and pore size the vapor pressure exceeds the capillary pressure. As noted on the graph, for the fine-pore Feltmetal ($\epsilon = 0.2$), the capillary pressure is in excess of 180 Torr at a vapor pressure of 10 Torr.

The graph also shows comparisons of uniform sphere size versus capillary tube size. For instance, the curve for uniform sphere grains at a porosity of 0.3 is identical to a bundle of capillary tubes with a diameter of 7.0 μ.

4. Burst Disc

A requirement of this feed system is that the cesium in the reservoir must be protected from atmosphere during storage and assembly. Previous feed systems have used a diaphragm and an electromechanical piercing mechanism for this purpose. A smaller, lighter, and simpler device was considered desirable for this system.

A study of available burst discs as a replacement for the Hughes designed piercing mechanism demonstrated the necessity of designing this component specifically for the low burst differential pressure of 14 pounds per square inch (psi) and the package requirements of the feed system. Preliminary negotiations were undertaken with two prospective vendors to manufacture such a device. Evaluation of the vendor capability in this area indicates that the concept is technically feasible.

A vendor sample of a low-pressure burst disc was received and tested. The results were satisfactory with burst pressure consistently in the range of 13.2 ±0.5 psia during 20 tests. Figure 24 shows this burst disc assembly after rupture of the diaphragm. Note that the disc ruptures by tearing with no resultant loose pieces.
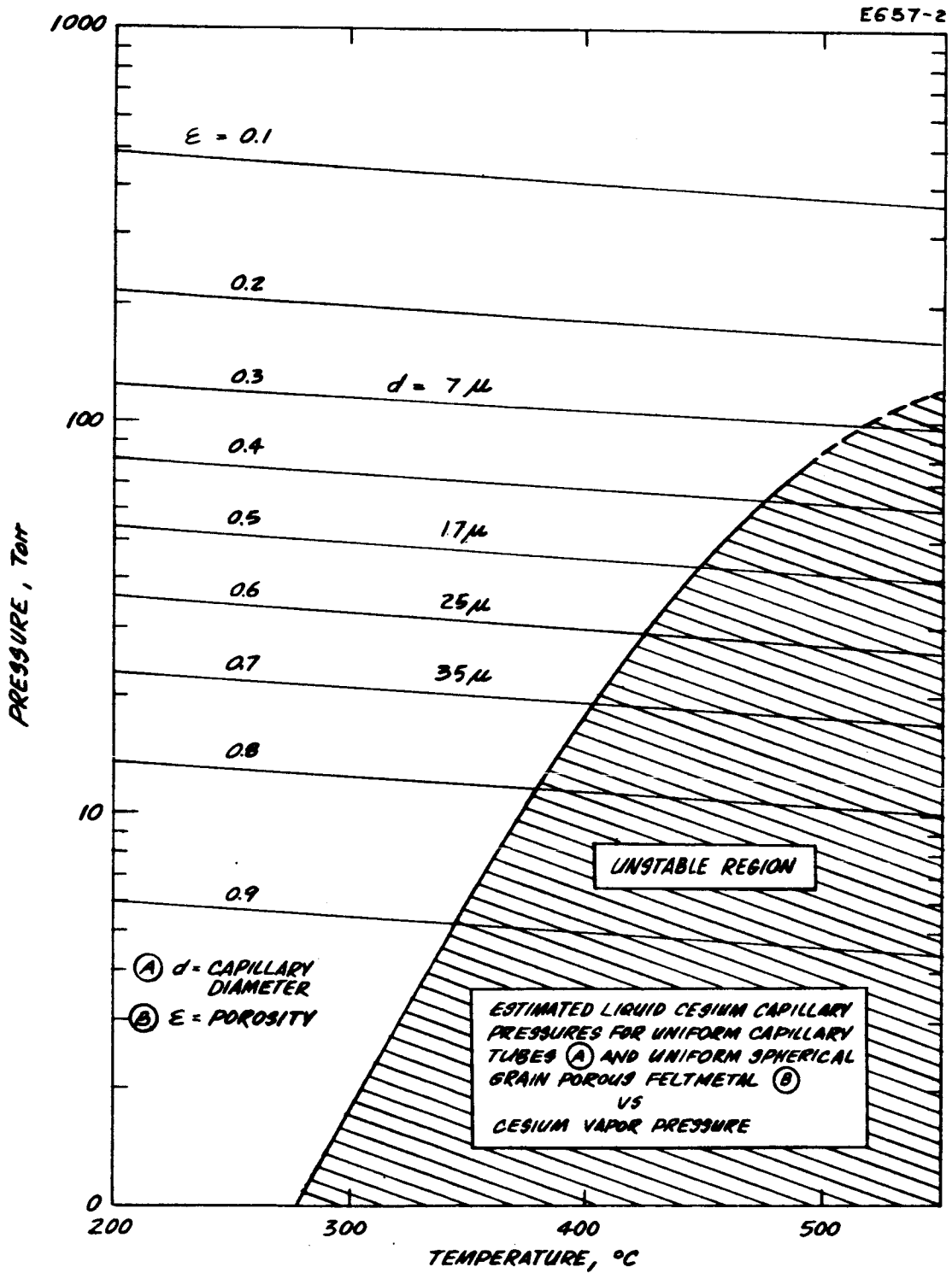
Fig. 23.   Approximate liquid cesium capillary pressures for uniform
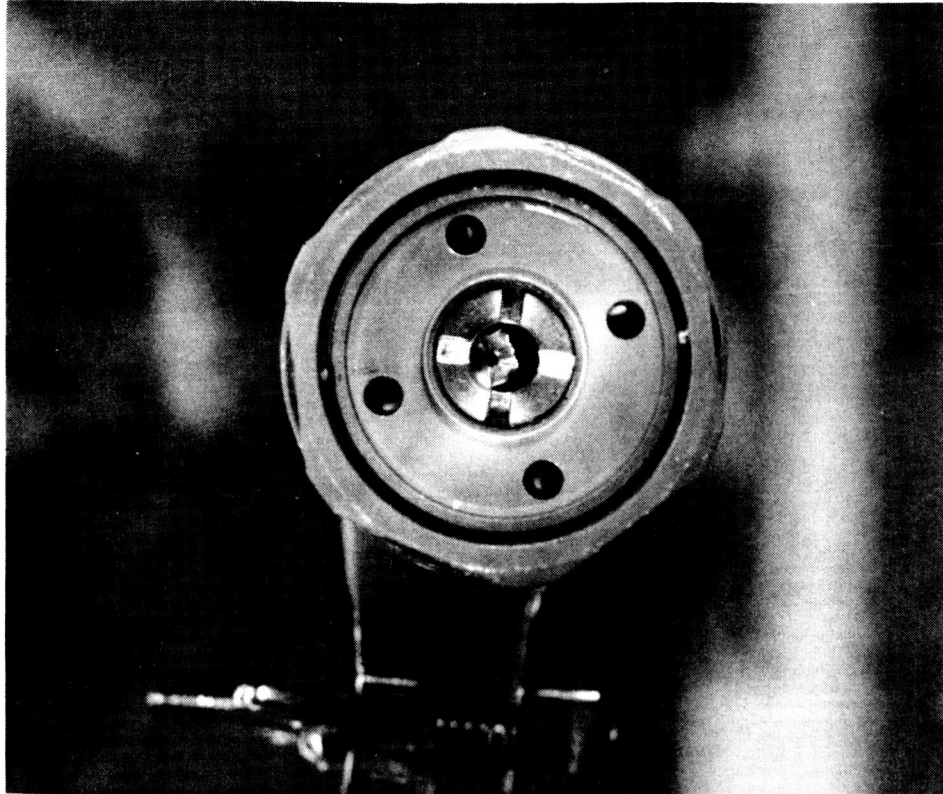tubes and for uniform spherical-grain porous nickel.

M4474

Fig. 24. Burst disc assembly after rupture of diaphragm.

When the cesium reservoir is to be filled, the last step will be to backfill with argon to a pressure of 1 atm. The feed system then will be sealed with the burst disc which will rupture when the ion engine system is exposed to tank or space vacuum.

C.   THERMODYNAMIC ANALYSIS

The first phase of the dynamic studies involving the liquid feed system necessarily required analog computer simulation of heat transfer and thermodynamic properties of the feed system design. As a result of the analog study, design criteria were established for the device which should provide fast thermal response for all conditions of operation. Figure 25 shows the present configuration of the feed system thermodynamic model based on the design presented in Fig. 19. Appendix C presents the complete analysis of the original feed system design which includes the feed system, schematic diagram, thermodynamic model, physical equations and coefficients describing the thermodynamic model, nomenclature, component sizings, and the analog computer mechanization of the mathematical model. The only difference between the design and the original model is that the contoured heat sink has been eliminated. This decision was based on the analytic results.

Consider now the results of the computer simulation. Figure 26 illustrates the cesium vaporizer temperature response for thrustor manifold demands of 1, 10, and 20 Torr vapor pressure for engine "pulse on" and "pulse off" times of 150 sec. This simulates a hypothetical pulse mode condition of operation. Initial system temperature was assumed to be 300°K for all cases. For cyclic operation, the vaporizer section average temperature rises at a rate of approximately 40°K/hour but appears to be approaching an equilibrium condition. In this case, an ionizer heat contribution of 1 W was assumed to be conducted down the feed tube. Figure 27 shows the feed system response for the system with a "full charge" and a "depleted charge" of liquid cesium. The computer results indicate an average "startup" and "shutdown" time of approximately 15 sec utilizing an electron bombardment heater to supply power to the vaporizer section. A large increase in
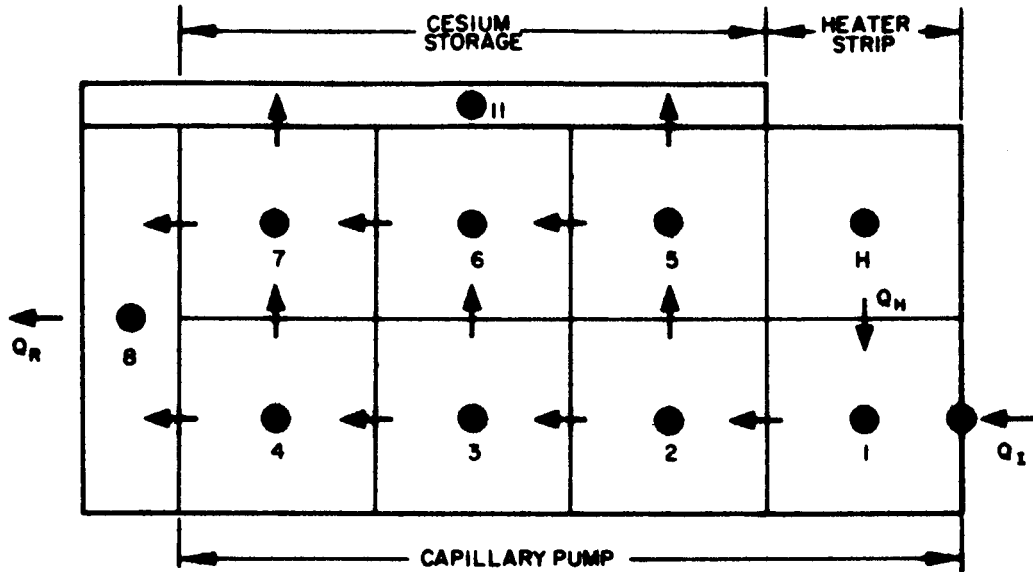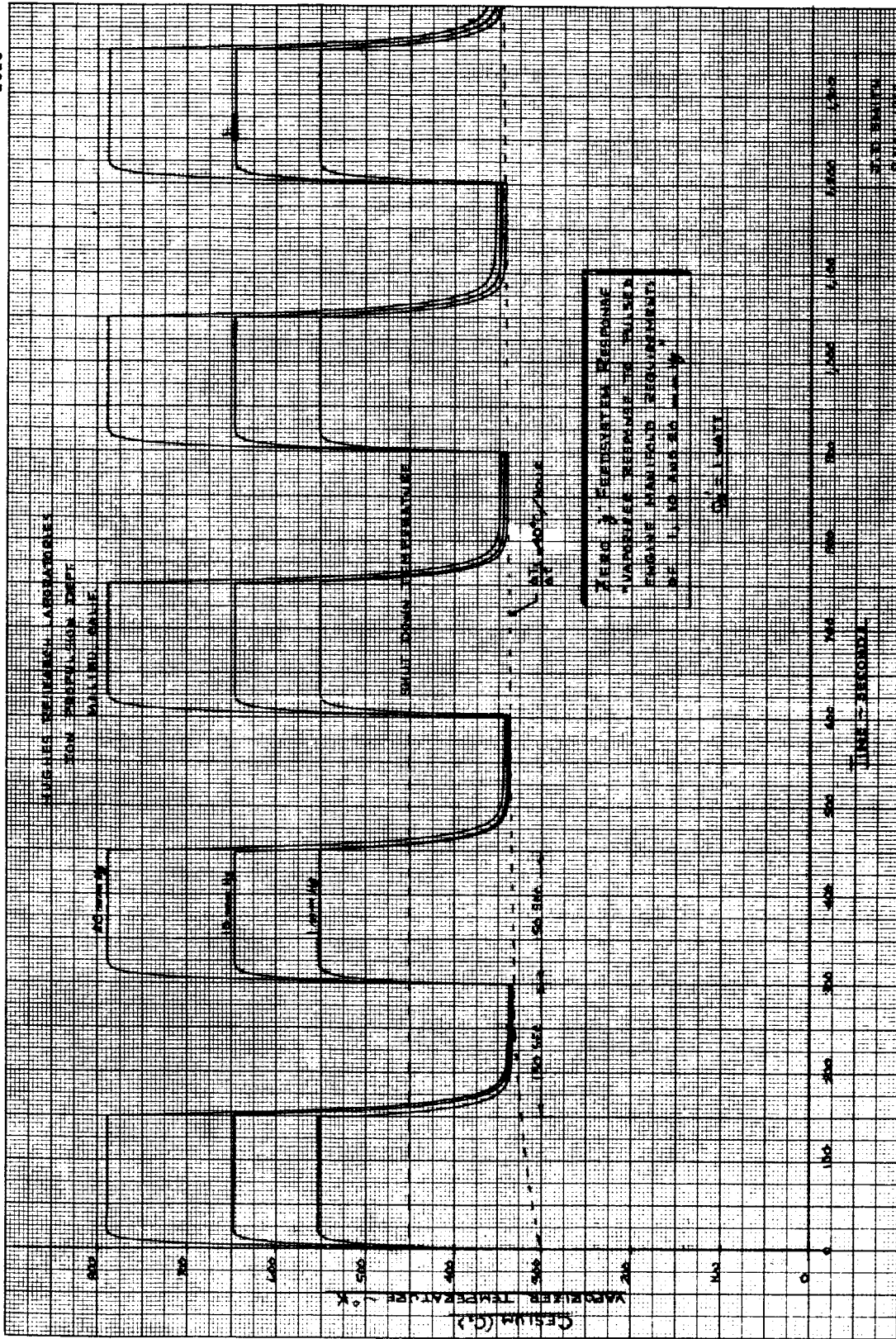
Fig. 25. Liquid cesium feed system thermodynamic model.

Fig. 26. Cesium vapor temperature and pressure dynamic characteristics for several thrustor manifold pressure requirements.
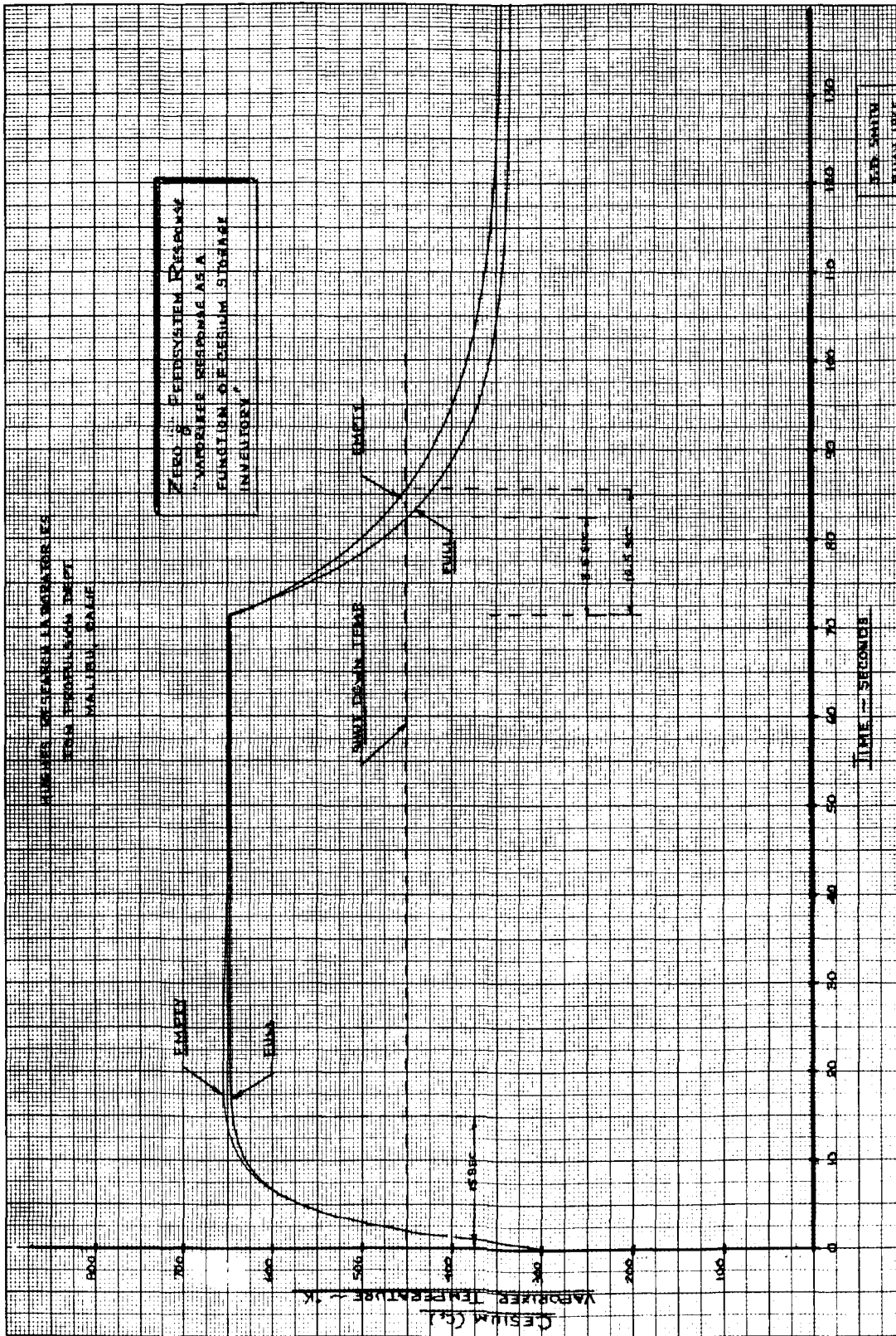
Fig. 27. Liquid cesium feed system vaporizer thermal response.

system response time occurs if a conventional coaxial heater is used instead of the electron bombardment heater. Since the analytical model assumed instantaneous application and removal of vaporizer heat, the results of the dynamic studies must be interpreted as optimistic; longer system response times should be expected for less ideal heating elements. For the case shown in Fig. 27, vapor pressure was closed-loop controlled to 10 Torr (650°K). Turnoff temperature for the valveless system was assumed to approximately 450°K, or 0.03 Torr. As noted in Fig. 27, the cesium vapor pressure can be reduced to 1% of the steady state value (10 Torr) in about 8 sec for the "full" case and in about 10 sec for the "empty" or depleted-supply case. This rapid response shows that pulse-mode operation is feasible for an ion thrustor coupled to this type of "valveless" feed system. For each condition of the fuel supply, a steady state heat contribution of 1 W from the ionizer manifold was assumed.

Figures 28 and 29 are presented to illustrate the relative dynamic behavior of the following system parameters:

Channel	Parameter
1	Vaporizer heater power, W
2	Ionizer heat contribution, W
3	Vaporizer temperature, Node (1), $^{\circ}$K
4	Temperature Node (2), $^{\circ}$K
5	Temperature Node (3), $^{\circ}$K

In both Figs. 28 and 29, the power input demand for "turn on" is a function of the command level of thrust. For the "turn off" condition, vaporizer power is terminated abruptly. The response of the feed system is thus closed-loop controlled around the thrust level command. For instance, Figs. 28 and 29 show the vaporizer temperature response to a demand engine manifold pressure of approximately 3.2 Torr ($T_3 = 600^{\circ}$K). Average "turn on" and "turn off" times are about 15 sec. These data represent the "closed loop" control system.
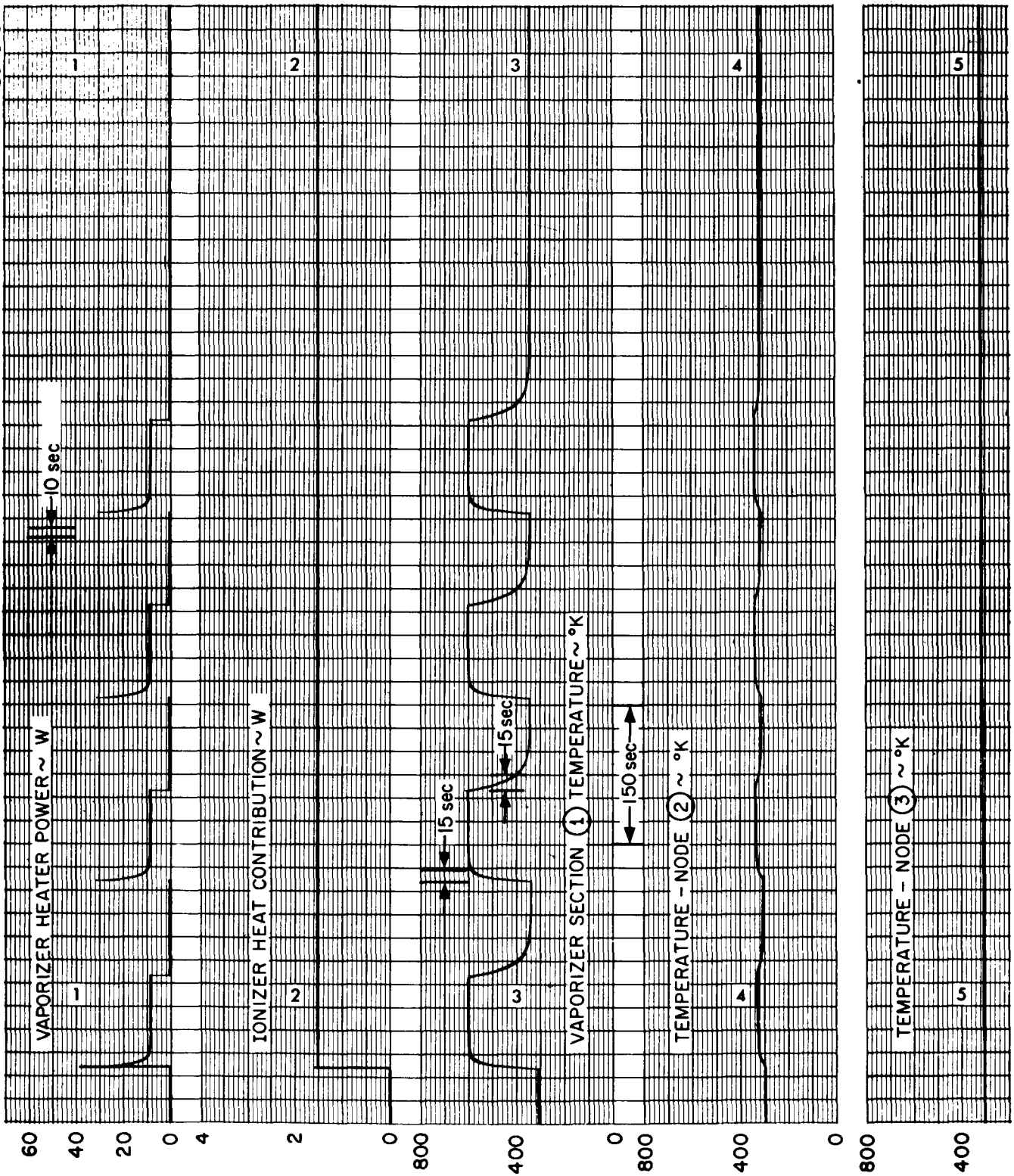
Fig. 28. Liquid cesium feed system thermal response with ionizer heat contribution of 1.5 W.

58

E643-4

VAPORIZER HEATER POWER~W

IONIZER HEAT CONTRIBUTION~W

VAPORIZER SECTION ① TEMPERATURE ~ °K

TEMPERATURE – NODE ② ~°K

TEMPERATURE – NODE ③ ~°K

10 sec
150 sec →
15 sec
15 sec

60 40 20 0 4 2 0 800 400 0 800 400 0 800 400
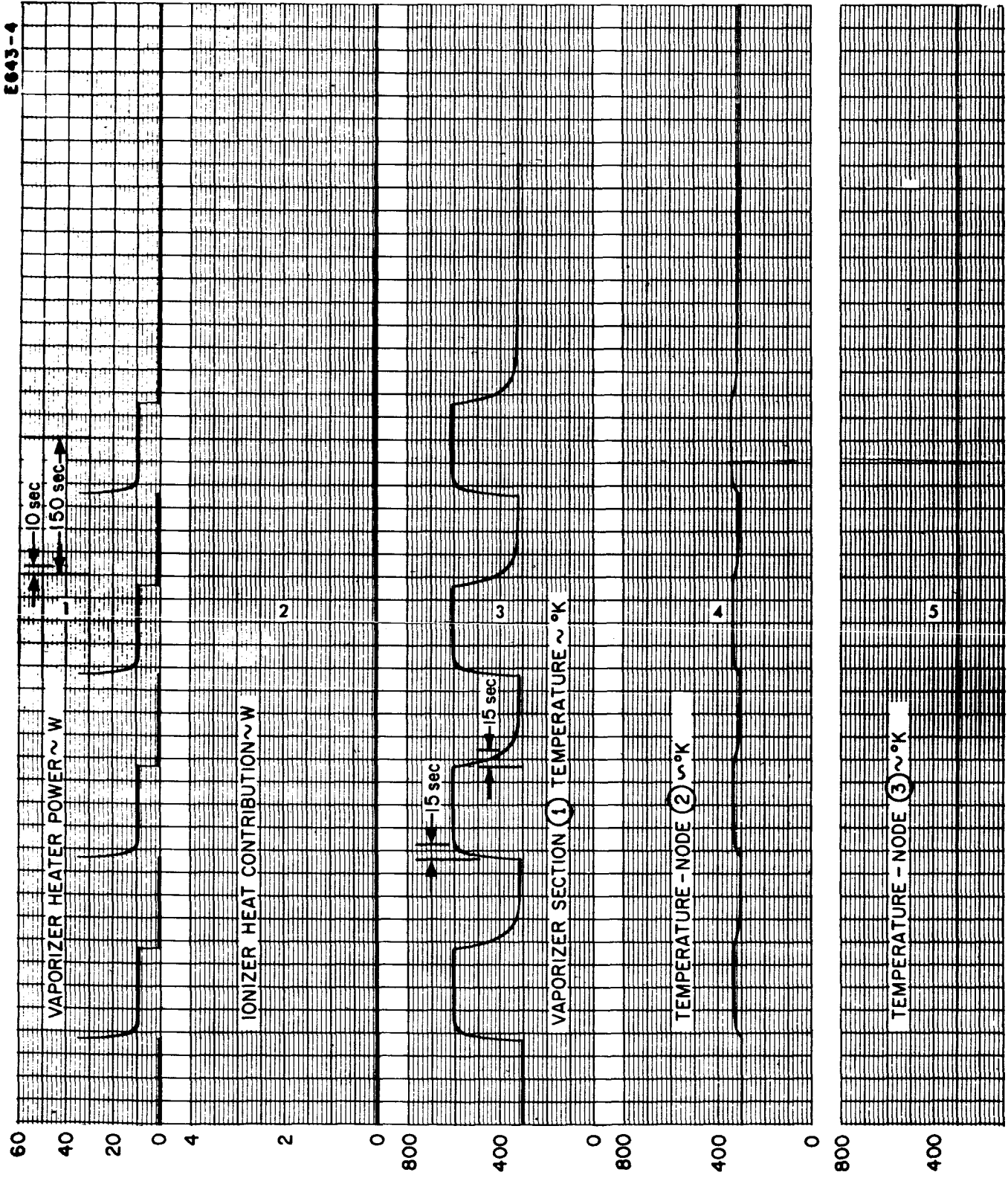
Fig. 29. Liquid cesium feed system thermal response for zero ionizer heat contribution.

59

Figure 28 presents the case where heat from the ionizer manifold provides a 1.5 W contribution. Figure 29 illustrates the case in which the heat contribution from the ionizer (Channel 2) to the vaporizer is near zero. These results show that low ionizer manifold heat has a negligible effect on feed system transient response.

Figure 30 presents the transient response of the vaporizer as a function of various ionizer heat contributions and power demand. Note that with a heat contribution from the ionizer of approximately 5.25 W, the vapor pressure cannot be reduced to less than 0.03 Torr. Therefore, it is important that the feed system be designed for minimal heat contribution from the ionizer. Figure 31 shows the closed loop heater power requirement at 10 Torr vapor pressure for various ionizer heat contributions. To attain the fast transient response shown in previous figures, the heater element must be capable of providing an instantaneous 40 W of power to the vaporizer section. The power demand is halved after about 4 sec. Figure 30 shows that a time of 8.5 sec. is needed to reduce the cesium vapor flow to 1% of its normal level. In addition, it can be noted from either Fig. 30 or 31 that the over-all feed system time constant (γ) is approximately 3.7 sec; therefore, the approximate time to steady state is

$$t_{ss} \approx 4\gamma = 4 \ (3.7 \text{ sec}) = 15 \text{ sec.}$$

This feed system concept suggests that it would be possible for a single storage element to provide cesium to a number of vaporizer wicks. Fine flow control of the individual vaporizer sections permits the individual mass flow control of vapor to a number of thrustors, as well as individual thrustor startup and shutdown.

60

Fig. 30. Liquid cesium feed system thermal response as a function of ionizer heat input.

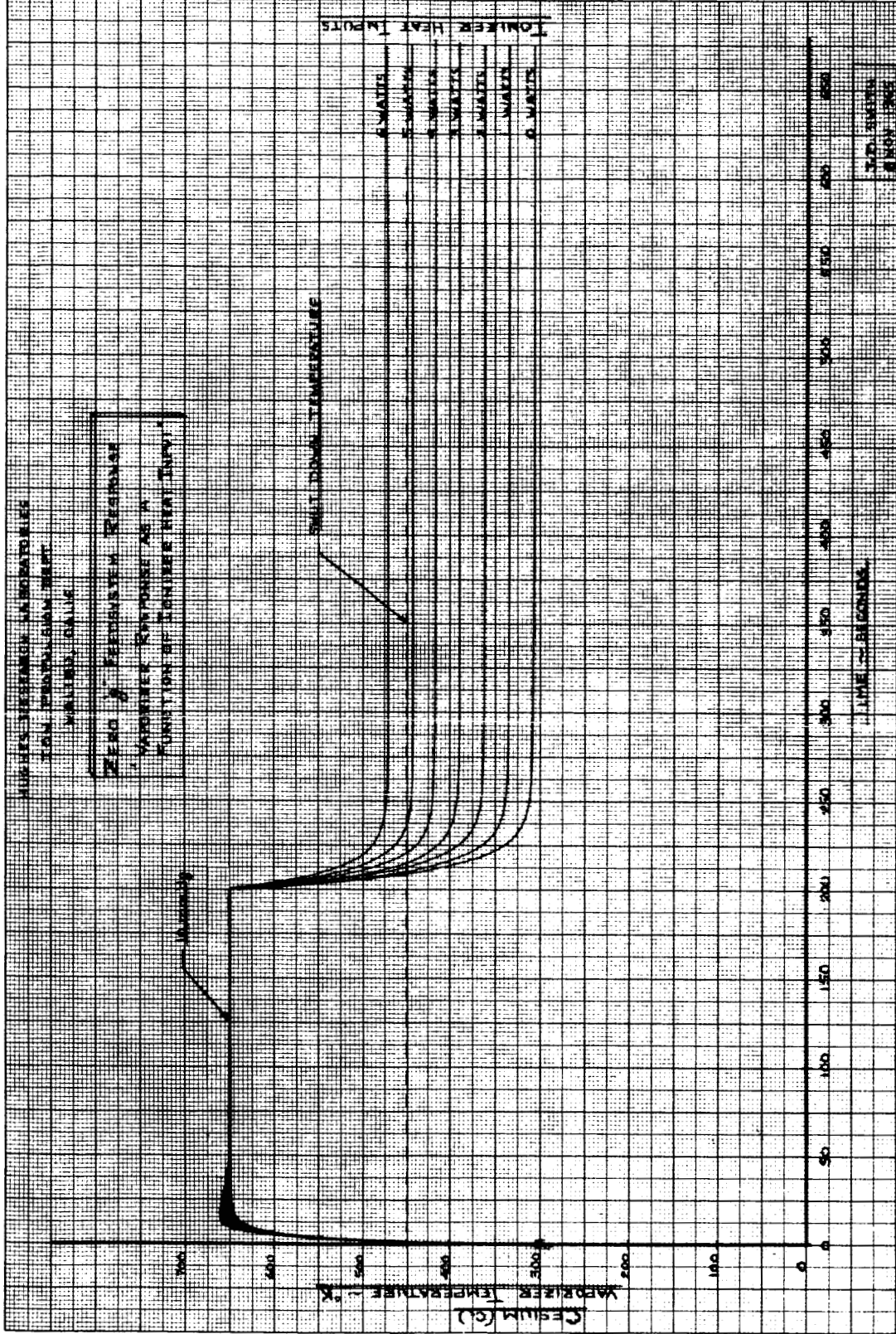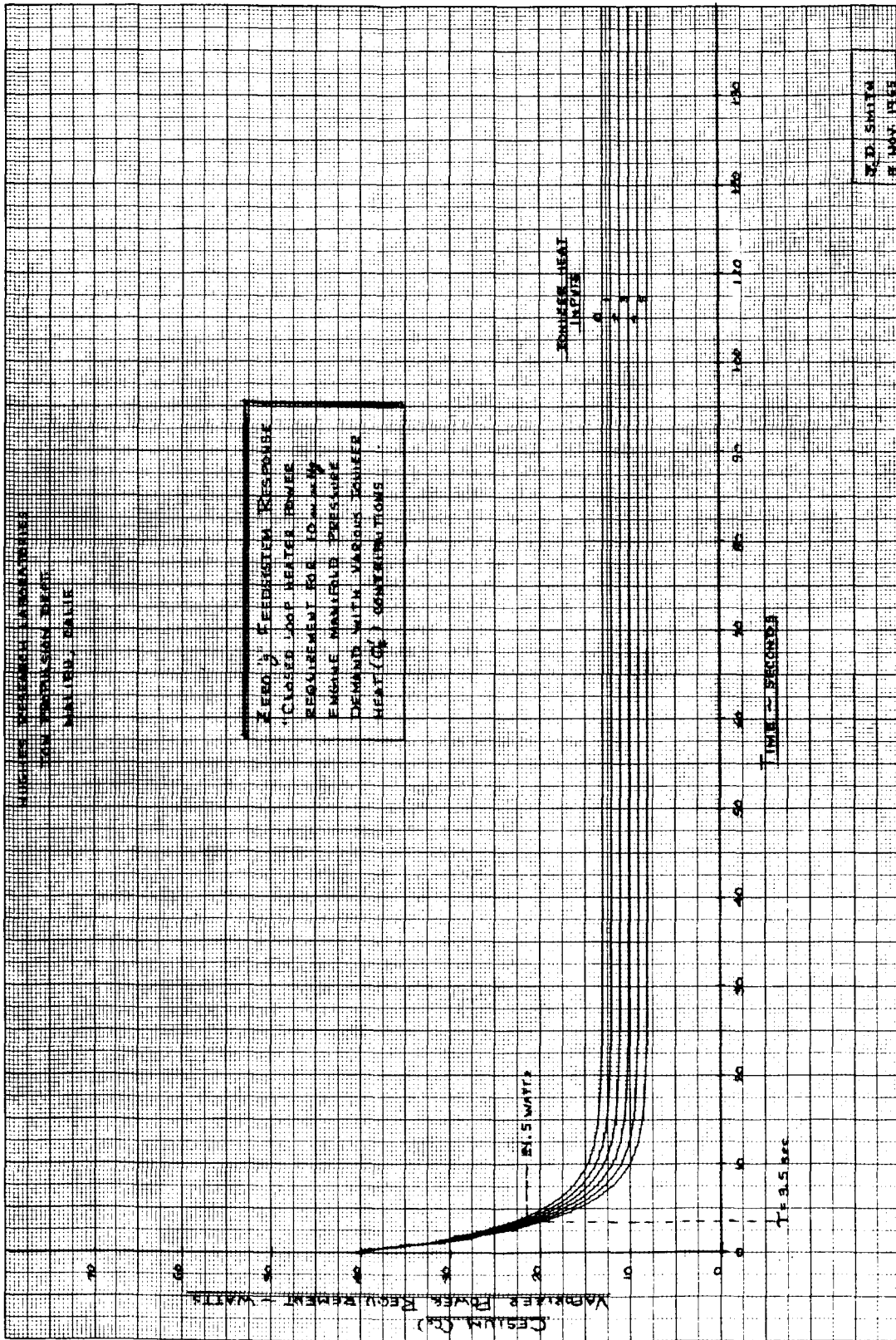Fig. 31. Liquid cesium feed system thermal response showing closed-loop vaporizer heater power requirements for 10 Torr ionizer manifold demand with various ionizer heat contributions.

V.   THRUSTOR ADVANCED DEVELOPMENT

This phase of the contract effort is concerned with those ad-
vanced developments which are pertinent to upgrading of the thrustor
thermal, mechanical, and electrical design and performance. Included
in this task is the design, fabrication, and test of a two-thrustor beam-
deflection station, including feed system.

A.   THERMAL IMPROVEMENT

The initial steady-state thermal tests on a Model LD thrustor, to
determine whether a more effective heat shielding technique is feasible,
have been completed. The results to date are promising, and this effort
will be concluded during the next reporting period.

The focus electrode was modified for the thermal tests as illus-
trated in Fig. 32. The side facing the ionizer manifold was relieved in
an area 0.030 in. deep and 0.275 in. wide on either side of the ionizer.
Two layers of molybdenum shielding and three layers of Fiberfrax
(Al_2O_3 and SiO_2) were inserted into the space while the critical optical
surface of the electrode remained undisturbed. This change was in-
tended to reduce the radiation to the focus electrode, which along with
the accel electrode forms a double heat shield between parts of the
ionizer assembly and the ambient thermal environment.

Figure 33 shows the results of testing to date. Normal LD
engine performance utilizing several layers of molybdenum shields
is consistently in the range of $0.75 \leq \epsilon/\eta \leq 0.80$, where ϵ is the
ionizer on emissivity and η is the heater efficiency. After the change
to a configuration of alternate layers of molybdenum shields and
Fiberfrax totaling approximately 3/8 in. thick, plus the insertion of
focus electrode shields, the thermal performance improved to
$\epsilon/\eta = 0.70$. This represents a saving of about 15% in heater power.
A spread in the data results because of a $15^\circ C$ temperature gradient
between the hottest and coolest portions of the ionizer.

FOCUS ELECTRODE   Mo SHIELD   2 SHIELDS + FIBER FRAX IN THIS SPACE

IONIZER
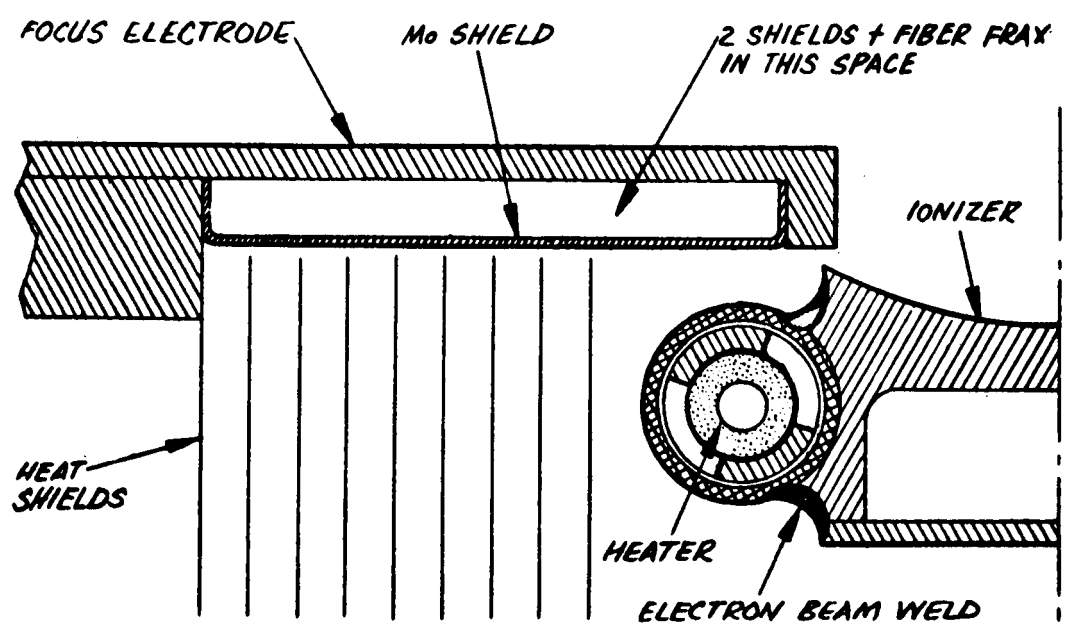
HEAT SHIELDS

HEATER

ELECTRON BEAM WELD

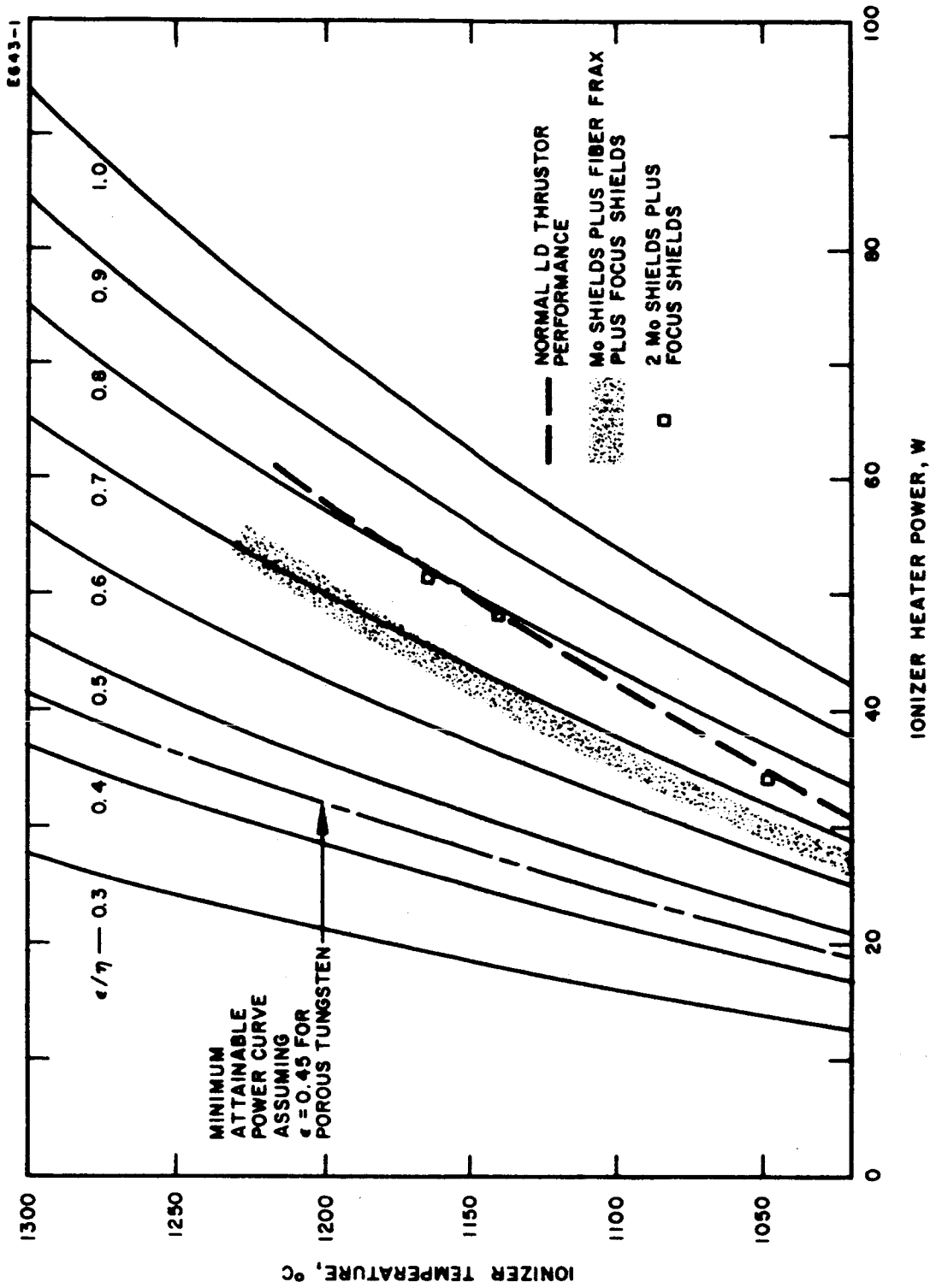Fig. 32. Schematic diagram of focus electrode thermal shielding.

Fig. 33. Steady-state thermal characteristics of thrustor LD-1 (4.6 cm long ionizer) for two different heat shield configurations.

65

When the alternate layers of molybdenum and Fiberfrax were removed from around the manifold and only the focus shields and the inner and outer molybdenum shields were retained, the thrustor operated as efficiently as when several layers of molybdenum shielding (no Fiberfrax) were present. The tentative conclusion based on these initial tests is that the combination of metal shields and Fiberfrax is more efficient than metal shields alone. It remains to be determined whether the configuration of two molybdenum shields containing only Fiberfrax between them is as good as alternative layers of metal shielding and Fiberfrax. When the best combination of materials is found, the arrangement will be incorporated into future thrustor designs. Varying the shield thickness may produce additional benefits; however, the thickness of the side and end shielding is already at the maximum permitted by current structural design.

B. ION OPTICS

In order to correlate theory with the experimental effects observed following the 2000 hour life test of the single-strip cesium-contact ion thrustor LXB-7, the paths of charged particles were studied on the trajectory tracer-analog computer. The results of these studies for the thrustor electrode configuration used for the 2000 hour test is shown in Fig. 34. The region of charge exchange ion bombardment corresponds closely to that observed in the experimental thrustor. Note that the neutralizer wire, in the absence of a decel electrode, is swamped in a negative potential electric field region. This is an unfavorable circumstance for transfer of electrons from the neutralizer into the ion beam. From this point of view it appears highly desirable to include a decel electrode in this modified Model 70 optical system in order to confine the negative equipotentials to a smaller volumetric region closer to the accel electrode.
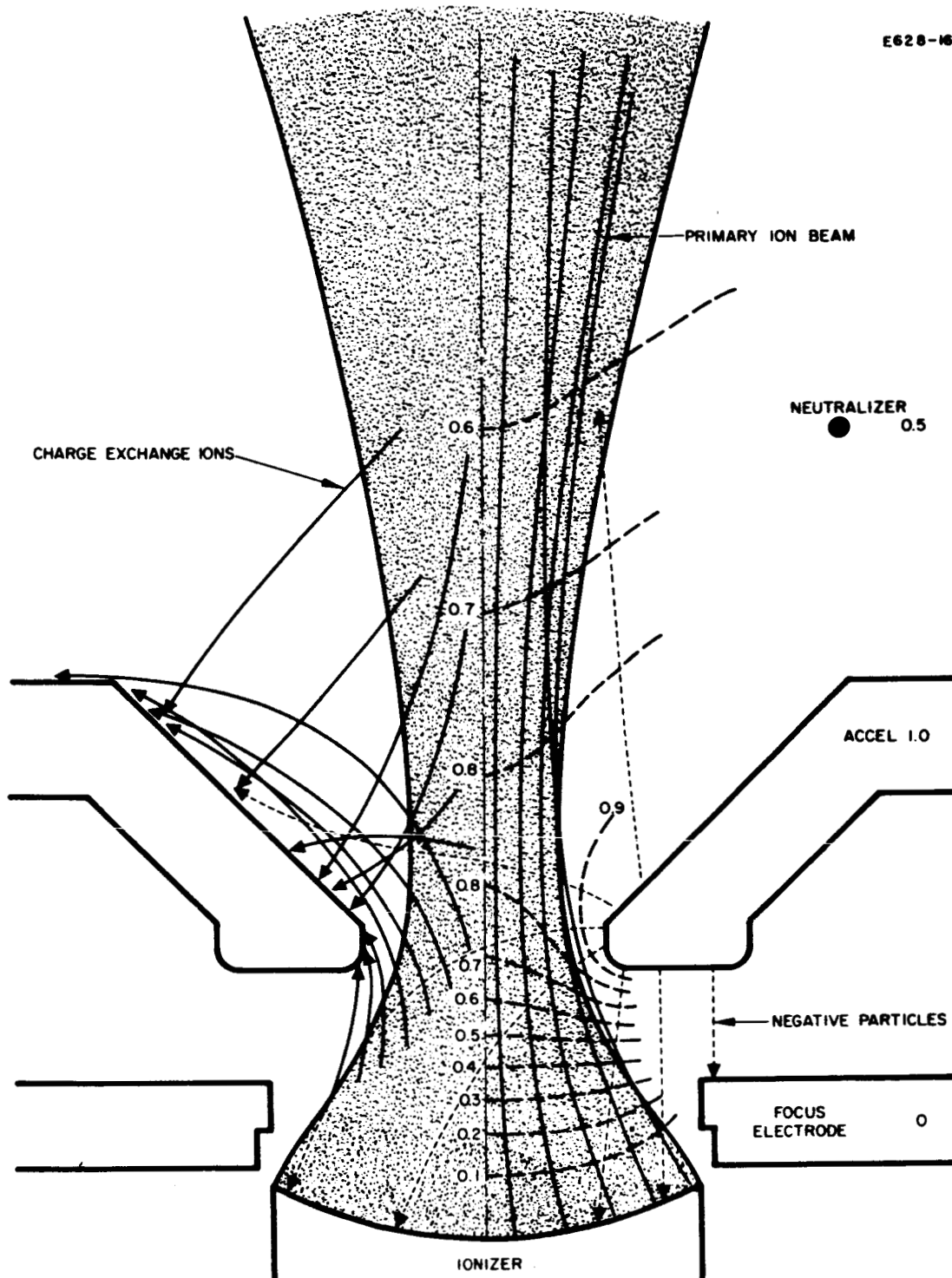
66

Fig. 34. Charged particle trajectories in the linear, single-strip ion
thrustor (Model 70 optics) used for the successful 2000 hour
steady state life test. Solution is for 3/4 of full space charge.

With this in mind, the same electrode system was studied but with the addition of a decel electrode downstream from the accel electrode. The trajectory results for simulation with 75% of full space charge are shown in Fig. 35. It is seen that the equipotentials are better defined and the negative equipotential lines do not extend to the region where a neutralizer filament would be placed. Consequently, this system is better suited for transferring neutralizing electrons into the ion beam. The choice of 75% full space charge was dictated by the fact that experimental engines are typically operated slightly flow-limited, rather than full space-charge-limited. Notice in Fig. 35 that the charge exchange ion trajectories are essentially unaffected by the presence of the decel electrode, and the ion bombardment is in the same general region of the accel electrode.

In Figs. 34 and 35 it is seen that the primary ion beam diverges at a half angle of about 10°. In order to determine the change in beam divergence for a different electrode structure, a thin accel Model 70 optical system was studied and the results are shown in Fig. 36. Because of the enhanced confinement of the negative equipotentials in the region of the accel electrode, it is seen that the primary ions experience a force which tends to spread the ion beam slightly more than that shown in Figs. 34 and 35. Furthermore, the thin accel electrode system with a decel electrode results in a wider distribution of the charge exchange ions. In particular, the ion bombardment occurs on both sides of the accel electrode and some bombardment of the decel electrode is experienced. This has an unfavorable effect on the long life capability of the ion thrustor. With the above considerations in mind, it appears that the thin accel electrode system is not desirable for use in operating ion thrustors intended for long life applications and that addition of a decel electrode to the present electrode structure will improve the effectiveness of the neutralizer.
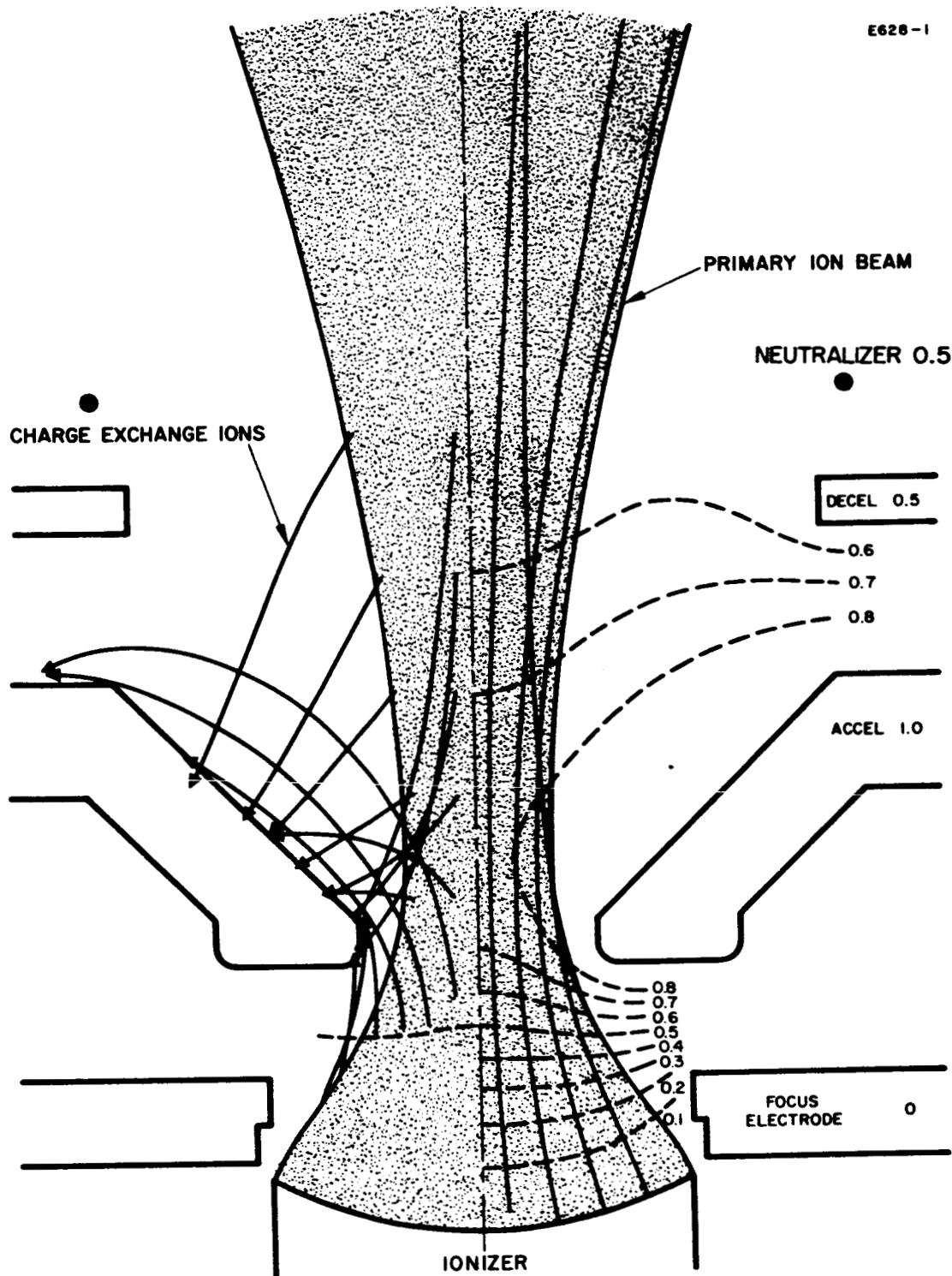
Fig. 35. Ion trajectories for the single-strip engine Model 70 optics with the addition of a decel electrode. Solution is for 3/4 of full space charge.
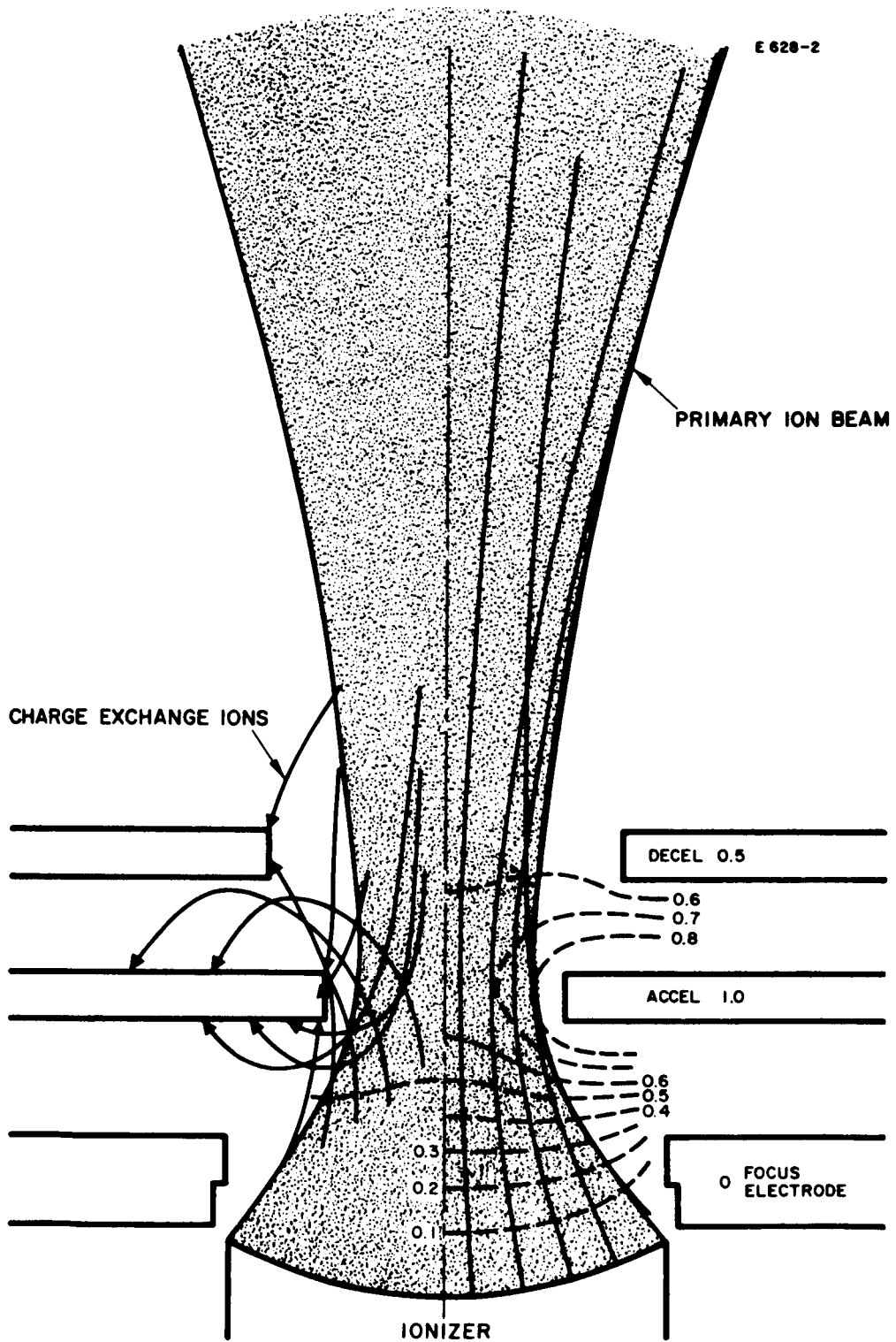
Fig. 36. Ion trajectories in a "thin-accel" Model 70 optical design including decel electrode. Solution is for 3/4 of full space charge.

C.   ION BEAM DEFLECTION

In order to apply linear-strip ion thrustors to a satellite attitude control station-keeping system, a minimum of six thrustors are required for the attitude control function and at least two additional thrustors are needed to provide translation forces for station keeping. The standby power requirements of such a system are determined in part by the energy needed to heat the cesium feed systems. Through careful thermal design, the power requirements for any one reservoir with a 2 lb capacity have been reduced to the order of 10 W. It is clearly desirable to operate several thrustors from a single feed system since individual feed systems for each of the eight thrustors would result in prohibitive standby power requirements.

Company funded work at Hughes Research Laboratories has shown that the beam from an ion thrustor can be deflected electrostatically in the accel structure. Much of this work was disclosed to NASA in HRL Proposal No. 65M-49847/A8764. Further work performed since that time has shown that the beam may be deflected to angles approaching 30°. With this deflection, half of the thrust can be directed at right angles to the normal thrust vector and a single linear-strip thrustor can be used for both station keeping and attitude control about one axis. If two such thrustors are mounted with the ionizers in one plane and with the electrode structures perpendicular to each other, two-axis control from a single station is possible. Figure 37 shows the general outline of such a station mounted to a single feed system. A single two-thrustor station with electrostatic beam deflection performs the functions of five static thrustors.

Additional advantages to the two-thrustor station approach are summarized below:

1.   Redundant thrustor operation — Since the thrust from each engine is normally directed the same way, the thrustors can be operated alternately without changing the forces on the spacecraft.
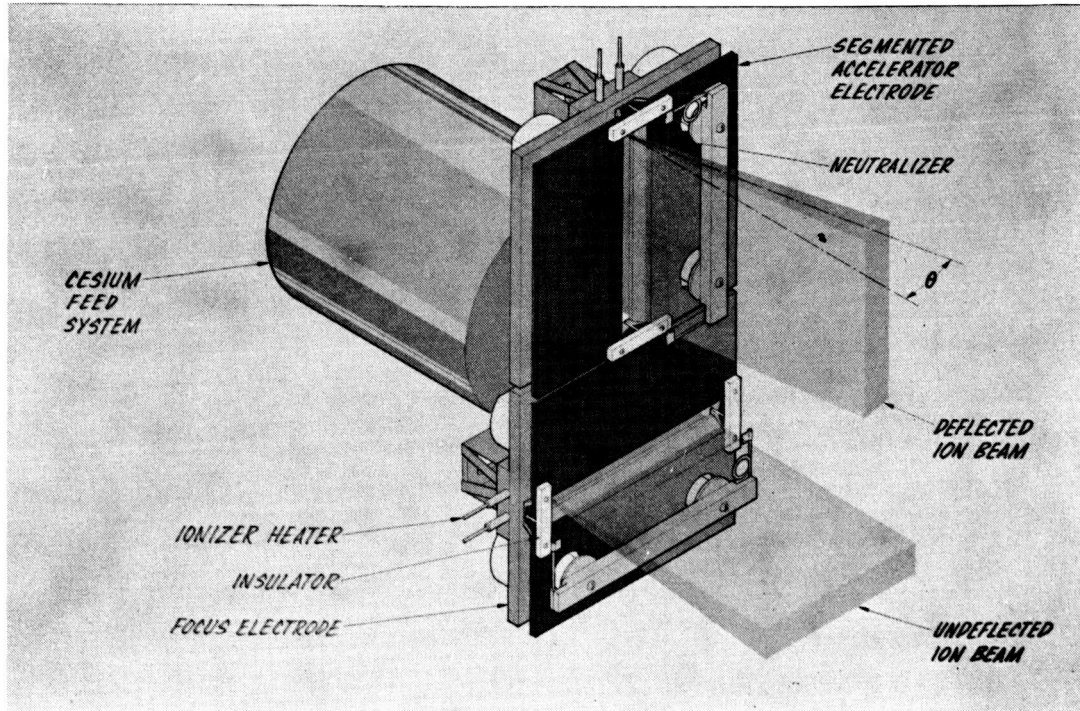
Fig. 37. Isometric of two-thrustor station with
electrostatic deflection of the ion beam.

2.   Vernier control of translation force — In a spacecraft it may be highly desirable to correct for minor misalignment in the thrust vector from an engine operating continuously. The direction of the thrust vector can be varied by ground command to a precision of better than 0.01 deg.

3.   Control system simplification — Electrostatic beam control permits a much faster and more flexible satellite control system than the original design based on static thrustors. Since disturbance torques as high as 5000 dyne-cm can be accommodated, the new system concept is applicable to a wide variety of satellites.

Ion beam deflection experiments have been conducted with the single-strip thrustor design. In these experiments thrustor LC-1 (5 cm long ionizer) was mounted in the 5 foot vacuum chamber. The electrostatic fields for deflection were provided by a bias voltage applied between two lengthwise halves of a split accel electrode. No decel electrode or neutralizer was present, but a ground plane was provided about 1/8 in. downstream from the accel electrode. For measurement of deflection angles, nitrogen gas was leaked into the chamber to a total pressure of 8×10^{-5} Torr to permit photographic recording. The deflection angle data were taken at a beam current of 10.5 mA with a peak ion gun voltage at the accel plane of 5 kV. Final beam voltage was 4 kV. The results of this experiment are shown in Fig. 38, where deflection angle is plotted versus the normalized deflection voltage and compared with theory. It is seen that correlation with the electrolytic tank analog computer theory is reasonably good. Additional data were taken without leaking nitrogen gas into the chamber to determine sensitivity of accel current to beam deflection voltage. It was shown that for a beam potential of 6 kV at the accel plane and deflection voltages from 0 to 700 V, the accel current rose from 26 µA
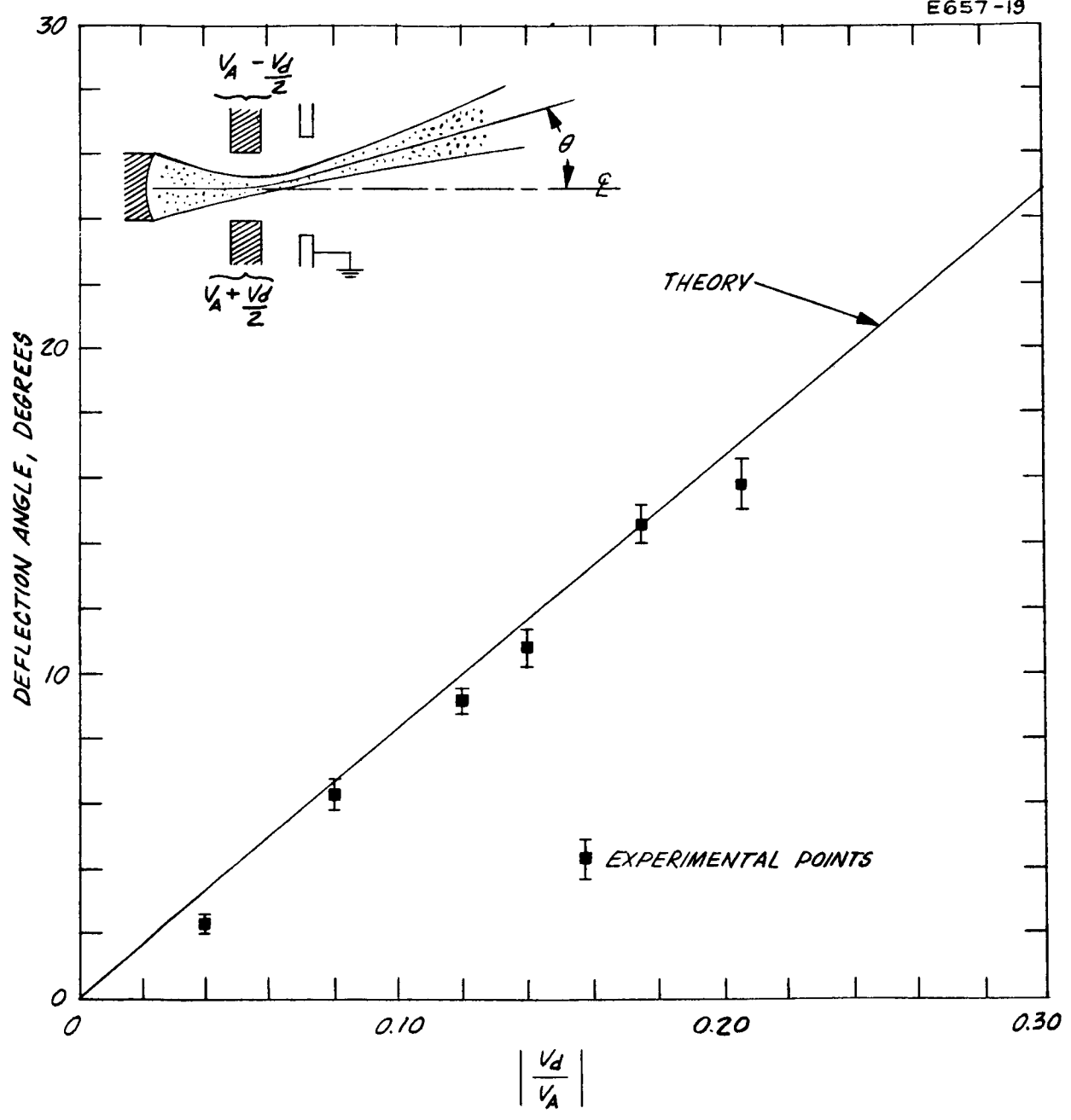
Fig. 38. Comparison of experiment and theory for ion
beam deflection in the linear ion thrustor.

to 30 μA. The beam current was 14.5 mA. This set of experimental data clearly demonstrates that in the present single-strip thrustor only a minor increase in the accel current occurs for deflection angles up to about 10°. These experiments will be continued to determine thrustor characteristics at deflection angles higher than 10°.

VI. CONCLUDING REMARKS

The thrustor vibration tests conducted to date have shown a low frequency resonance at about 200 cycles when a two-point mounting is used. It is expected that refining the mathematical model used in the analysis and repeating the calculations will confirm the low-frequency experimental data. At that time a means for reducing or eliminating this low frequency resonance will be investigated, including the use of a four-point mounting structure. Correlation between the analytical and experimental results will permit rapid evaluation of design changes without the delays and expense often associated with vibration tests.

The major area of uncertainty in this program is the dynamic behavior of the cesium feed system. The test plan will be pursued vigorously in order to obtain experimental verification of the present design as soon as possible. Studies indicate that use of a thrustor at the output end of the cesium feed system provides the best and most sensitive detection method available. Consequently, stable operation of a single-strip ion thrustor attached to the new liquid-cesium feed system will provide the principal experimental verification of the feed system design.

Advanced development toward improving the thermal performance of the present thrustor appears promising and will be pursued. Furthermore, the high voltage integrity of the present thrustor can be improved by rearranging the high voltage insulators. An electrical test of the thrustor with the new high voltage structural arrangement will be conducted to verify operation at 10 mA/cm^2. In agreement with the NASA Project Manager, it appears desirable to conduct a few thrustor experiments using a different accel material which has a sputtering yield lower than that of copper. The purpose of these experiments is to provide a comparison of thrustor performance for possible future steady-state life tests.

APPENDIX A
THRUSTOR VIBRATION ANALYSIS

Presented here are the results of a study of the dynamical behavior of a linear strip ion thrustor for attitude control and station keeping. Estimates of expected principal vibrational modes and frequencies with maximum expected deflection and accelerations are presented.

1. INTRODUCTION

The objective of this study was to provide information concerning the dynamical behavior of the ion thrustor when subjected to a vibration environment. This information will be used for design modifications and for comparison with vibration tests. Specifically this study provides:

1. Estimates of resonance frequencies and mode shapes of the thrustor supported by its two attachment points on the bottom plate.

2. Estimates of dynamic deformation resulting from a 1 g input at points where interference may be a problem.

3. Transmissibility to a 1 g input of certain vital points in the system.

2. STRUCTURAL MODEL

In the analysis, the neutralizer filament assembly was treated separately. It was assumed that this assembly would have little dynamical effect on the rest of the system because of its relatively small mass. The results of this analysis are discussed in Section 3.

The ion engine (neglecting the neutralizer filament assembly) was simulated by a series of lumped masses connected by elastic members as shown in Fig. A-1. The weight breakdown and appropriate moments of inertia for each mass are given in Table A-1. The model was assumed to have a damping coefficient of 1% of critical for all modes and to be fixed at Stations 10 and 12.
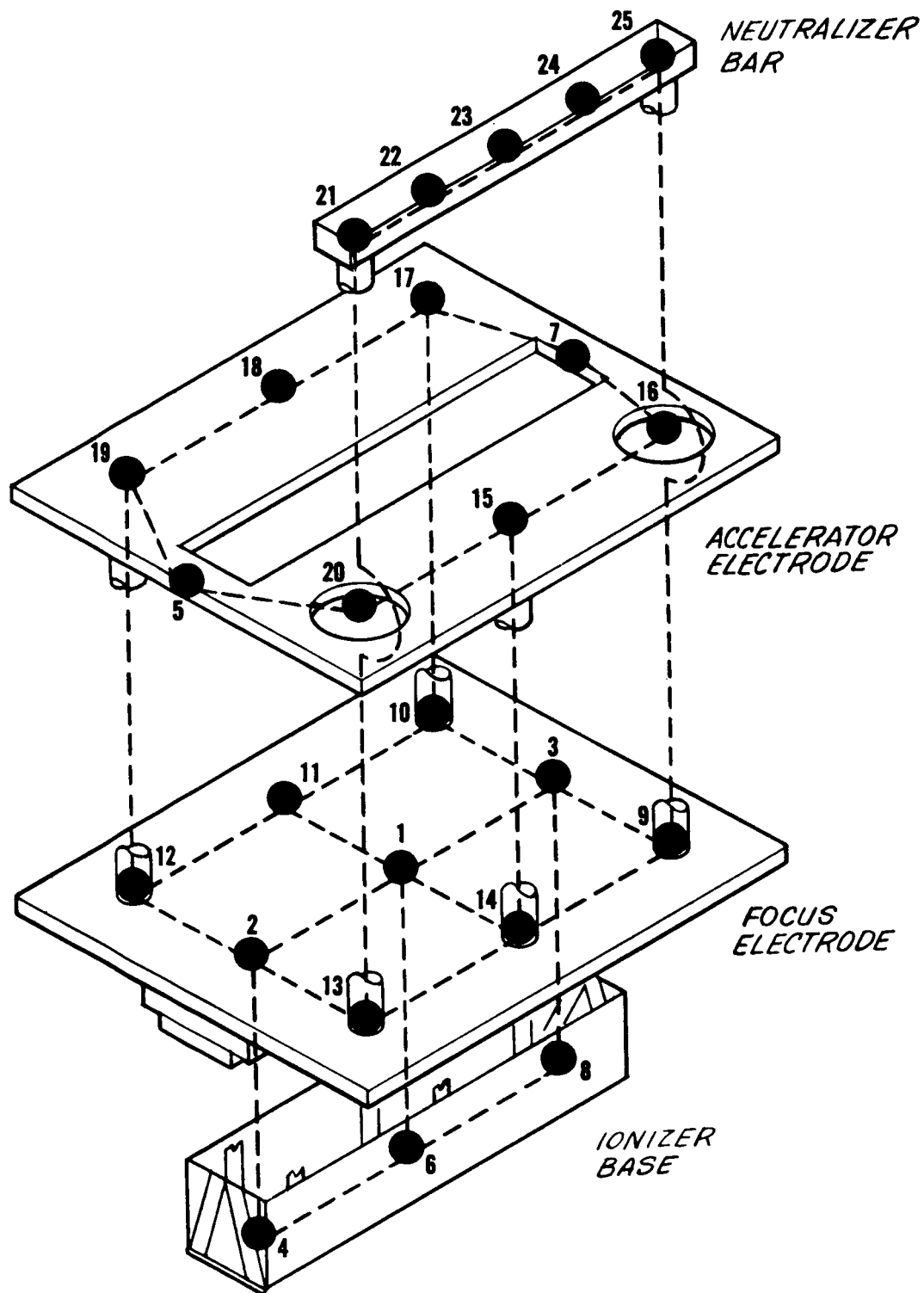
Fig. A-1(a). Mathematical model simulating single-strip ion engine.
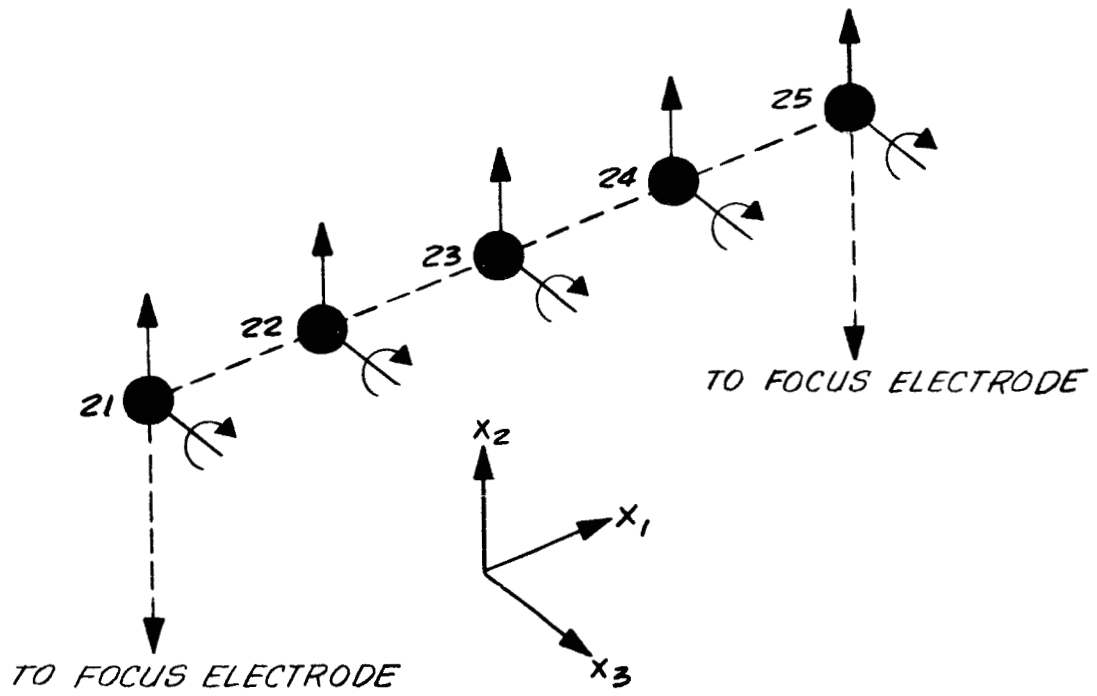
Fig. A-1b. Neutralizer Bar — Degrees of Freedom
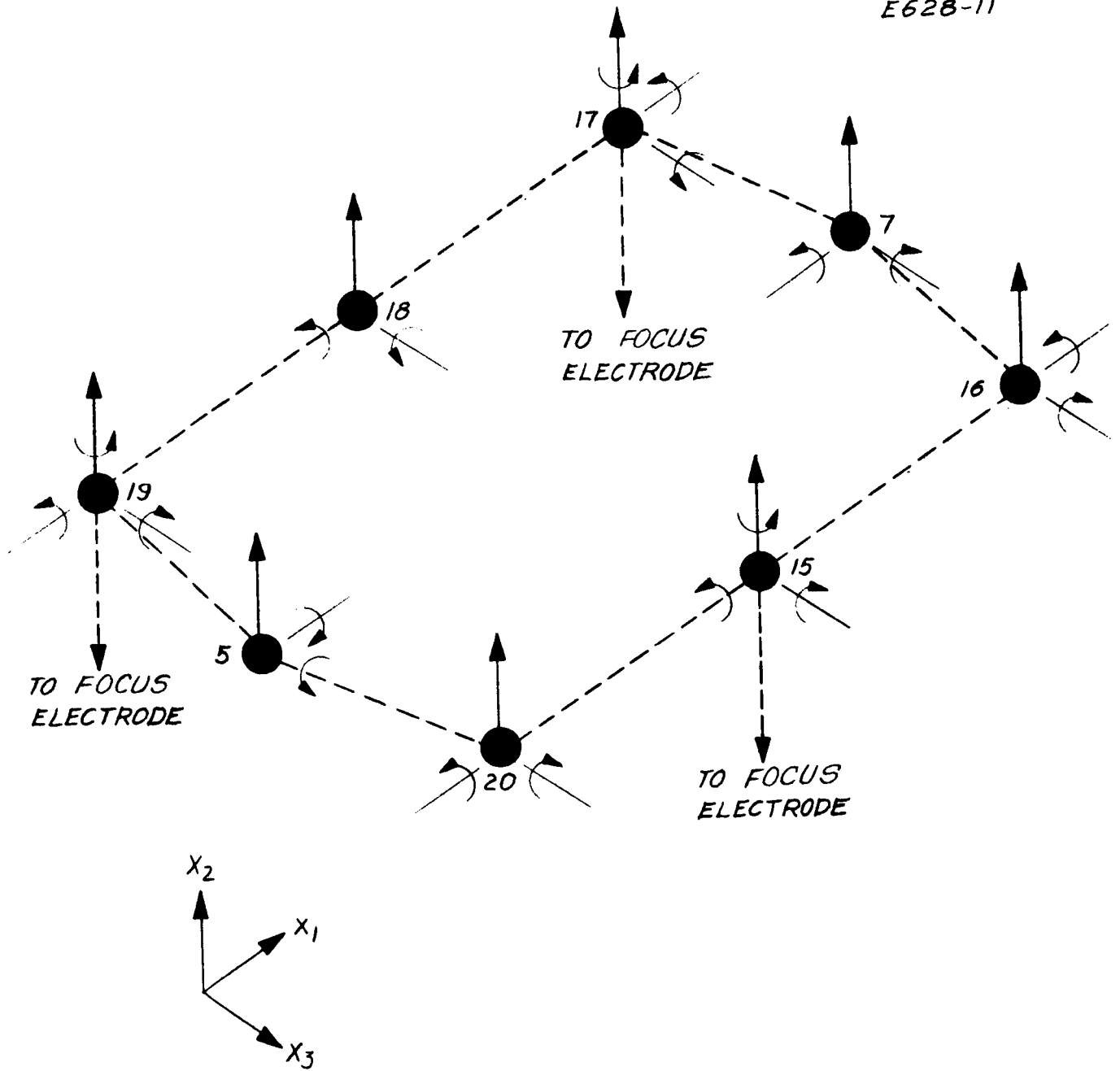
Fig. A-1c. Accelerator Electrode — Degrees of Freedom
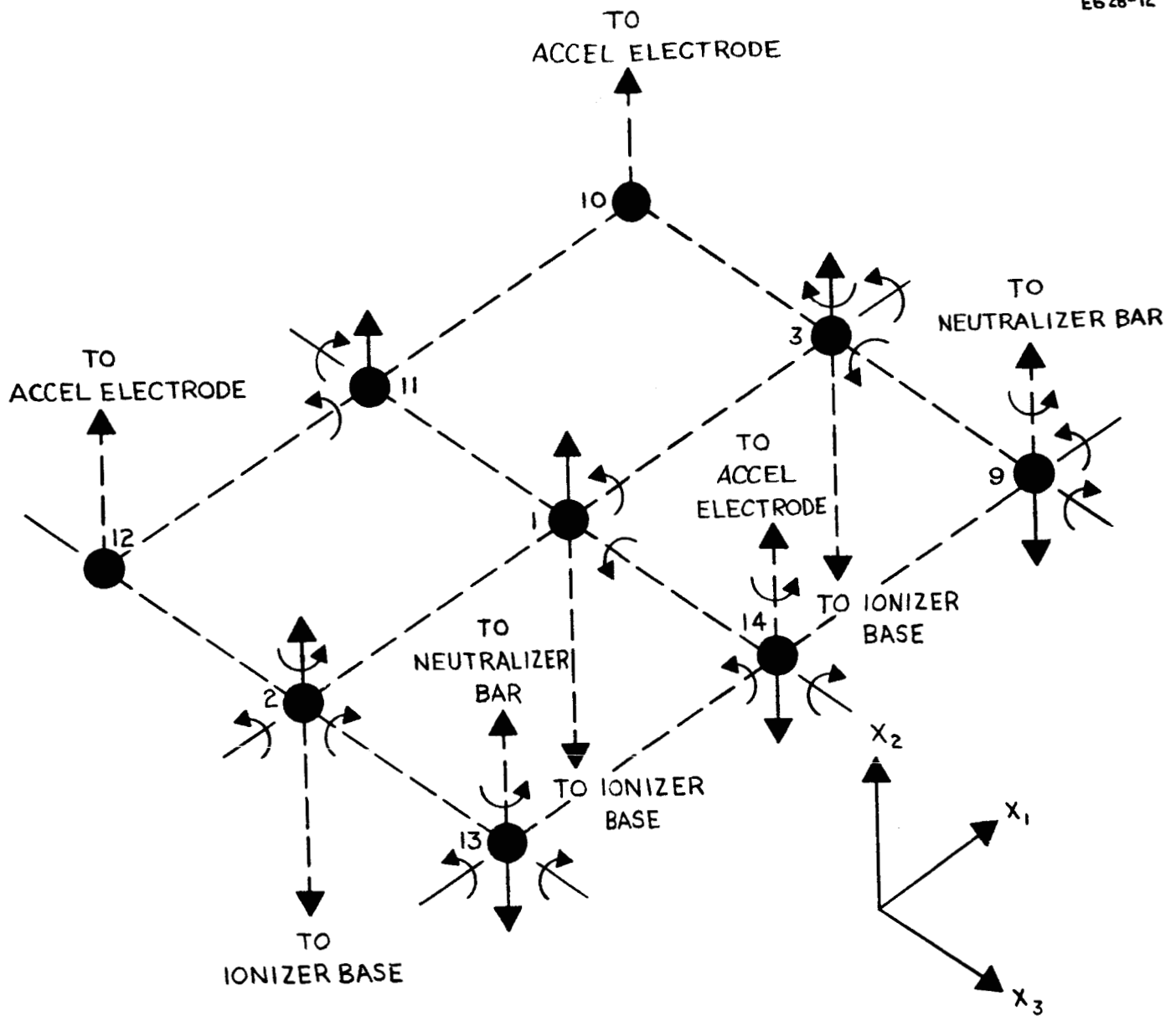
Fig. A-1d. Focus Electrode — Degrees of Freedom.
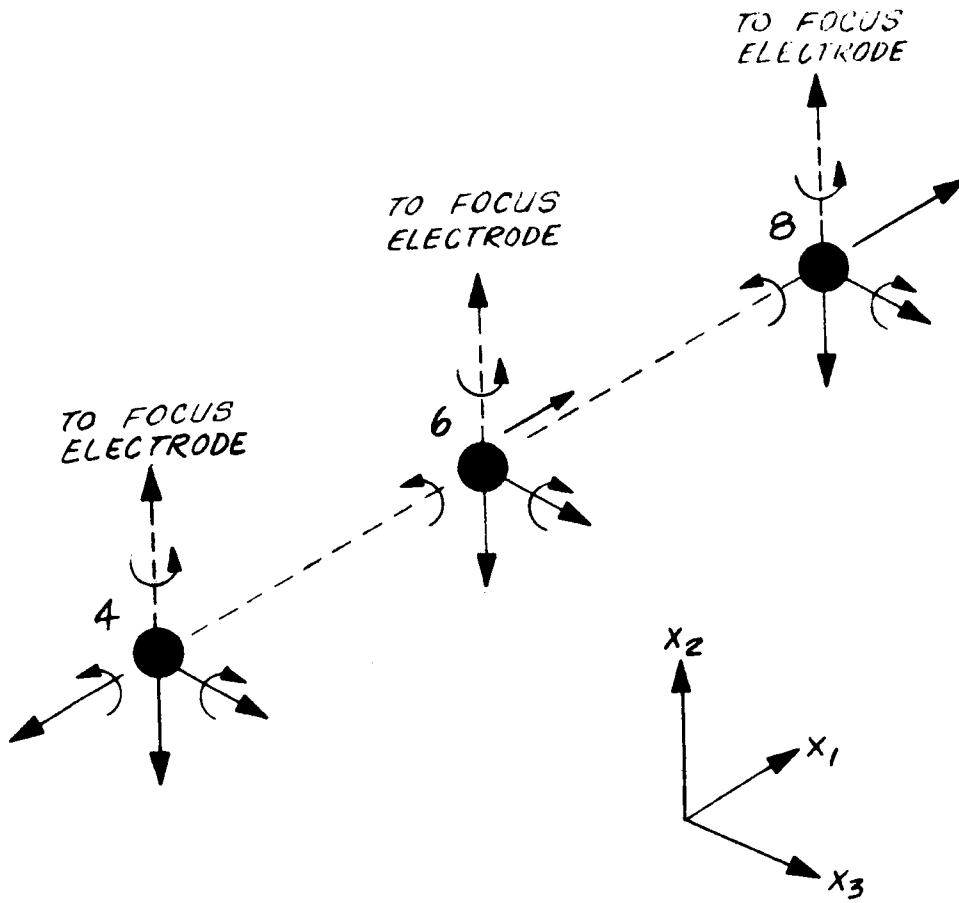
Fig. A-1e. Ionizer Base — Degrees of Freedom

TABLE A-I
Weights and Moments of Inertia

Location	Weight, lb	I_{x_1}, lb-in.^{2}	I_{x_2}, lb-in.^{2}	I_{x_3}, lb-in.^{2}
1	0.02464	0.0001928	0.0001562	0.00515
2	0.02700	0.002065	0.00370	0.00191
3	0.02700	0.002065	0.00370	0.00191
4	0.00715	0.0001103	0.000161	0.0000592
5	0.000843	0.0000694	0.000007	0.0000694
6	0.01020	0.0001103	0.000161	0.0000592
7	0.000843	0.0000694	0.000007	0.0000694
8	0.00715	0.0001103	0.000161	0.0000592
9	0.0350	0.001671	0.00299	0.001671
10	0.0350	0.001671	0.00299	0.001671
11	0.0763	0.00364	0.00652	0.00364
12	0.0350	0.001671	0.00299	0.001671
13	0.0350	0.001671	0.00299	0.001671
14	0.10887	0.00520	0.00927	0.00520
15	0.0198	0.000945	0.00169	0.000945
16	0.0190	0.000927	0.00166	0.000927
17	0.194	0.000945	0.00169	0.000945
18	0.0194	0.000927	0.00166	0.000927
19	0.0194	0.000945	0.00169	0.000945
20	0.0190	0.000927	0.00169	0.000927
21	0.00405	0.0000152	0.0000552	0.0000468
22	0.00302	0.0000152	0.0000552	0.0000468
23	0.00302	0.0000152	0.0000552	0.0000468
24	0.00302	0.0000152	0.0000552	0.0000468
25	0.00405	0.0000152	0.0000552	0.0000468

3. NEUTRALIZER FILAMENTS ASSEMBLY

In the analysis, the neutralizer filaments and leads were considered separately from the rest of the thrustor. Natural frequencies of this assembly are summarized in Table A-II. Because of the large loop in the neutralizer sping-lead it is difficult to calculate its specific resonance frequency. The filament assembly is shown in Fig. A-2.

TABLE A-II

Natural Frequencies of Neutralizer Filaments Assembly

Neutralizer Filament	422 cps
Dummy Neutralizer Filament	188 cps
Neutralizer Lead	4000 cps
Neutralizer Spring-Lead	200 to 700 cps
Dummy Filament Lead	515 cps
Dummy Filament Spring-Lead	252 cps

4. RESONANCE FREQUENCIES AND MODES

The first two natural frequencies of the thrustor, excluding the neutralizer assembly, occur at 1774 cps and 2473 cps. In these modes the neutralizer bar experiences rather large motion relative to the rest of the system; the mode shapes are shown in Fig. A-3. The third and fourth mode of free vibration occur at 2618 and 3569 cps; in both of these modes, the accelerator electrode experiences relatively large motion. The modes are shown in Fig. A-4.

5. DEFORMATIONS

Because of the high fundamental frequencies, the maximum deflection is very small. All maximum displacements occur at 1774 cps. The largest displacement occurs in the center of the neutralizer bar with a magnitude of 0.0003 in. for a 1 g excitation acceleration. The

E628-13

Fig. A-2. Neutralizer filament assembly.

E628-6

SECOND MODE

STATIC MODE

FIRST MODE

25

24

23

22

21
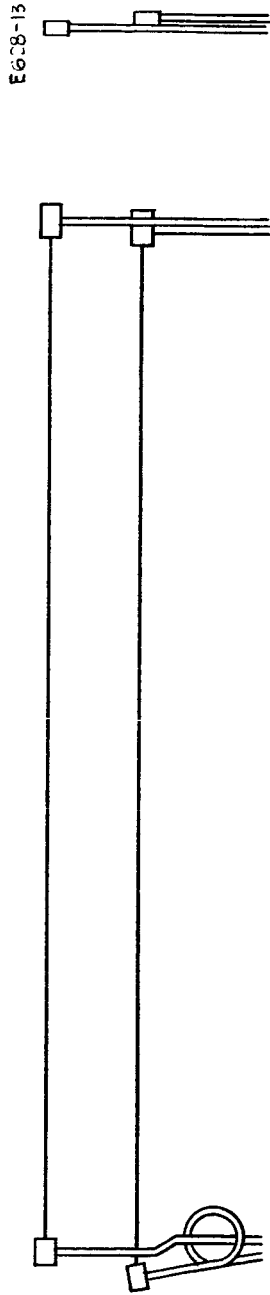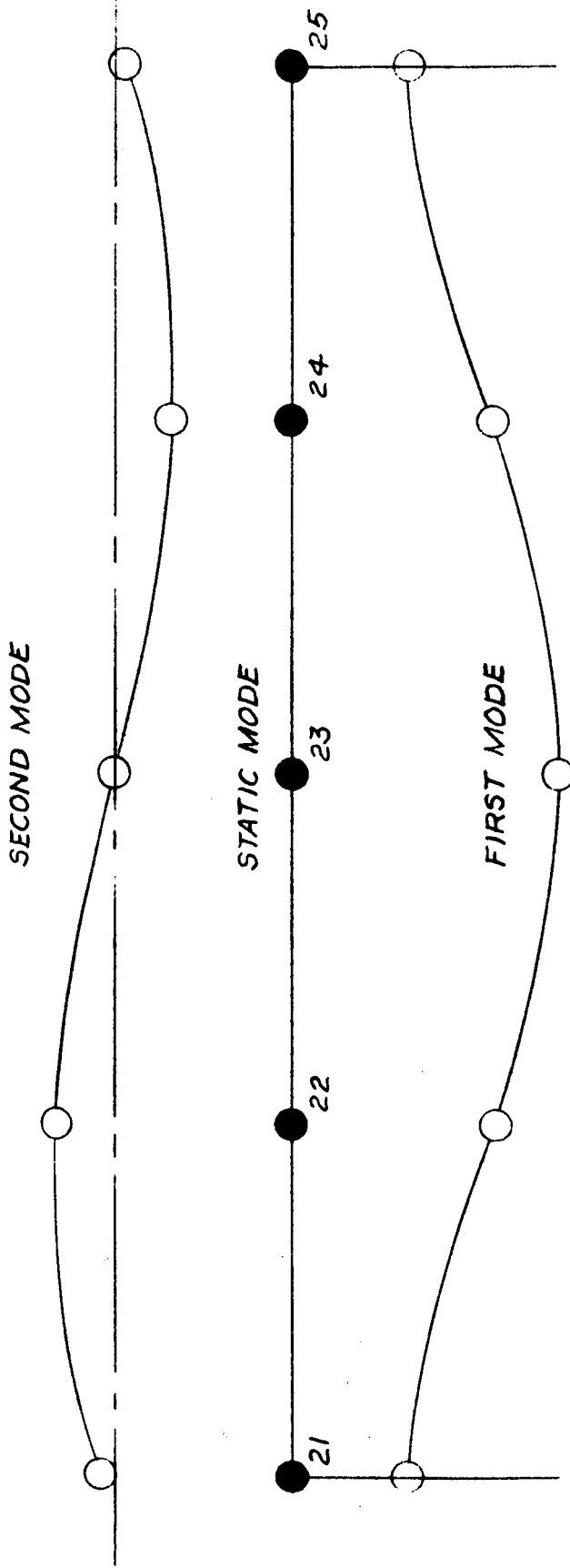
Fig. A-3. First two vibration mode shapes of neutralizer filament.

88
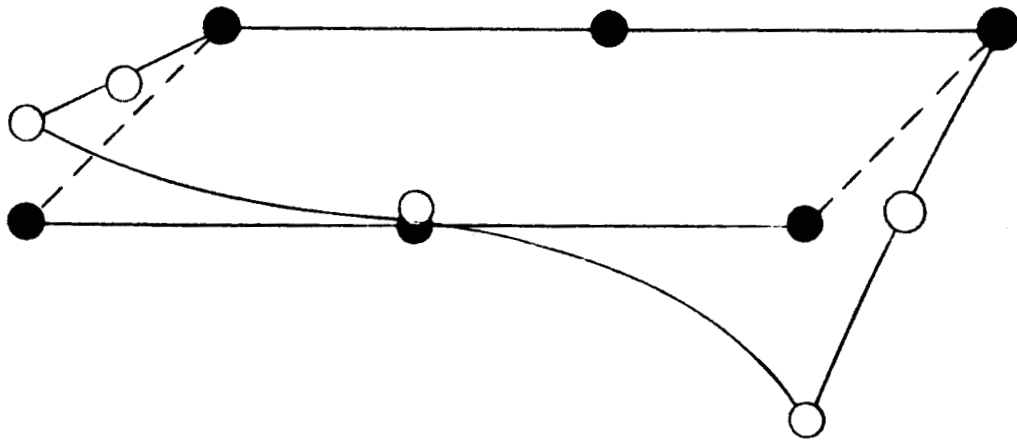
THIRD MODE
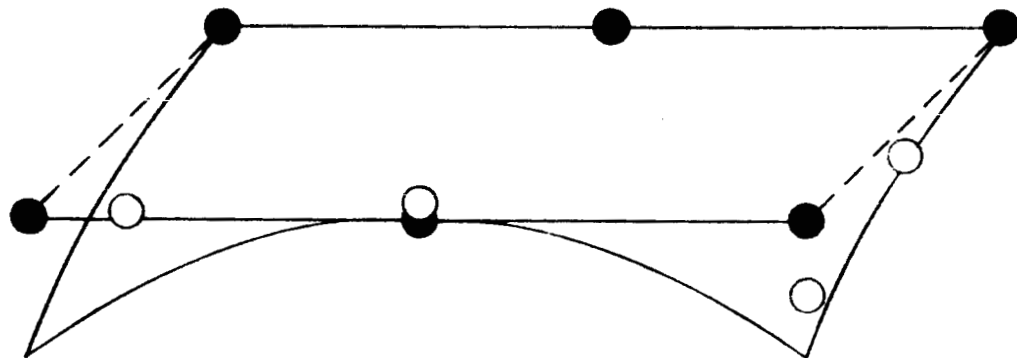
FOURTH MODE

Fig. A-4. Accelerator electrode mode shapes for the third and
fourth natural frequencies of the single-strip thrustor.

maximum relative displacement of the accelerator electrode to the ionizer electrode is 0.000025 in. (for a 1 g excitation acceleration), and is shown in Fig. A-5. For a complete list of maximum displacements at 1 g excitation, see Table A-III.

6.   TRANSMISSIBILITY

The absolute value of the largest transmissibility is plotted in Fig. A-6. This is also a response envelope for the entire system. The maximum acceleration occurs in the center of the neutralizer bar at 1774 cps with a magnitude of 95 g for a 1 g excitation acceleration.

7.   CONCLUSION

Based on outputs from LESAR I and II and hand calculations, the following conclusions are reached:

1.   The first fundamental frequency of the thrustor assembly, excluding the neutralizer filament assembly, is 1774 cps and occurs in the neutralizer bar.

2.   The first fundamental frequency of the neutralizer filament assembly is 188 cps and occurs in the dummy filament.

3.   The relative displacement between the accelerator electrode and the ionizer electrode is not more than 0.000025 in. for a 1 g excitation acceleration.

4.   Maximum displacement occurs in the center of the neutralizer bar and is 0.0003 in. for a 1 g excitation acceleration.
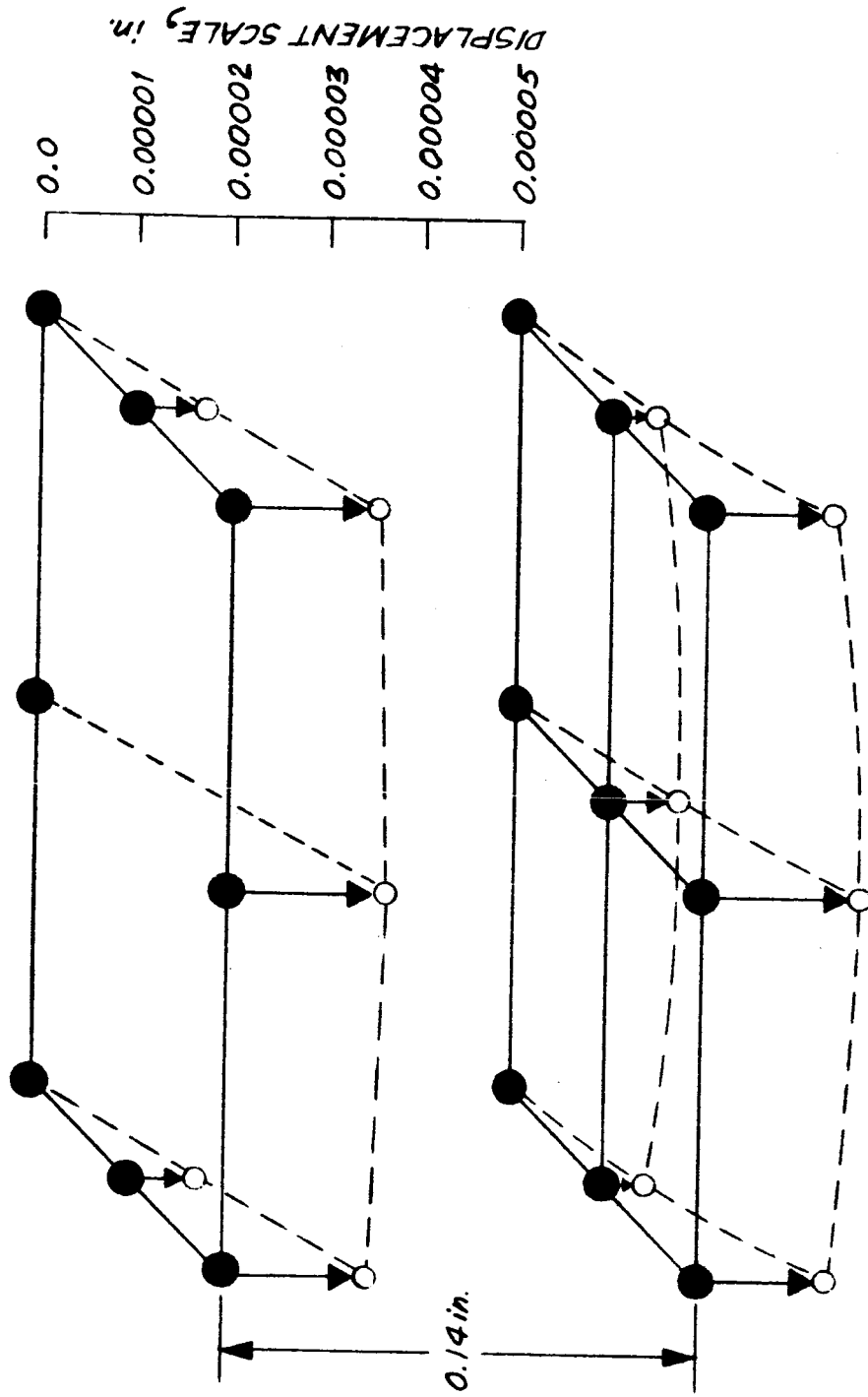
Fig. A-5. Maximum displacement of the accelerator electrode relative to the ionizer.
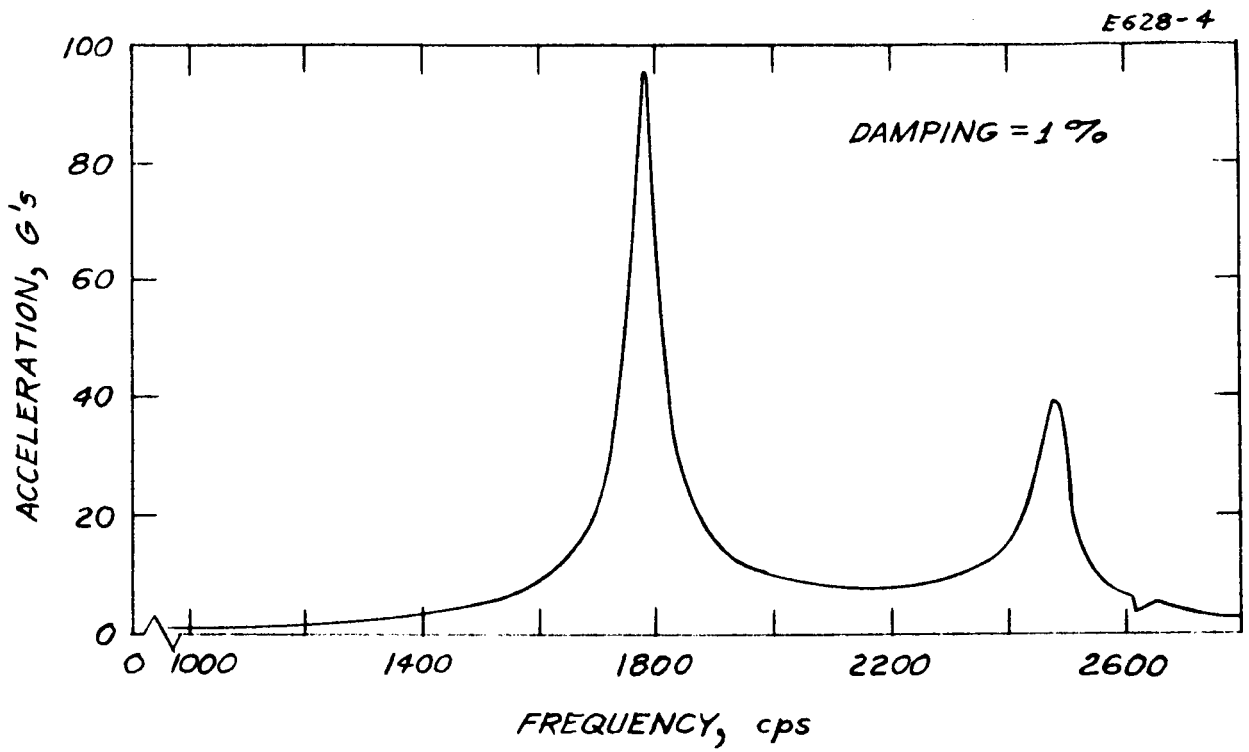
Fig. A-6. Response envelope for the entire single-strip ion engine.

TABLE A-III

Maximum Displacements

Location	Displacement in X_2 Direction, 10^{-4} in.
1	0.77
2	0.48
3	0.48
4	0.50
5	0.72
6	0.73
7	0.72
8	0.50
9	1.36
10	0
11	0.08
12	0
13	1.36
14	1.66
15	1.67
16	1.54
17	0.01
18	0.01
19	0.01
20	1.54
21	1.37
22	2.29
23	2.99
24	2.29
25	1.36

APPENDIX B
LITERATURE REVIEWED.

1.   "Liquid Behavior Investigations Under Zero and Low G Conditions," E. W. Schwartz, Convair Astronautics, Paper presented at Zero G Symposium, Norair, Hawthorne, California, July 1960.

2.   "Hydrodynamic Considerations for the Designs of Systems For Very Low Gravity Environments," TR LG-1, W. C. Reynolds, Stanford University, September 1961.

3.   "Ion Rocket Engine System for Attitude Control and Station Keeping," Proposal No. 62M-0751/A0258 Book I, Hughes Research Laboratories, July 1962.

4.   "Design, Fabrication and Testing of a Cesium Ion Engine," NAS 5-517, HRL 5-517 II-S, Hughes Research Laboratories, September 1962.

5.   "Applied Research on Contact Ionization Thrustors," AF 33(657)-8157, Report No. ASD TDR 63-571, Electro Optical Systems, August 1963.

6.   "Design, Fabrication, and Testing of a Cesium Ion Rocket Engine," NAS 5-517, HRL 5-517 III-S, Hughes Research Laboratories, March 1964.

7.   "Applied Research on Contact Ionization Thrustor," AF 33(657)-10980, Report No. APL TDR 64-52, Electro-Optical Systems, May 1964.

8.   "Ion Rocket Engine System Research and Development," NAS 3-2516, NAS CR 54067, EOS Report 3670 Final, Electro Optical Systems, June 1964.

9.   "Ion Rocket Systems Research and Development," NAS 3-5250, NASA CR 54025, EOS Report 4920-Q-1, Electro Optical Systems, June 1964.

10.   "Cesium Electron Bombardment Ion Engines," AIAA Paper No. 65-373, R. C. Speiser, et al., Electro Optical Systems, July 1965.

APPENDIX C

LIQUID CESIUM FEED SYSTEM THERMODYNAMIC ANALYSIS

This Appendix presents the design, analysis, and analog computer mechanization of the heat transfer and thermodynamic equations for the liquid cesium feed system. The final design (presented in the body of the report) is a result of the dynamic simulation of the mathematical model presented in this Appendix. The preferred design differs from the original in that the contoured heat sink was eliminated from the system design during the computer design study.

This Appendix contains the original general model of the feed system. The subjects presented in this Appendix are listed below:

1.   Schematic diagram (Fig. C-1)
2.   Thermodynamic model (Fig. C-2)
3.   Heat transfer and thermodynamic equations
4.   Gas diffusionmodel (Fig. C-3)
5.   Nomenclature list
6.   Component sizings
7.   Analog computer mechanization (Fig. C-4 and C-5).
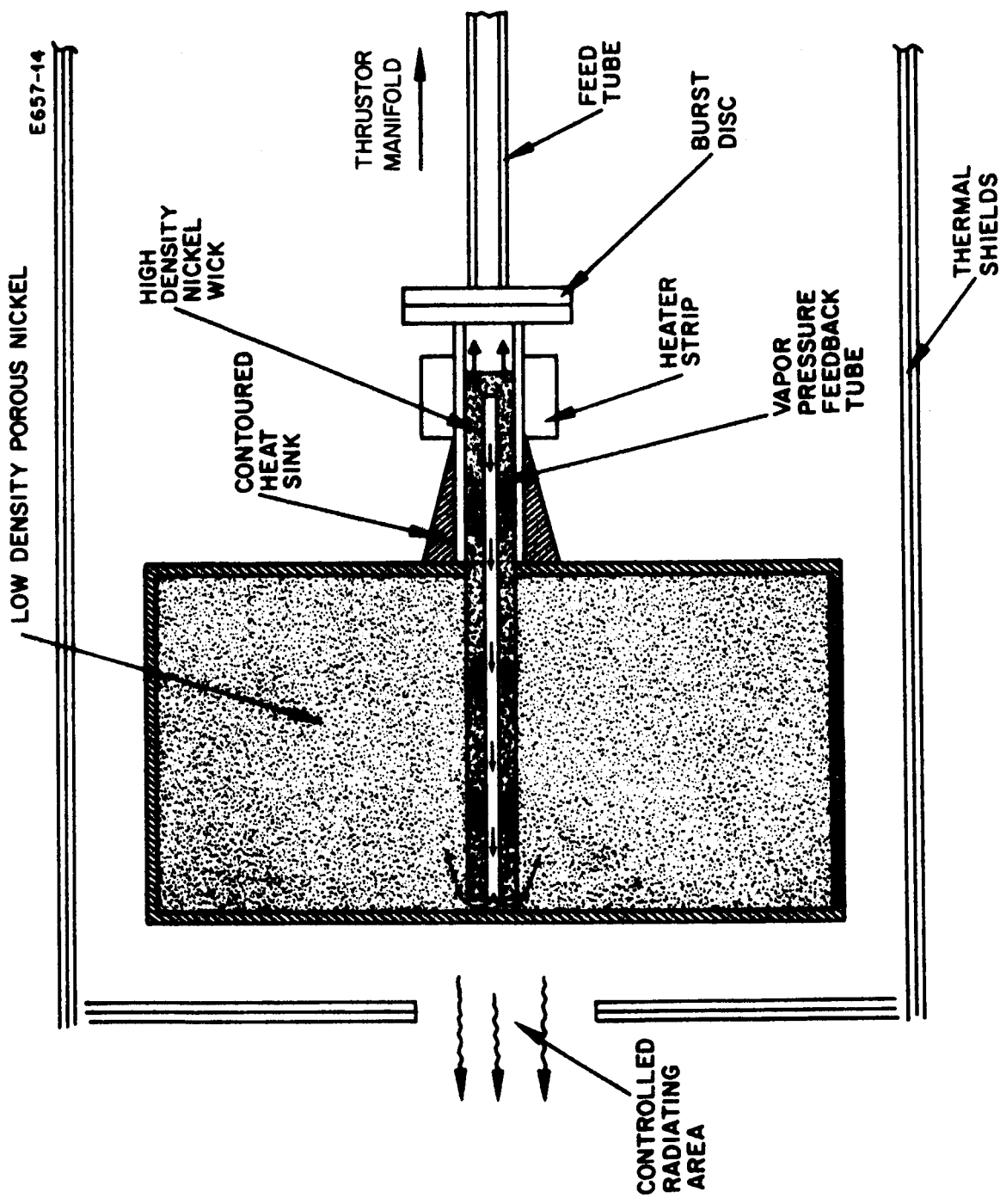
Fig. C-1. Schematic of original liquid cesium feed system design.
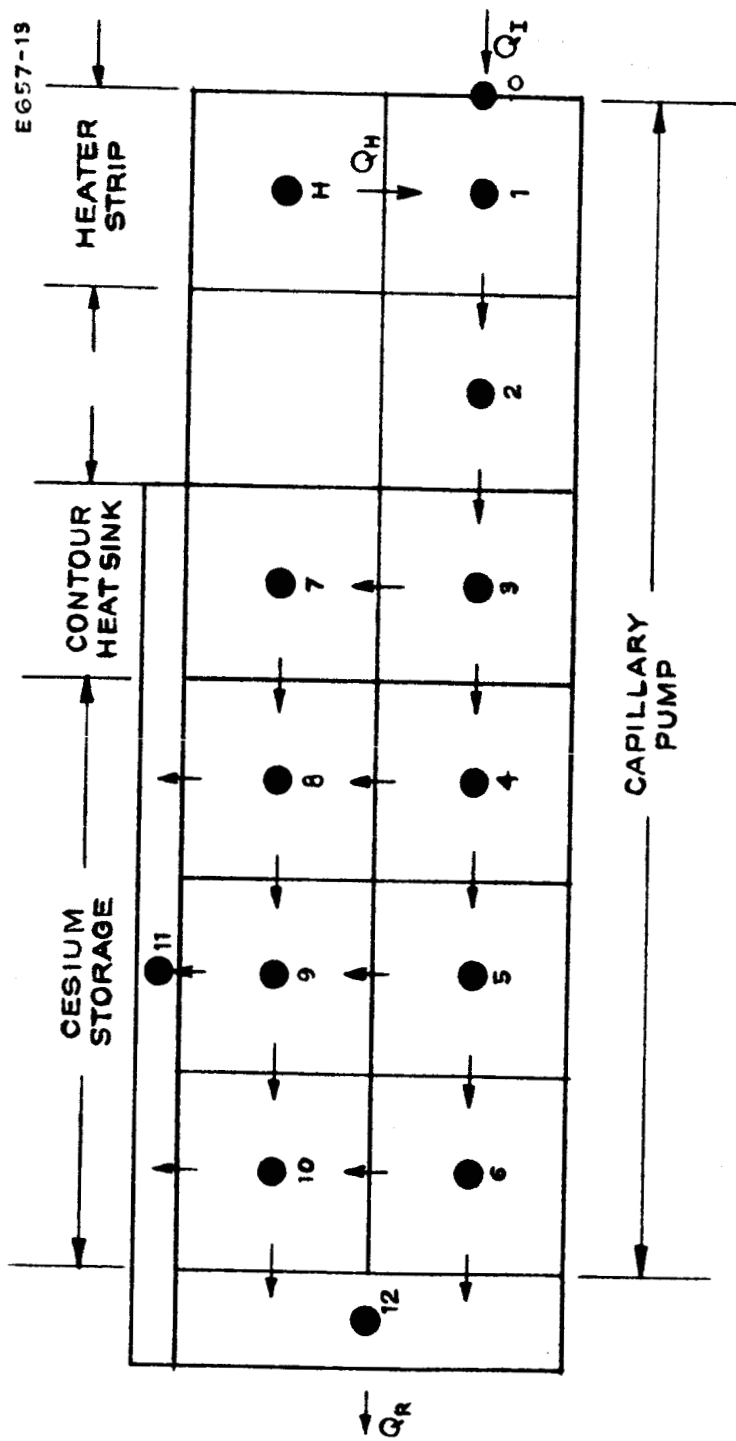
Fig. C-2. Thermodynamic model of original liquid cesium feed system.

3. <u>Zero "g" Feed System Thermodynamic Model</u>

1. $$\dot{T}_1 = \frac{1}{(MC)_1} \left[Q_I + Q_H - K_{12} (T_1 - T_2) \right]$$

2. $$\dot{T}_2 = \frac{1}{(MC)_2} \left[K_{12} (T_1 - T_2) - K_{23} (T_2 - T_3) \right]$$

3. $$\dot{T}_3 = \frac{1}{(MC)_3} \left[K_{23} (T_2 - T_3) - K_{34} (T_3 - T_4) - K_{37} (T_3 - T_7) \right]$$

4. $$\dot{T}_4 = \frac{1}{(MC)_4} \left[K_{34} (T_3 - T_4) - K_{45} (T_4 - T_5) - K_{48} (T_4 - T_8) \right]$$

5. $$\dot{T}_5 = \frac{1}{(MC)_5} \left[K_{45} (T_4 - T_5) - K_{56} (T_5 - T_6) - K_{59} (T_5 - T_9) \right]$$

6. $$\dot{T}_6 = \frac{1}{(MC)_6} \left[K_{56} (T_5 - T_6) - K_{610} (T_6 - T_{10}) - K_{612} (T_6 - T_{12}) \right]$$

7. $$\dot{T}_7 = \frac{1}{(MC)_7} \left[K_{37} (T_3 - T_7) - K_{78} (T_7 - T_8) \right]$$

8. $$\dot{T}_8 = \frac{1}{(MC)_8} \left[K_{48} (T_4 - T_8) + K_{78} (T_7 - T_8) - K_{89} (T_8 - T_9) \right.$$
    $$\left. - K_{811} (T_8 - T_{11}) \right]$$

9. $$\dot{T}_9 = \frac{1}{(MC)_9} \left[K_{89} (T_8 - T_9) + K_{59} (T_5 - T_9) - K_{910} (T_9 - T_{10}) \right.$$
    $$\left. - K_{911} (T_9 - T_{11}) \right]$$

10. $$\dot{T}_{10} = \frac{1}{(MC)_{10}} \left[K_{910} (T_9 - T_{10}) - K_{1011} (T_{10} - T_{11}) \right.$$
    $$\left. - K_{1012} (T_{10} - T_{12}) \right]$$

11. $\dot{T}_{12} = \frac{1}{(MC)_{12}} \left[K_{612} (T_6 - T_{12}) + K_{1012} (T_{10} - T_{12}) \right.$

$$\left. - \sigma\epsilon A_{12} (T_{12}^4 - T_\infty^4) \right] + K_{1112} (T_{11} - T_{12})$$

12. $K_{12} = K_{23} = K_{34} = K_{45} = K_{56} = \frac{A_i}{\Delta X_i} \left[0.1 k_{Cs} + 0.9 k_{Ni} \right]$

13. $A_i = \frac{\pi d_i}{4}$

14. $Q_H = \text{Heater Power} = K_{H1} (T_H - T_1)$

15. $\dot{T}_H = \frac{1}{(MC)_H} \left[I_H^2 R_H - K_{H1} (T_H - T_1) \right]$

16. $K_{37} = \dfrac{2\pi L_3}{\dfrac{\ln(2)}{(0.1 k_{Cs} + 0.9 k_{Ni})} + \dfrac{\ln[0.5 (1 + V_7/V_3)]}{k_{ss}}}$

16a. $\dot{T}_{11} = \frac{1}{(MC)_{11}} \left[K_{1011} (T_{10} - T_{11}) + K_{911} (T_9 - T_{11}) \right.$

$$\left. + K_{811} (T_8 - T_{11}) + K_{1112} (T_{11} - T_{12}) \right]$$

17. $K_{48} = \dfrac{2\pi L_4}{\dfrac{\ln(2)}{(0.1 k_{Cs} + 0.9 k_{Ni}}) + \dfrac{\ln\left[0.5 \left(1 + \frac{1}{8}/\frac{1}{4}\right)\right]}{(0.9 k_{Cs} + 0.1 k_{Ni})}}$

18. $K_{59} = \dfrac{2\pi L_5}{\dfrac{\ln(2)}{(0.1 k_{Cs} + 0.9 k_{Ni})} + \dfrac{\ln[0.5 (1 + V_9/V_5)]}{(0.9 k_{Cs} + 0.1 k_{Ni})}}$

19. $$K_{610} = \dfrac{2\pi L_6}{\dfrac{\ln(2)}{(0.1\,k_{Cs} + 0.9\,k_{Ni})} + \dfrac{\ln[0.5(1 + V_{10}/V_6)]}{(0.9\,k_{Cs} + 0.1\,k_{Ni})}}$$

20. $$K_{89} = \dfrac{k_i A_i}{L_i} = \dfrac{\pi}{4}\,\dfrac{(d_8^2 - d_4^2)(0.9\,k_{Cs} + 0.1\,k_{Ni}}{L_8}$$

21. $$K_{910} = \dfrac{\pi}{4}\,\dfrac{(d_9^2 - d_5^2)(0.9\,k_{Cs} + 0.1\,k_{Ni})}{L_9}$$

22. $$K_{1012} = \dfrac{\pi}{4}\,\dfrac{(d_{10}^2 - d_6^2)}{\dfrac{L_{10}}{2(0.9\,k_{Cs} + 0.1\,k_{Ni})} + \dfrac{L_{12}}{2\,k_{ss}}}$$

23. $$K_{1112} = \dfrac{\pi}{4}\,\dfrac{(d_{11}^2 - d_{10}^2)\,k_{ss}}{L_{11}/2}$$

24. $$K_{12} = K_{23} = K_{34} = K_{45} = K_{56} = \dfrac{\pi}{4}\,\dfrac{d_1^2(0.1\,k_{Cs} + 0.9\,K_{Ni}}{L_1}$$

25. $$K_{612} = \dfrac{\pi d_1^2}{4}\,\dfrac{1}{\dfrac{L_6}{2(0.1\,k_{Cs} + 0.9\,k_{Ni})} + \dfrac{L_{12}}{2\,k_{ss}}}$$

26. $$K_{78} = \dfrac{\pi}{4}\,\dfrac{(d_7^2 - d_3^2)}{\dfrac{L_8}{2(0.9\,k_{Cs} + 0.1\,k_{Ni})} + \dfrac{L_7}{2\,k_{ss}}}$$

4.   Gas Diffusion Equations

$$K\nabla^2 \rho_i = \frac{\partial \rho_i}{\partial t} + v_{xi} \frac{\partial \rho_i}{\partial x}$$

$$K\nabla^2 \rho_i = \frac{\partial}{\partial x}\left(D_i \frac{\partial \rho_i}{\partial x}\right) \quad \text{(One dimensional flow)}$$

$$\therefore \quad \frac{\rho_i}{\partial t} = \frac{\partial}{\partial x}\left(D_i \frac{\partial \rho_i}{\partial x}\right) - v_{xi} \frac{\partial \rho_i}{\partial x} \qquad\qquad \text{(C.1)}$$

$$D_i \equiv \text{diffusion coefficient} \sim cm^2/sec$$

$$v_{xi} \equiv \text{velocity of liquid-vapor interface} \sim cm/sec$$

$$\rho_i \equiv \text{concentration of mass} \sim gms/cm^3$$
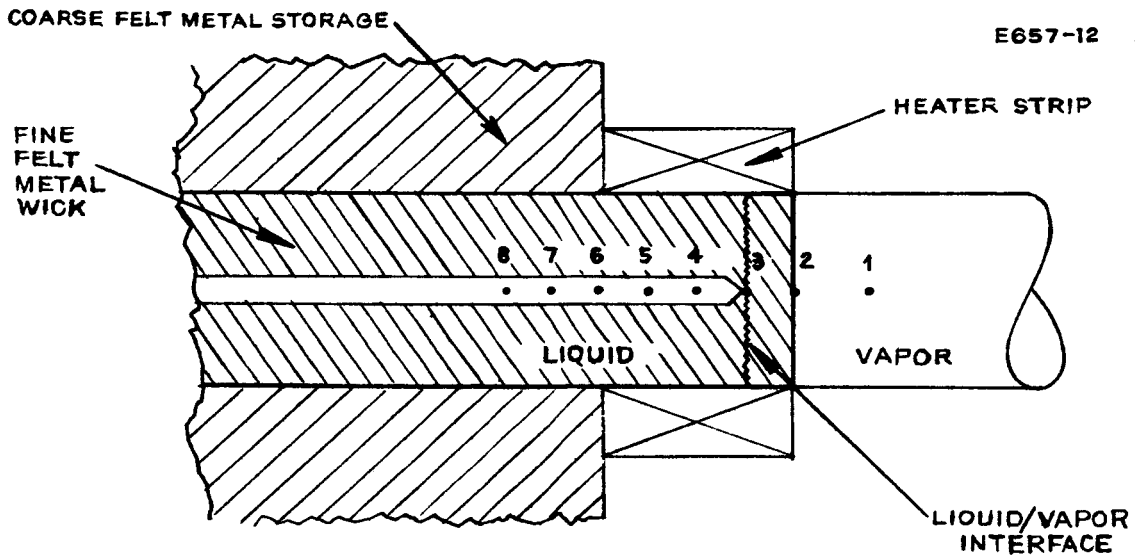
Fig. C-3. Schematic fluid-dynamic model of vaporizer section.

Finite Difference Approximation

$$\rho_{i+1} \qquad \rho_i \qquad \rho_{i-1}$$

$$\circ\!\!-\!\!-\!\!-\!\!-\!\!\circ\!\!-\!\!-\!\!-\!\!-\!\!\circ$$
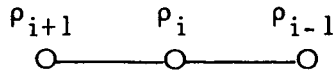
$$\frac{\partial \rho_i}{\partial x} \cong \frac{\rho_i - \rho_{i+1}}{\Delta x_{i+1}} \qquad \text{(backward difference approximation)}$$

$$\frac{\partial \rho_i}{\partial x} \cong \frac{\rho_{i-1} - \rho_i}{\Delta x_{i-1}} \qquad \text{(forward difference approximation)}$$

$$\frac{\partial \rho_i}{\partial x} \cong \frac{\rho_{i-1} - \rho_{i+1}}{(\Delta x_{i+1} + \Delta x_{i-1})} \qquad \text{(average difference approximation)}$$

$$\nabla^2 \rho_i \cong \frac{D_{i-1} \dfrac{\partial \rho_{i-1}}{\partial x} - D_{i+1} \dfrac{\partial \rho_{i+1}}{\partial x}}{\dfrac{\Delta x_{i+1}}{2} + \dfrac{\Delta x_{i-1}}{2}} \qquad \text{(central difference approximation)}$$

$$\therefore \nabla^2 \rho_i \cong \frac{D_{i-1}(\rho_{i-1} - \rho_i)}{\Delta x_{i-1} \dfrac{(\Delta x_{i+1} + \Delta x_{i-1})}{2}} + \frac{D_{i+1}(\rho_{i+1} - \rho_i)}{\Delta x_{i+1} \dfrac{(\Delta x_{i+1} + \Delta x_{i-1})}{2}} \qquad \text{(C.3)}$$

$$v_{xi} = \dot{x} \qquad \text{(C.4)}$$

Combining eqs. (C.1), (C.2), (C.3), (C.4) yields

$$\boxed{\frac{\partial \rho_i}{\partial t} = \frac{2(\rho_{i-1} - \rho_i) D_{i-1}}{\Delta x_{i-1}(\Delta x_{i+1} + \Delta x_{i-1})} + \frac{2(\rho_{i+1} - \rho_i) D_{i+1}}{\Delta x_{i+1}(\Delta x_{i+1} + \Delta x_{i-1})} + \frac{\dot{x}(\rho_{i+1} - \rho_i)}{\Delta x_{i+1}}}$$

Diffusion Coefficient

$$D_i = K/\epsilon = \text{permeability/porosity}$$

$$K = \frac{B_o \overline{P}}{\eta} + \frac{4}{3} K_o \, \overline{v}$$

$$\overline{P}_i = \frac{(P_{i+1} + P_{i-1})}{2} = \rho_i RT_i \quad \text{(average pressure)} \sim \text{(dyn/cm}^2\text{)}$$

$$\eta_i = 0.807 \times 10^{-5} \sqrt{T_i} \quad \text{(viscosity)} \sim \text{(dyn-sec/cm}^2\text{)}$$

$$\overline{v}_i = 1,260 \sqrt{T_i} \quad \text{(mean velocity cesium atom)} \sim \text{(cm/sec)}$$

$$B_o = \frac{\pi}{8} N r^4 \quad \text{(cm}^2\text{)}$$

$$K_o = \frac{\pi}{2} J_1 N r^3 \quad \text{(cm)}$$

$$\epsilon = N \pi r^2 \quad \text{(porosity)}$$

where

$$J_1 = 0.9$$

$$r \equiv \text{average radius of pores} \sim \text{(cm)}$$

$$N \equiv \text{number of pores per unit area.}$$

Substituting into the diffusion equation

$$D_i = 756 \; r \sqrt{T_i} \left(\frac{cm}{sec\text{-}°K^{1/2}} \right) \left[20.5 \; r \, \rho_i R \left(\frac{cm \text{ - } °K}{dyn} \right) + 1 \right]$$

5. Nomenclature for Cesium Liquid-Vapor Separator

Symbol	Description	Units
A_i	Surface area of node i	cm^2
C_{csl}	Heat capacity of liquid cesium	W-sec/g-°C
C_{csg}	Heat capacity of cesium vapor	W-sec/g-°C
C_{Ni}	Heat capacity of nickel	W-sec/g-°C
C_{SS}	Heat capacity of 316 stainless steel	W-sec/g-°C
d_i	Diameter of node i	cm
ϵ_{SS}	Emissivity of 316 stainless steel	—
k_{csl}	Thermal conductivity of liquid cesium	W/cm-°C
k_{csg}	Thermal conductivity of cesium vapor	W/cm-°C
k_{Ni}	Thermal conductivity of nickel	W/cm-°C
K_{SS}	Thermal conductivity of 316 stainless steel	W/cm-°C
L_i	Length	cm
$(MC)_{ffm}$	Heat capacity of fine felt metal	W-sec/°C
$(MC)_{cfm}$	Heat capacity of coarse felt metal	W-sec/°C
$(MC)_{csg}$	Heat capacity of cesium vapor	W-sec/°C
$(MC)_{csl}$	Heat capacity of liquid cesium	W-sec/°C
$(MC)_H$	Heat capacity of heater strip	W-sec/°C
P_S	Separator output vapor pressure	Torr
Q_{Ri}	Radiant heat loss from node i	W
Q_S	Separator input heater power (E^2/R)	W
T_i	Temperature at node i	°K

Symbol	Description	Units
T_S	Cesium vaporization temperature	$^{\circ}K$
T_{∞}	Background temperature	$^{\circ}K$
V_i	Volume	cm^3
V_{fc}	Void fraction, coarse felt metal	—
V_{ff}	Void fraction, fine felt metal	—
$\dot{W}_{cs}$	Cesium flowrate	g/sec
σ	Stefan-Boltzman constant	$W/cm^2 - {^{\circ}C}$
ρ_{csg}	Density cesium vapor	g/cm^3
ρ_{csl}	Density liquid cesium	g/cm^3
ρ_{Ni}	Density nickel	g/cm^3
ρ_{SS}	Density 316 stainless steel	g/cm^3

6.   Cesium Liquid-Vapor Separator Sizing List

Symbol	Value or Range
C_{csl}	0.239 W-sec/g-$^\circ$C
C_{csg}	0.156 W-sec/g-$^\circ$C
C_{Ni}	0.544 W-sec/g-$^\circ$C
C_{SS}	0.502 W-sec/g-$^\circ$C
d_i	5.00 cm
ϵ_{SS}	0.22
k_{csl}	0.0184 W/cm-$^\circ$C
k_{csg}	0.000057 W/cm-$^\circ$C
k_{Ni}	0.0606 W/cm-$^\circ$C
k_{SS}	0.0199 W/cm-$^\circ$C
P_S	approx. 1-20 Torr
Q_S	approx. 10 W
T_S	approx. 551-680 $^\circ$K
T_∞	approx. 300° K
V_{fc}	90%
V_{ff}	10%

7.   Analog Computer Mechanization

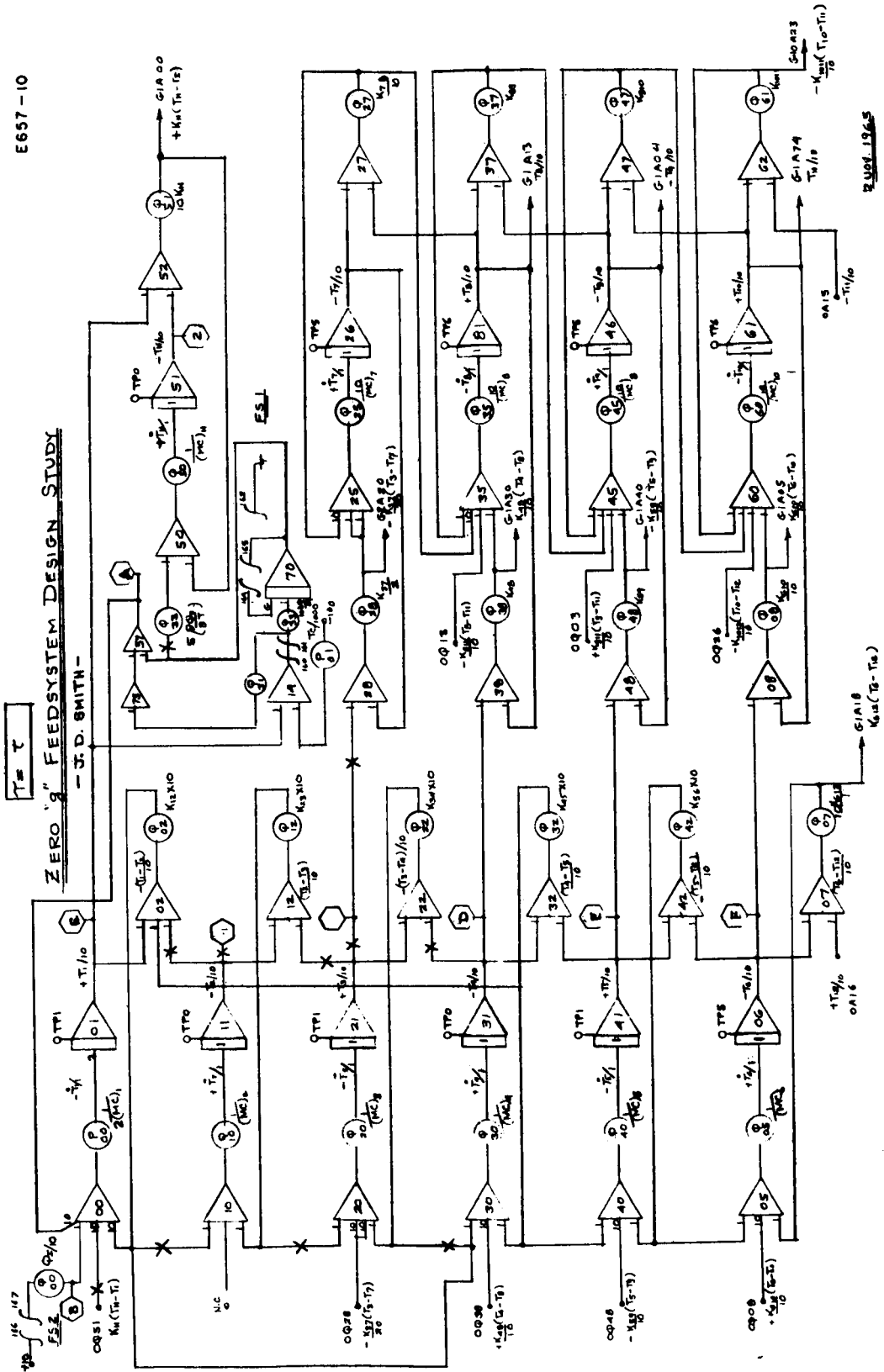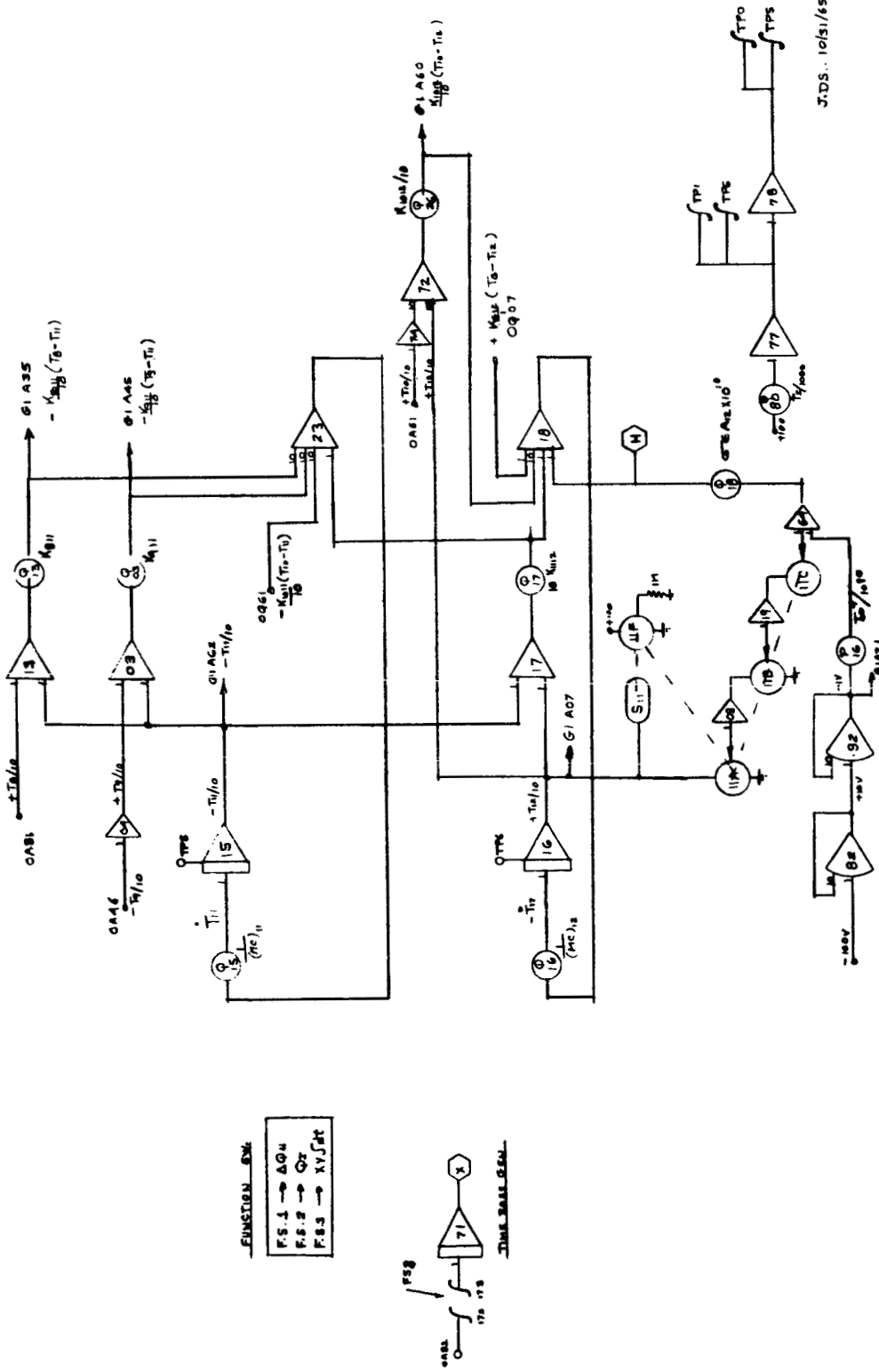The analog computer mechanizations for the zero-g feed system design study are shown in Fig. C-4 and C-5.

Fig. C-4. Analog computer mechanization for zero-g design study.

Fig. C-5. Analog computer mechanization for zero-g design study.

111

DISTRIBUTION LIST

	Address	Semiannual
1.	NASA Headquarters FOB-10B 600 Independence Avenue, S.W. Washington, D.C. 20546 Attn: RNT/James Lazar	1
2.	NASA-Lewis Research Center 21000 Brookpark Road Cleveland, Ohio 44135 Attn: Spacecraft Technology Procurement	
	Section (M.S. 54-2)	1
	Technology Utilization Office	
	(M.S. 3-19)	1
	Library (M.S. 3-7)	2
	Spacecraft Technology Division	
	a. C. C. Conger (M.S. 54-1)	1
	b. D. L. Lockwood (M.S. 54-3)	2
	c. J. T. Kotnik (M.S. 54-3)	1
	d. D. M. Shellhammer (M.S. 54-3)	4
	Electrical Propulsion Laboratory	
	a. W. Moeckel (M.S. 301-1)	1
	b. H. R. Kaufman (M.S. 301-1)	1
	c. E. A. Richley (M.S. 301-1)	1
	Report Control Office (M.S. 5-5)	1
3.	NASA Scientific and Technical Information Facility P. O. Box 33 College Park, Maryland 20740 Attn: NASA Representative RQT-2448	6
4.	NASA-Marshall Space Flight Center Huntsville, Alabama 35812 Attn: Ernest Stuhlinger (M-RP-DIR)	1
5.	Research and Technology Division Wright-Patterson AFB, Ohio 45433 Attn: AFAPL (APIE-2)/R. F. Cooper	1
6.	AFWL Kirtland AFB, New Mexico Attn: WLPC/Capt. C. F. Ellis	1

7.   Aerospace Corporation
     P. O. Box 95085
     Los Angeles, California 90045
     Attn: Library/Technical Documents Group   1

8.   Jet Propulsion Laboratory
     4800 Oak Grove Drive
     Pasadena, California 91103
     Attn: J. W. Stearns   1

9.   Electro-Optical Systems, Inc.
     300 North Halstead Street
     Pasadena, California 91107
     Attn: R. C. Speiser   1

10. TRW Inc.
     TRW Systems Group
     One Space Park
     Redondo Beach, California
     Attn: D. B. Langmuir   1

11. Westinghouse Astronuclear Laboratories
     Electric Propulsion Laboratory
     Pittsburgh, Pennsylvania 15234
     Attn: H. W. Szymanowski   1

12. General Electric Space
     Flight Propulsion Laboratory
     Cincinnati, Ohio 45215
     Attn: M. L. Bromberg   1

13. Hiram College
     Department of Physics
     Hiram, Ohio
     Attn: Professor L. Shaffer   1

14. Field Emission Corporation
     Melrose Avenue at Linke Street
     McMinnville, Oregon 97128
     Attn: L. W. Swanson   1

15. Litton Precision Products
     960 Industrial Road
     San Carlos, California
     Attn: G. K. Wehner   1

	Address	Semiannual
16.	Princeton University Department of Aeronautical Engineering Princeton, New Jersey Attn: Professor J. B. Fenn	1
17.	University of California Space Science Laboratory Berkeley 4, California Attn: H. P. Smith	1
18.	Aerojet-General Nucleonic Division San Ramon, California Attn: J. S. Luce	1
19.	North American Aviation, Inc. 12214 Lakewood Avenue Downey, California Attn: Technical Information Office Department 4096-314	1
20.	NASA-Langley Research Center Langley Field Station Hampton, Virginia 23365 Attn: Technical Library	1
21.	Colorado State University Fort Collins, Colorado Attn: L. Baldwin	1
22.	Rocketdyne 6633 Canoga Avenue Canoga Park, California Attn: J. F. Hon	1
23.	MSA Research Corporation Callery, Pennsylvania Attn: R. C. Werner	1
24.	U. S. Atomic Energy Commission P. O. Box 62 Oak Ridge, Tennessee 37831 Attn: Division of Technical Information Extension	1

	Address	Semiannual

25. USAF
Office of Scientific Research
Washington, D. C. 20025
Attn: M. Slawsky   1

26. Cornell University
Graduate School of Aeronautical Engineering
Ithaca, New York
Attn: E. L. Resler, Jr.   1

27. The Martin Company
P. O. Box 5837
Orlando, Florida
Attn: Engineering Library MP30   1

28. AVCO Corporation
Research and Advanced Development Division
201 Lowell Street
Wilmington, Massachusetts
Attn: R. R. John   1
       R. J. Cybulski   1

29. The Royal Institute of Technology
Stockholm 70, Sweden
Attn: B. Agduv   1

30. Swiss Federal Institute of Technology
Zurich, Switzerland
Attn: The Library

31. Nagoya University, Chikusa-ku
Institute of Plasma Physics
Nuclear Fusion Research Group
Research Information Center
Nagoya, Japan
Attn: Y. Y. Terashima   1

32. Air Force Plant Representative
Hughes Aircraft Company
Culver City, California
Attn: RWRAAC-2   1
       RWRAPS-9   1

ERRATA

NASA CONTRACTOR REPORT CR-54684

DEVELOPMENT OF

LINEAR STRIP ION THRUSTORS

by J. R. Anderson, R. Kuberek, J. W. Pfeifer,
J. D. Smith, S. A. Thompson, and M. D. Benton

Hughes Research Laboratories

The subject report was incorrectly numbered as NASA CR-54684. Please
change this number to NASA CR-54685 on the cover and title page.